Systems biology analysis of iron metabolism

D i s s e r t a t i o n

zur Erlangung des akademischen Grades

d o c t o r r e r u m n a t u r a l i u m

(Dr. rer. nat.)

im Fach Biophysik

eingereicht an der

Mathematisch-Naturwissenschaftlichen Fakultät I

der Humboldt-Universität zu Berlin

von

Herrn Tiago Jose da Silva Lopes

Präsident der Humboldt-Universität zu Berlin

Prof. Dr. Dr. h.c. Christoph Markschies

Dekan der Mathematisch-Naturwissenschaftlichen Fakultät I

Prof. Dr. Andreas Herrmann

Gutachter:

1. Prof. Edda Klipp
2. Prof. Martina Muckenthaler
3. Prof. Hermann-Georg Holzhutter

Tag der mündlichen Prüfung: 05.December.2010

For my family.
For my friends from the past, present and future.

Contents

Chapter 1

1 - Introduction

Iron is a chemical element present in key biochemical processes of virtually every living cell. It exists in two interconvertible ionic forms, Fe^{2+} (ferrous ion, reduced) and Fe^{3+} (ferric ion, oxidized). This is the basis for numerous oxido-reductive electron transfers which are a vital element of living cells. The high reactivity of ionic iron, however, is also a danger, since it may lead to chemical radicals which are detrimental to biological macromolecules. An example for this is a reaction of the so-called Fenton type, where ferrous iron becomes oxidized by hydrogen peroxide. The reaction produces a hydroxyl anion and a hydroxyl radical, which can damage cell membranes and essential components like DNA or proteins.

$$Fe^{2+} + H_2O_2 \rightarrow Fe^{3+} + OH\cdot + OH^-$$

It is therefore important for the organism to exert a critical control over its free iron, otherwise its beneficial reactive characteristics can turn into a threat for the cell.

In mammals, a very important role of iron is related to its presence in hemoglobin, a protein directly involved in oxygen transport through the body. The synthesis of hemoglobin is an essential step in the production of red blood cells (RBC). In the human body this step requires approximately 20 mg iron per day. In adult humans as well as in many other mammals the RBC production takes place predominantly in the bone marrow and represents the greatest demand of iron in the body.

In the muscles, iron is present in myoglobin. This protein provides a reservoir of readily accessible oxygen. This is intracellular buffer for the case of intermittent anoxia [1]. Other cell types of the body contain iron as a reserve store, bound to ferritin. This protein is able to bind free iron in considerable amounts and keeps it non-toxic, releasing it only until required by other metabolic functions.

Every cell of the body incorporates a certain amount of iron into a host of iron-containing proteins (heme proteins, Fe-S-cluster proteins) which fulfill essential functions of cellular life.

The only natural source of iron for mammals is the diet. A tightly controlled mechanism exists to determine the exact amount allowed to enter the body. Disorders in this absorptive process, in either direction – too much or too little iron – have serious public health implications. Iron deficiency anemia is the most prevalent nutrition disease worldwide and affects every society, irrespective of race, cultural and social-background [2]. On the other hand is hemochromatosis a hereditary disease that provokes an excessive intake of iron from the diet. Since the human body is incapable of excreting iron in a well-regulated manner, an accumulation of this metal can take place, which damages the liver and other parenchymous organs and leads to liver cirrhosis and finally to liver cancer. The liver absorbs the excess of iron and so protects other organs, but unfortunately ends up damaging itself.

In the brain, iron varies according to three factors: the anatomic region, the developmental stage of the organism and the species being studied [3]. In this organ iron plays a not-well characterized role. A strong correlation was observed between accumulation of this metabolite and neurodegenerative diseases like Parkinson, Alzheimer and Huntington [4, 5].

Uptake and distribution of iron in the body have been investigated in detail, but we have no complete picture of the molecular mechanisms that regulate these processes. There are still missing components that are at present being revealed through the use of modern molecular techniques. The use of transgenic mice technology opened a range of possibilities and helps to elucidate the regulatory pathways of iron metabolism.

From a systemic point of view the iron metabolism displays two different hierarchical levels. One level concerns the well regulated iron metabolism within the multifarious types of cells and tissues of the body. The other level is the regulated exchange of iron between cells and tissues and the control of its uptake. The cellular and the organismal aspect are intimately connected and cannot be satisfactorily understood in isolation of each other. The study of isolated cells has led to a deeper understanding of the regulation within certain cells. However, the interpretation has been limited by the fact that the cell lines so studied were usually not fully functional and could not communicate with the extracellular environment and with other organs. On the other hand, the study of iron flux between tissues has led to important quantitative data, but was limited to a phenomenological level that described aptly what happened in the body, but not why it happened as it did. These two limitations have now been overcome by the modern gene construction techniques. They allow the study of animal iron metabolism applying certain well-designed genetic constructions which reveal, by knock-out or by enforced gene expression, the fine-tuning of iron-related reactions in the healthy as well as in the diseased organism. The so-called Cre-Lox-technology makes it even possible to change a certain gene in a selected target cell, by causing the attempted effect (knock-out, knock-in or enforced expression) only under the control of cell-specific promoters. So it became possible to address certain cell types and tissues with experimental changes, thereby avoiding the often deleterious effect of whole-body genetic mutations.

A holistic understanding of iron metabolism in its various physiological and pathological states requires a deeper systemic understanding. This can be advanced by the method of mathematical modeling. Many ingenious mathematical studies of iron metabolism of the whole body have been published. Most of the earlier work concentrated on the interpretation of the tracer elimination curve in human blood plasma after an intravenous injection [6, 7]. Marsaglia, in cooperation with Finch and Hosain [8] devised a method to estimate the passage time through bone marrow and the return time of tracer into blood. Pollycove and Mortimer [9] published a study that tried to estimate the organ distribution of iron fluxes on the basis of scintillation measurements of tracer projected to the body surface. Nathanson and coworkers [10] studied the absorption and distribution kinetics of iron in dogs. Berzuini et al. [11] and later on Stefanelli et al. [12] developed whole-body models on data from human subjects, after tracer injection into blood or as colloidal tracer absorbed by the reticulo-endothelial system. A whole-body iron distribution study by Vácha et al. [13] attempted at a quantitative description of a mouse strain (C57BL/10ScSnPh) which is related to the strain to be modelled in this dissertation. This paper contained a series of ad-hoc assumptions on fluxes for which a precise biochemical characterization was not possible, but the resulting mathematical model fitted the measured ferrokinetic data quite satisfactorily. A first attempt to model iron metabolism as compartment system with inclusion of the recently discovered hormonal signals (especially the hepcidin loop) was published by Lao and Kamei [14]. The intracellular aspect has in all these papers been studied only in a black-box manner because iron motion within the cell occurs in a complex membranous environment. This precludes the classical biochemical kinetics which has been so successfully applied to the analysis of cytosolic and mitochondrial biochemistry.

The dissertation presented here proposes a comprehensive description of iron metabolism in the form of an *in silico* simulation of the iron exchange and its regulation for the mouse strain C57BL6. We chose this special model animal for two reasons: It is the preferred strain for the afore-mentioned genetic constructs, and it is possible to obtain most of the experimental data that are required for a quantitative description of iron metabolism. A generic cell model will be presented which comprises the main features of iron metabolism

that are common to all cell types, due to the fact that every cell expresses the same set of iron-related mRNA and proteins. Specific cellular flavor is obtained by adapting the values of certain crucial parameters of the cell model accordingly. The different cell and tissue types the iron profile of which is being specified in this way are then integrated in accordance with their relative abundance into a whole-body balance sheet to which the most important regulatory signals (iron-related hormone hepcidin, erythron-related hormone erythropoietin, intracellular regulators of the IRP/IRE system) are added. We show that certain of the salient features of iron metabolism in the normal state as well as under physiological or pathological challenge are being satisfactorily simulated with quantitative approximation to experimental data.

Chapter 2

2 - Models and Experimental Methods

2.1 General Structure of Iron Metabolism

Iron metabolism has been reviewed in several monographs from which the general structure can be extracted as basis for a mathematical model [15-17].
Iron is contained in every cell of the mammalian body and also in the extracellular space. Only tiny amounts appear as free ionic iron. All the other iron is in bound form, as hemoproteins, as oxygen carriers, as iron-sulfur proteins, in non-haem enzymes (such as transferrins), or as iron transporters in cellular membranes.

2.2 General Flux Network of Iron in the Organism

Mammalian organisms absorb iron from the intestinal tract, mainly via the duodenal epithelium, and loose it predominantly by exfoliation of intestinal epithelium, by desquamation of the skin, by occasional or repeated loss of blood, and to a lesser extent via excretion of a non-reabsorbed fraction of bile and urine. Duodenal absorption transfers iron into plasma where it is bound to transferrin. Transferrin-bound iron is distributed to peripheral tissues in accordance with their expression level of the transferrin receptor (TFR1). This stream into the periphery can be measured after injection of radioactive ^{59}Fe into plasma as rate of appearance of the tracer in the periphery. This intake of iron into cells is balanced by an out- stream back into plasma of similar strength, mediated by iron export protein ferroportin [18].
This global scheme of iron uptake and distribution into the periphery and its reflux into plasma is adequately represented by a “mammillary” compartment system with reversible flux. The layout of the general flux model is depicted in fig. 2.1.

Plasma and extracellular fluid contain transferrin-bound iron that equilibrates quickly (< 1 day) between both compartments [6, 19], which are therefore treated as one central compartment. Other tissues form peripheral compartments. The erythropoetic compartment of bone marrow has a high expression level of the transporter TFR1 and rapidly integrates iron into hemoglobin [20, 21]. Both fluxes as well as the filtering-out of senescent blood cells are irreversible. In contrast, the expression level of ferroportin in bone marrow is low. This allows us to model the iron pathway from plasma over bone marrow, erythrocyte pool, and RES (emphasized by thick arrows in fig. 2.1) as a circular irreversible flux without reflux. A smaller flux from bone marrow into the Reticulo-Endothelial System (RES) has to be included. It represents partly spleen erythropoiesis in mice and partly “ineffective erythropoiesis” [22].

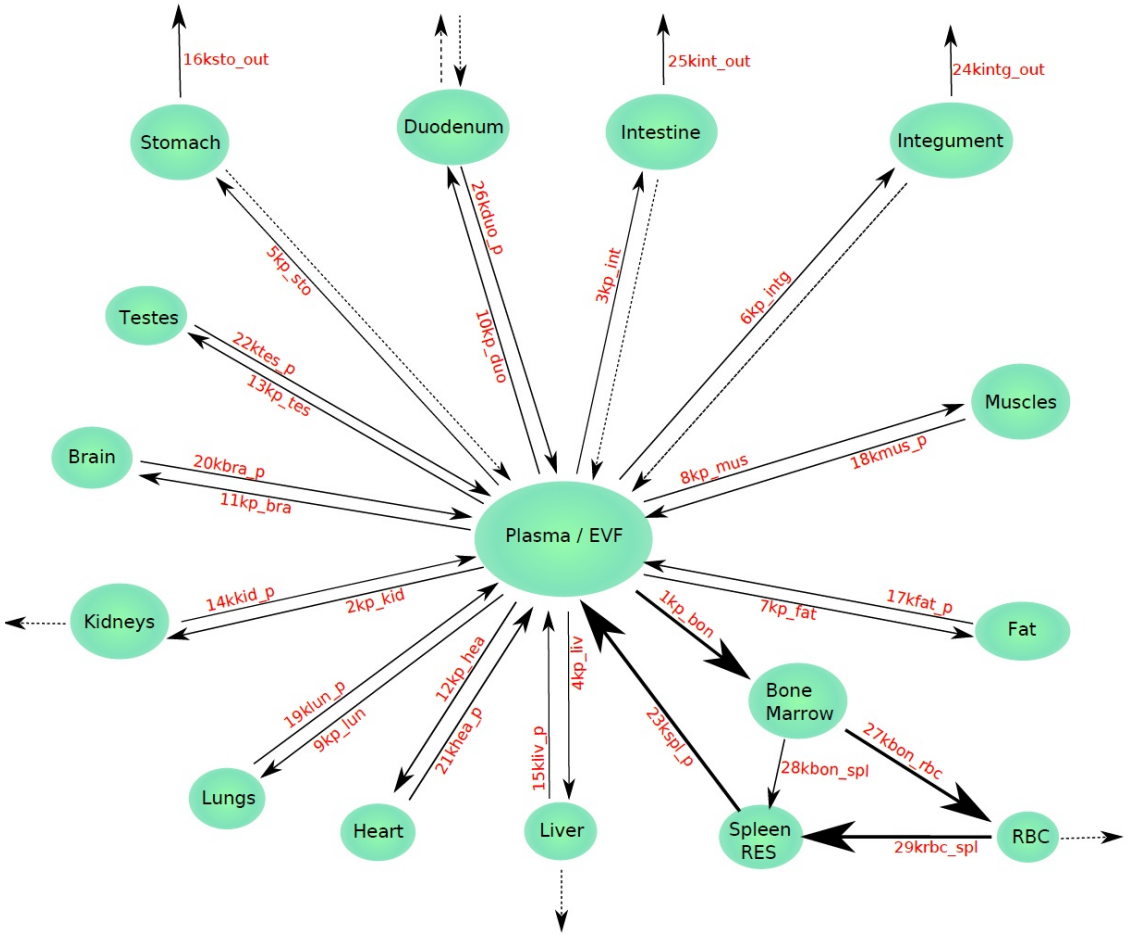

Figure 2.1: Global flux model layout. In green are shown the compartments representing each organ, the arrows are iron flows between compartments and plasma or directly between organs (bone marrow, RBC and Spleen). Dashed arrows represent fluxes that are known to exist but were omitted in our model because they were combined with the dominant outflux from the same compartment (to avoid parameter indeterminacy).

Some of the peripheral compartments have two outlets, one leading back into the central compartment and the other one leaving the system by loss of cells or excretion. The clearance of radioactive tracer can be estimated in these cases, but not the partition between these two outlets. Loss of tracer from the body is difficult to measure, and the plasma curve is not sufficiently sensitive to small variants of back-flux from those tissues. For parameter estimation an *a priori* decision had to be made about which of the double outflows is quantitatively the more important. In the intestine and integument, with the exception of the duodenum, iron losses from the body are assumed to be the main route. This reflects the rapid exfoliation of intestinal epithelium (around 4 days), as well as the slower, but of larger volume, desquamation of skin and integumental adnexes. In the duodenum the ^{59}Fe influx from plasma counters the physiological uptake of unlabelled iron from the lumen. In erythrocytes, liver, and kidney it was decided that the main pathway balancing iron uptake is reflux into plasma rather than loss out of the body.

The compartments in fig. 2.1 represent organs and tissues. They are not kinetically homogenous, as every organ consists of cell types that may differ in their iron metabolism. Iron content in such compartments and intercompartment fluxes represent therefore a weighted mean over different cell types. Mixture compartments of this type are liver, spleen and muscle.

2.3 Iron balance: absorption from duodenum and loss from the body

Iron is being distributed in various amounts over all body cells. The exchange traffic is mainly mediated via the transferrin pool in plasma (about 1.5 µg iron per mouse body). The absorption of iron takes place in the duodenal and upper jejunal lumen. The rate of absorption is tightly controlled and amounts to about 3 µg per mouse body per day. The adult healthy mouse is in a steady state, because the rate of iron loss is the same, amounting to 0.5% of the total body iron per day [23, 24]. This happens mainly through desquamation of skin cells, loss of hair, and shedding of stomach and intestinal mucosa. In our model it will be formulated as aggregated iron 'leakage' where the whole cell is lost from the body, loosing its iron content. The rate of iron leakage is small and varies with different cell types.

2.4 Numerical Scales of Pools and Turnover Rates.

2.4.1 Scaling of iron content to the whole mouse organism

The generic model of fig. 2.1 has to be quantitatively specified. The assumed reference organism of all data in this paper is an adult mouse of 25 g body mass; all other references are transformed to this scale. Comparing relevant data from other species involves a scale factor of approximately 10 from mouse to rat and 2500 to 3000 from mouse to humans. Compartments are envisaged as iron aggregates ("pools") the iron content of which is a systemic variable, expressed in units of µg iron per animal. Fluxes into and out of a compartment are expressed in units of µg iron per animal per day.

The systemic structure of this model is specified by "content" data ("concentration" of iron in its various biochemical forms in the different compartments), and by "turnover" data, usually obtained from tracer studies. Both data sets must be scaled up to the whole organism. The model must have a mathematical structure that reflects statics and dynamics. Its parameters are to be estimated from the empirical data.

An important indicator of the iron status of cells or of the whole body is the iron content in the various biochemical fractions of iron.

The quantitatively dominating biochemical form of iron in the mammalian body are:

- as coordination atom in the heme group (ion haemoglobin, about 600 µg per mouse body;
- in myoglobin, about 100 µg per mouse body;
- minor contents in other cellular hemoproteins
- non-heme iron (iron bound to ferritin, about 300 µg per mouse body;
- other iron-containing proteins (e.g. FeS-cluster), small fraction of heme iron;
- in blood plasma bound to transferrin (about 1.5 µg per mouse body)

The biochemical status of free ionic iron in the cell is not quite clear. One fraction is called Labile Iron Pool (LIP), ([25]) can be extracted by chelating agents, and is said to the crossroads of biosynthetic and biodegrading pathways in the cell. Its concentration is very small in all cells, well below 1 µM, e.g. in liver [26]

LIP can serve as theoretical indicator of the iron state in mathematical models. A better measurable indicator of cellular iron is the amount bound to ferritin, which can be extracted and measured. Here we record both variables, LIP and holoferritin.

2.4.2 Contribution of organs and tissues to whole body mass

An important scale factor is the fractional contribution of each organ or tissue to the mass of the whole body. Table 2.1 provides data for organ weights of C57BLC mice litter mates [27]. We include the estimates of plasma and blood volume of the whole body corrected for the bias of peripheral venous measurement [28].

Table 2.1: The values were taken from [27]. Blood values were scaled to the whole body hematocrit according to [28]. It is being assumed that the organ weights do not considerably change between different dietary regimes in a healthy mouse. * Liver weight per mouse. Data from [27] ** Barbee et al. [29] give 2.3 ml / 25 g mouse * Mass of bone marrow in mouse (body weight 23 g) calculated from Lee et al. [30] p.484) is 192 mg, here scaled up to a mouse body of 25 g.**

Organ weight in g per animal (ca 25 g)		Standard deviation	% of body weight
Liver*	1.22	0.10	4.75
Spleen	0.07	0.01	0.27
Bones	1.80	0.25	7.01
Heart	0.14	0.02	0.55
Kidneys	0.38	0.05	1.48
Lungs	0.13	0.05	0.51
Stomach	0.18	0.04	0.70
Intestine	1.22	0.19	4.75
Duodenum	0.04	0.01	0.16
Integument (fur)	3.97	0.73	15.50
Fat	0.31	0.07	1.21
Muscle	13.42	1.21	52.30
Brain	0.47	0.01	1.83
Testicles	0.24	0.07	0.94
Plasma	1.36	0.03	5.30
Blood cells	0.71	0.02	2.77
Whole blood**	2.07	0.04	8.07
Bone marrow***	0.21	0.03	0.84

2.4.3 Upscaling of iron content to the whole organism

To scale up the specific iron concentration (f, expressed as µg iron per g wet organ) to the total contribution of an organ or tissue compartment we multiplied such data by the total weight w (in g) of the organ(s) per body, i.e. f * w. The standard deviation was calculated from the standard deviations h(f) and s(w) of the factors according to the formula 2.23 on p.7 of [31]:

$$\mathrm{SQR}\left(f^2 * s^2 + w^2 * h^2 + h^2 * s^2\right)$$

which assumes that the measurements of organ mass and iron content are independent random variables.

2.5 Ferrokinetic study of tracer distribution

As pointed out in the introduction it is intended to specify the model to the iron status of the mouse strain C57BL6. There are two basic sources of quantitative information available: biochemical assays of the “iron status” of the animal, and tracer-kinetic measurement of the fluxes between the iron compartments of cells and tissues. The former type of information has been assembled from a detailed study of the published literature on this mouse strain. The latter type of information was derived from experiments done in the laboratory of Professor K. Schümann, TU Munich, complemented again by literature data.

2.5.1 Experimental Setting

The data used for the model have been derived from ferrokinetic data [27]. In brief, male young adult mice (C57BL6 strain; 18-20 g) underwent a 5-week period (growth up to 25 g) with a diet controlled for iron content (iron content of diet induction of deficiency: 6 mg/kg; for adequate supply: 180 mg/kg; for iron overload 25000 mg/kg). The experiment was started by intravenous administration of ionic radioactive tracer (Fe^{59} nitrate in complex with nitrolotriacetic acid). It is known that this equilibrates quickly with the transferrin-bound iron pool [32]. The single tracer dose contained about 0.285 µg per mouse, which is less than 2% of plasma iron and in the range of 0.01% of body iron. At certain intervals between 12 hours and 28 days animals (n = between 3 and 7) were sacrificed, blood was collected and their main organs were dissected, weighed, and their iron status (non-heme iron) was measured. Hematocrit and haemoglobin content of blood were measured, and aliquots were separated into plasma and red blood cell compartment. The weight of organs and tissue samples was measured and normalized to the whole body (25 g). The ambient Fe^{59} content of organs and blood compartments was measured by scintillation counting and also converted to a whole body value. The tissue contents of tracer were corrected by subtraction of the tracer in the residual blood, by a calculation scheme that was derived from parallel model experiments with Fe^{59}-labeled erythrocytes as indicator [27].
All tracer data were corrected for the decay of radioactivity during the experiment by normalizing them with the help of the radioactivity of the injection solution measured at the same time.
Data concerning the total iron clearance rate were obtained from Trinder et al. [33], as they were obtained on control mice of the same strain under very similar dietary regimes.

2.5.2 Raw data corrected for blood content

The raw data obtained from the experiments are given in (see Appendix A tables 1, 2 and 3). In iron-deficient mice the tracer content of the spleen dropped to zero after a short time and even reached apparent negative values. This is clearly an overcorrection for blood-related Fe^{59}, as the spleen contains a large extravascular blood pool that cannot be removed completely by perfusion. The true tracer content of the splenic tissue was obviously close to zero at those time points (see Appendix A, table 1). Therefore, we set these small negative values equal to zero. This manipulation did not appreciably change the fractional clearance parameter of the iron-deficient spleen.

2.5.3 Averaged tracer content in the intestine

As the precise organ weights of intestinal subsections, such as ileum/coecum/colon were not established, we replaced the tracer concentrations in Appendix tables 1, 2 and 3 by a mean ascribed to the intestine as a whole. The standard deviation of this derived quantity was calculated according to the SQR-forluma sketched above.

2.5.4 Normalization of the data set

It is technically difficult to inject exactly the same small fluid dose of radioactive iron-solution. Therefore, the Fe^{59} content of an organ at a given time point was expressed as the Fe^{59} concentration normalized according to the formula:

Sum of radioactivity in the body at time t = 100% * exp h ,

were t is expressed in days.
This describes the long-term rate of iron loss from the murine body [23, 24]. [34] give a somewhat lower rate of ~ 0.004 per day. The process of normalization smoothed the ups and downs of determined tracer contents. It indicates a loss of about 13% of the injected tracer over an experimental period of one month, which is in accordance with previous estimates (10-15%) [35].

2.5.5 Mathematical structure of the compartment model of tracer distribution

The generic structure of the model is a set of balance equations describing time course and steady-state of the iron content of kinetically relevant pools:

$$\frac{dC_i}{dt} = \sum_j v_{ij} - \sum_j v_{ji} + v_{io} - v_{oi} \qquad (1)$$

where

C_i (≥ 0) - “pool size”: iron content of the i-th compartment, i = 1…n (number of pools) - chosen scale is µg per body
v_{ij} (≥ 0) - rate of iron (in-) flux from compartment j to i (j = 1…n; j ≠ i) (µg per body per day)
v_{ji} (≥ 0) - rate of iron (out-)flux from compartment i to j (µg per body per day)
v_{io} (≥ 0) - rate of iron flux from outside the system into compartment i (µg per body per day); only influx into duodenum of “cold” iron has a value > 0
v_{oi} (≥ 0) - rate of iron flux from compartment i out of the system (µg per body per day; values > 0 only for intestine, stomach, integument).

2.5.6 Clearance mode of model description and derivation of motion equations.

Each of the rates is a function of the status of some of the pool sizes and of kinetic parameters. One may introduce fractional clearance coefficients (letter k) by the following definitions:

$$k_{ij} \equiv \frac{v_{ij}}{C_j} \qquad (2)$$

$$k_{oi} \equiv \frac{v_{oi}}{C_i}$$

These coefficients describe the ambient tendency of a given flux to clear the pertinent source pool. They apply also to the dynamics of the tracer content. If fluxes and pool sizes do not change substantially during the experiment (steady-state of the bulk of “cold” iron

fluxes and pools during the experiment by the tiny amount of tracer), the k´s become constant and a system of ordinary linear differential equations with constant coefficients describes the motion of the tracer content (x – being measured as specific radioactivity, i.e. counts per mass of compartment iron, normalized to initial tracer dose):

$$\frac{dx_i}{dt} = \sum_j k_{ij} * x_j - \sum_j k_{ji} * x_i - k_{oi} * x_i \quad (i = 1\ldots n) \qquad (3)$$

where a term $k_{io} * x_o$ has been dropped because re-absorption of excreted radioactivity can be neglected, if the tracer has been applied to the plasma compartment. The k-values for non-existing fluxes (out of the system or non-reversible) are set to zero. The system of differential equations describing the tracer motion is found in the next sections.

2.5.7 Residence time

Time scale is an important aspect of any metabolic model [102]. Interpretation of systems dynamics is simplified by introduction of expected residence times of molecules of defined biochemical state within a compartment:

$$\Theta_i \equiv \frac{1}{(\sum_j k_{ji} + k_{oi})} \qquad (j=1\ldots n;\ j \neq i) \qquad (4)$$

2.6 System of Ordinary Differential Equations for Tracer Motion

We established a mathematical description of the tracer content and the inter--compartmental tracer flow using linear ordinary differential equations. This choice is justified as it can be assumed that pools and fluxes are approximately constant during the experiment. Under these conditions are the linear coefficients of tracer clearance constant quantities. The system of equations is shown below. For designations, refer to Figure 2.1. Parameter names in the computer program were assigned according to the convention k_{a_b}, meaning clearance parameter of flux from a into b:

d(Plasma) / dt = Plasma(t) * (-1kp_bon - 2kp_kid - 3kp_int - 4kp_liv - 5kp_sto -6kp_intg
-7kp_fat - 8kp_mus - 9kp_lun -10kp_duo - 11kp_brain - 12kp_hea
- 13kp_tes)
+14kkid_p * Kidneys(t) + 15kliv_p * Liver(t) + 16ksto_out * Stomach(t)
+ 17kfat_p * Fat(t) + 18kmus_p * Muscle(t) + 19klun_p * Lungs(t)
+ 20kbra_p * Brain(t) + 21khea_p * Heart(t) + 22ktes_p * Testes(t)
+ 23kspl_p * Spleen(t)

d(Bone Marrow) / dt = 1kp_bon * Plasma(t) -Bone Marrow(t) * (27kbon_rbc + 28kbon_spl)

d(Liver) / dt = 4kp_liv * Plasma(t) - 15kliv_p * Liver(t)

d(Spleen) / dt = - 23kspl_p * Spleen(t) + 29krbc_spl * RBC(t) + 28kbon_spl * Bone Marrow(t)

d(Heart) / dt = 12kp_hea * Plasma(t) - 21khea_p * Heart(t)

d(Testes) / dt = 13kp_tes * Plasma(t) - 22ktes_p * Testes(t)

d(Lungs) / dt = 9kp_lun * Plasma(t) - 19klun_p * Lungs(t)

d(Kidneys) / dt = 2kp_kid * Plasma(t) - 14kkid_p * Kidneys(t)

d(Muscle) / dt = 8kp_mus * Plasma(t) - 18kmus_p * Muscle(t)

d(Fat) / dt = 7kp_fat * Plasma(t) - 17kfat_p * Fat(t)

d(Integument) / dt = 5kp_intg * Plasma(t) - 24intg_out * Integument(t)

d(Duodenum) / dt = 10kp_duo * Plasma(t) - 26kduo_p * Duodenum(t)

d(Stomach) / dt = 5kp_sto * Plasma(t) - 16ksto_out * Stomach(t)

d(RBC) / dt = 27kbon_rbc * Bones(t) -29krbc_spl * RBC(t)

d(Intestine) / dt = 3kp_int * Plasma(t) - 25int_out * Intestine(t)

d(Brain) / dt = 11kp_brain * Plasma(t) - 20kbra_p * Brain(t)

d(Outside) / dt = 25int_out * Intestine(t) + 26kduo_p * Duodenum(t)

+ 24intg_out * Integument(t)

At time = 0 the injection of a tracer dose (scaled to 100%) into plasma sets the boundary condition of this system (plasma (0) = 100% all other compartments = 0%). This sets a relaxation into motion that follows the fluxes of the bulk iron through the body.

2.7 Parameter optimization pipeline

With a system of linear ordinary differential equations representing the major ferrokinetic processes, the next step was to find reasonable parameters values that correctly described the physiological exchange of iron in the body. For this purpose we created an optimization pipeline (Figure 2.2).

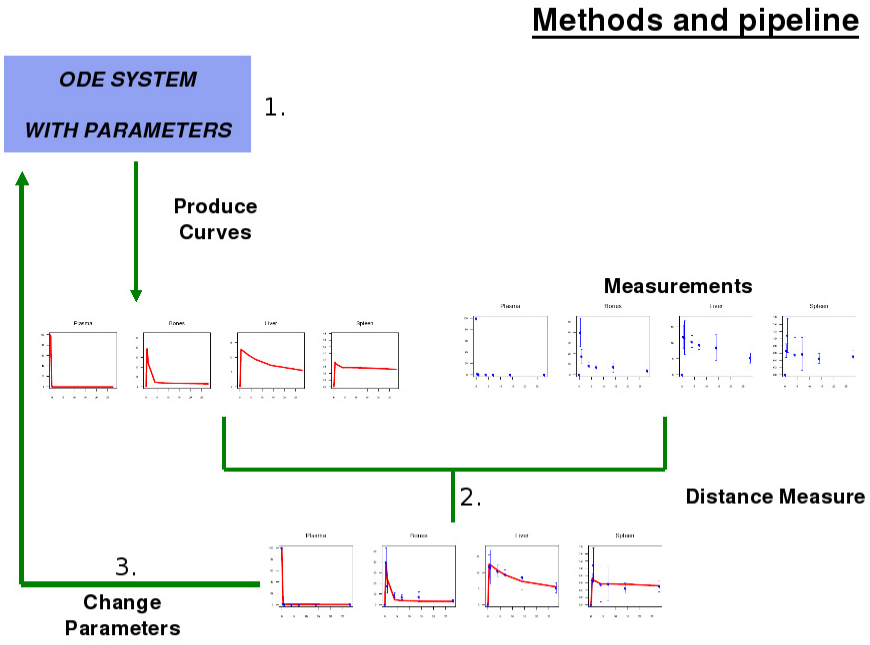

Figure 2.2: Optimization pipeline developed in this study. Starting with differential equations with arbitrarily chosen parameters the system is run and its results continuously compared to measurements. The difference between them is used by the optimization algorithm to improve the selection of parameters values for further runs.

The first step was to create a system of linear ordinary differential equations and define reasonable initial parameter values, which were mainly derived from literature extracts.

With this system of equations we produced simulated curves for each organ of our model (step number 1 in figure 2.2). We used an ODE solver from Matlab for stiff systems, since our system comprises different time scales, varying from minutes to days.

We then compared the generated curves with real ferrokinetic measurements used as input for our model (step 2 in figure 2.2). Three different distance measures were tried: simple squared distance, squared distance divided by the standard deviation and squared distance divided by variance. Our experiments demonstrated that in our model the choice of one distance measure did not produce strong differences in parameter estimates, so we chose the second, defined by the equation :

$$D = \sum_{j=1}^{16} \sum_{i=1}^{7} \frac{(e_{ij} - m_{ij})_2}{std} \qquad (5)$$

where e_{ij} is the estimated value produced by our model, and m_{ij} is the measured value obtained from radioiron injection and std stands for the standard deviation of the measured point m_{ij} . The index i runs from 1 to7 and corresponds to the 7 points of measurements in our experiments. The index j runs from 0-16 and corresponds to each organ of our system and experimental settings.

We then estimated the parameters of the equation system in order to minimize the distance between the model curves and the measurements (step 3 in figure 2.2).

The solution was to use a constraint optimization algorithm named Active-Set. This is a hill-climbing algorithm which receives as input: the initial parameter values and the system constraints. In our case only one constraint was defined, the sum of the parameters leaving

the central compartment (Plasma) to the peripheral organs should be 20. This is based on the principle that the iron clearance time is below 1 hour in mice [33].

2.7.1 Parameter Estimation by Convergence from different Starting Points

The parameter optimization step was performed using as input the datasets with measurements of organ radioactivity under different diets. It was checked that the algorithm always converged to a parameter set giving an equal value of the distance minimum. In order to test the statistical uncertainty of these parameter estimates we randomly perturbed the measured compartment radioactivities within the measured standard deviations around their mean values. This change was performed for every measurement in the three datasets and the optimization pipeline of figure 2.2 executed. This complete procedure was repeated 100 times for each dataset.

2.7.2 Quality of final fit

As an intuitive measure of the quality of the final fit we chose the root of mean of squared weighted deviation between prediction and the mean of measurements (table 3.2; “sq root of mean weighted squared dev”). We document the parameter set of the best fit together with an upper and lower bound obtained from a sextile-truncated sample of the empirically found parameter variation. In the case of a Gaussian distribution the interval thus defined would be twice the standard deviation.

2.7.3 The problem of interdependence of parameter estimates

Some parameters or sets of parameters are not identifiable by measurement in a model of given design. For instance, if ferrokinetic measurements are available only for the time course of changes in plasma concentration of tracer, the total clearance rate can be adequately assessed, but not the distribution into the network of body compartments. In contrast, if the first measurement was obtained after most of the tracer has left the plasma compartment, the relative distribution to the various organs can be assessed, but the flux dynamics of this distribution cannot. Even if parameters seem to be identifiable in the Laplace domain [36], the error structure of the data will make the ensuing algebraic treatment ill-conditioned and will expand the range of parameter estimates. They become meaningless. We tackled this problem by studying the parameter space using the alternating conditional expectation algorithm (ACE) [37, 38].
The essence of this strategy is to explore the total domain with all parameter values that support an acceptable fit, i.e. the criterion value of this fit is sufficiently close to the optimum. This is done by running a large number of parameter estimations from a large range of starting points. The result is a set of sometimes widely differing parameter vectors that yield very similar optimal values of the fit criterion. Interdependent and hence non-identifiable parameter combinations can be addressed by the information furnished by the ACE method. On the basis of this analysis one or more suitable parameters are chosen to be fixed or held in definite proportion to each other so that the other parameters became identifiable. The choice of suitable parameters for this reduction of parameter redundancy and of their fixed values is not always easy and requires a theoretical understanding of the dynamic structure of the model. Maiwald et al. [39] have developed software (“Potter´s wheel”) the tools of which support this computer-time-intensive study very effectively. Specific assumptions made to remove strong parameter intercorrelation will be mentioned explicitly below.

2.8 Flux rates and pools sizes derived from clearance parameters

2.8.1 Calculation of absolute flux rates from fractional clearances

The tracer data alone can be used to estimate fractional clearance parameters (per day) of flux out of plasma (k_{i_plasma}). To calculate flux rates (µg per day per mouse) one needs the iron content of plasma plus extracellular fluid ($C_{plasma/ECF}$):

$$v_{i\_plasma} = k_{i\_plasma} * C_{plasma/ECF} \qquad (6)$$

The iron pool of the plasma plus ECF is calculable from the iron concentration and the plasma volume plus the accessible volume of ECF.

2.8.2 Estimation of peripheral pool size from countercurrent clearance parameters and plasma pool

The iron content of body organs can be measured by chemical methods, mainly as hemoglobin, myoglobin, and non-heme iron. Cellular heme iron content as oxidoreductases and other proteins is less important quantitatively. Such direct measurements may be contrasted with tracer-accessible iron pool sizes. When in the steady-state influx and outflux are equal, the following equation relates the pool size C_i of a peripheral compartment to that of plasma

$$k_{i\_plasma} * C_{plasma/ECF} = k_{plasma\_i} * C_i \qquad (7)$$

If the data support estimates of the two rate constants (k_{i_plasma} defining the early phase and k_{plasma_i} characterizing the late phase of tracer distribution) and of the plasma/ECF iron content, then the size of the “accessible” pool C_i may be inferred.

2.8.3 Scaling of the system variables and parameters

All parameters and variables were scaled to be dimensionless. On rescaling to the in-vivo state variables and fluxes were transformed to units of µg per mouse (24 g) and µg per day per mouse, respectively. Turnover times and the inverse of related kinetic constants are expressed in days.

2.9 The Cellular Model of Iron Metabolism

So far we obtained a description of the physiological distribution of iron in mice. It aims at estimation of the cellular iron pools and iron fluxes between organs in the steady-state of the whole organism. In this section the layout a kinetic description of the iron turnover within and between cell types of the organism will be developed with the goal of predicting the steady-state of the whole organism of the mouse as a result of kinetic interaction of iron species in different cell types. The model will also comprise the most important regulatory mechanisms of iron metabolism. It will be based on quantitative literature data concerning the fine-tuning of iron metabolism. For obvious reasons it is not feasible to formulate such a model on the most elementary molecular and cell-biological level. This is because most types of kinetic measurements cannot be done on the intact tissue or cell in its natural environment. The reductive approach of experimental cell biology therefore provides in many cases qualitative data (molecular “mechanisms”), but no quantitative description. It will however be feasible, on the basis of existing physiological data and the established network structure of iron metabolism to derive a description of the core regulatory structure of the system.

The mechanistic skeleton of iron metabolism is very much the same in each cell type, because the genes and their products are the same. We therefore derive a generic model of iron metabolism within the cell. The specificity of tissue and cell types will be introduced in addition by modifying parameters of the regulatory structure of this generic model. Such core parameters are the iron status and the expression level of iron-related mRNA and/or protein of a specialized cell type.

2.9.1 Transfer across the cell membrane

- **Transferrin-mediated iron uptake:** Most part of iron is taken up by the cells through transferrin-receptor-1 mediated endocytosis [40]. The transferrin molecule, when it carries two iron atoms (apotransferrin) binds to the surface receptor and after conformational changes the complex is internalized. The iron molecules are released into the cell and the unloaded complex returns to the cell surface. To determine the kinetic constants involved in this process a pioneer study was conducted by Ciechanover [41]. Using HepG2 cells they determined the amount of surface receptors and the rate at which each step of the transferrin internalization cycle happens. We used those values to derive parameter values for the pertinent kinetic equations of this thesis
- **Non-Transferrin-mediated iron uptake:** In addition to the iron that enters the cell through the transferrin-transferrin receptor cycle, there is a certain amount of this metabolite that is taken up by the cells through other mechanisms. The duodenum absorbs iron from the diet by reduction from ferric to ferrous ion (calculated by the cytochrome b-like ferrireductase (Dyctb) and ensuing uptake by the divalent metal transporter 1 (DMT1). This surface receptor is expressed mainly in the brush border membrane of duodenal cells and is also responsible for the absorption of other metals. In addition, hepatocytes are able to take up iron molecules from blood that is not bound to transferrin.

2.9.2 Intracellular processes

- **Ferritin as Storage Compartment:** Once inside the cells, it is believed that iron molecules appear in the so-called Labile Iron Pool (LIP). The exact physicochemical status of this pool is not known except but it can be extracted and quantified by chelating agents [25] The amount of iron present as LIP is much smaller than that bound to ferritin. This protein is able to store up to 4500 iron atoms in one molecule. There exist two isoforms of this protein (Light and Heavy chains), of different expression in different cells and with different storing capacities. In our simplified model we do not make a kinetic distinction between them and combine them to one storage pool.

- **Biosynthesis of cellular proteins:** incorporating iron in prosthetic groups. These proteins are being synthesized in each growing cell and undergo turnover with specific time course in each cell. Two basically different subgroups of proteins may be distinguished.

- **Synthesis of Fe-S cluster**: The Fe-S cluster is present in more than a hundred different proteins and it plays an important role in different processes inside the cell.

- **Heme Synthesis:** The heme group in hemoglobin, myoglobin and a number of further proteins contains ferrous iron as catalysator. We include the hemoglobin pool in the erythropoetic system (in bone marrow and in red blood cells), the myoglobin pool mainly in red in muscle and a further unspecified combined pool of heme compounds in every other cell of the organism.

- **Iron Export from the Cell:** The only known exporter of ionic iron out of the cell is the ferroportin molecule. The expression level of ferroportin is regulated by the hormone hepcidin which is produced in the liver and then transported in the blood plasma to the sites of its regulatory effect. The molecular mechanism of its effect is exerted by binding to ferroportin thereby triggering its intracellular degradation. Ferroportin is expressed at high level in duodenum, liver and macrophages, but to a lesser extent also in most or all other cell types [18].

- **IRP Regulation:** Iron Regulatory Proteins have a dual role in the cell: either binding to the 3’ end of mRNA molecules and thus stabilizing them against degradation or binding to the 5’ region of the mRNA and consequently inhibiting translation. Whether one or the other function happens depends on the iron level in the cell (LIP level) and on the presence of iron responsive elements (IRE) in either the 3’ or the 5’ ends of the mRNA molecules [40]. In our model the two different IRP proteins are represented as different pools. They protect the mRNA of transferrin receptor 1 and DMT1 against degradation and inhibit the translation of the apoferritin, ferroportin mRNA and the translation of other biosynthetic pathways (into Fe-S-Cluster and heme synthesis). We take both basic types, IRP1 and IRP2, into account and formulate a combined formula for the effect of both together.

2.10 Iron flux network

2.10.1 Intracellular and transmembrane iron flux

The fig. 2.3 depicts how the different elements of intracellular iron metabolism interact with each other. The figure refers to a generic cell, i.e. to a cell that contains the main elements present in every body cell. Some special features of cell types that have a special role in iron metabolism are also sketched.

The upper part of the picture shows the transferrin cycle (fluxes *v1*, *v2*, v3 and *v4*) as

present in almost every cell. Depicted on the the left side is the iron uptake by DMT1 (*v5*) which is expressed in duodenal cells, as well as non-transferrin-mediated iron uptake (*v7*) which happens mainly in hepatocytes.
Iron taken up by the mechanisms modelled as *v1*, *v5* and *v7* is further transferred into the Labile Iron Pool (LIP) (fluxes *v3*, *v6* and *v7*).
LIP iron molecules undergo four possible fates: stored in ferritin (*w1*), deployed in heme synthesis (*w9*), biosynthesis of Fe-S cluster (*w3*), and export by ferroportin transferred onto holotransferrin (*w5* and *w6*). Stored iron may be mobilized (flux *w2*). Also iron bound in Fe-S clusters are re-utilized during the general protein turnover occurring with different time course in all cells that do not undergo cell loss. Heme iron may only be reutilized (*w12*) if the cell expresses the corresponding catabolic pathways (e.g. RES macrophages). Iron taken up into the erythropoetic pathway in bone marrow is converted to hemoglobin and added to the red blood cell compartment (*w10*). Red blood cells become senescent after a certain functional lifetime and the heme is transferred to macrophages of RES. There exists also a direct shuttle from bone marrow to RES [22] which has been explained as “ineffective erythropoesis”.
At last, on the right side of the picture, is a leakage term which is used to represent the iron loss of the system due cell death and removal, mainly of intestinal epithelium and skin and other integument cells. Since labile iron pool is present only in tracer amounts, this leakage will visibly affect only the holoferritin level, which is in equilibrium with LIP.

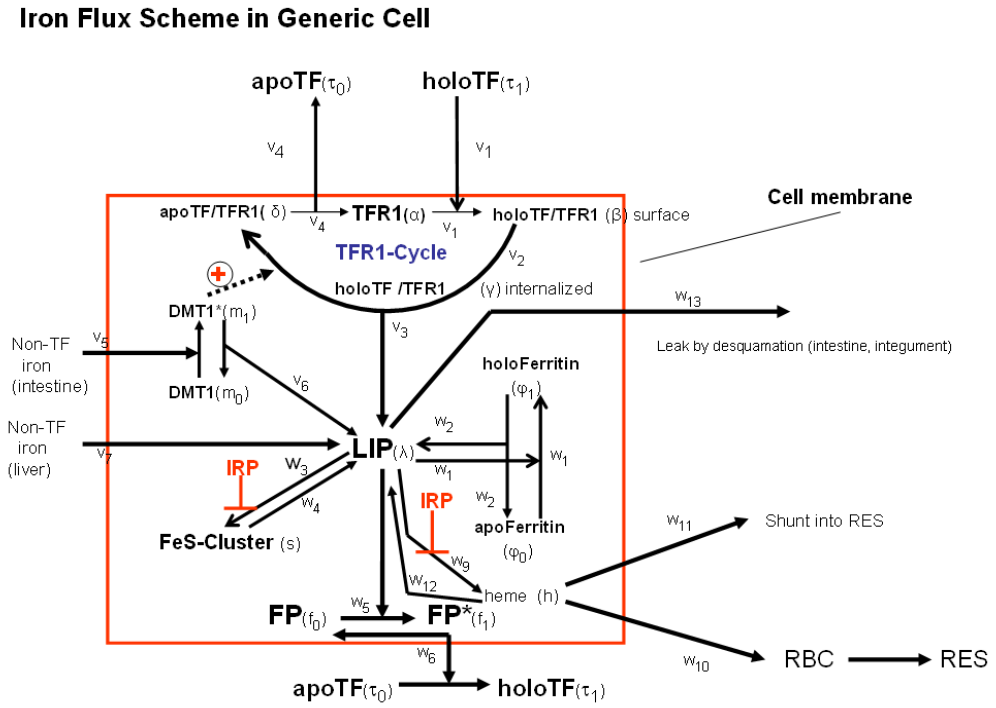

Figure 2.3: The figure shows the general cellular model shared by all organs in the model. What distinguished the cell-types are the parameter values defined for the equations. There are three pathways of iron input in the cell: TfR1 cycle, dietary uptake through DMT1 and non-TF bound iron. Inside the cell iron has some possible fates: be stored within ferritin, be exported to blood plasma by FPN1, participate in heme synthesis, be part of Fe-S clusters or in the case of bone marrow, be transferred directly to RES, due ineffective erythropoiesis.

2.11 Regulated turnover of iron-processing macromolecules

The macromolecules taking part in the regulatory scenario of this cellular model undergo continuous biosynthesis and degradation. This involves gene transcription into mRNA, translation of mRNA into protein and, after a certain characteristic life time within the cell, the degradation of mRNA catalyzed by RNAse and of proteins by the protein-degrading

machinery of the cell. We simplify the enormous complexity of these processes by formulating for each protein an overall rate of biosynthesis and a rate of degradation. The latter is assumed to be proportional to the ambient cellular expression level. Both processes are influenced by kinetic signals of specific regulatory factors. The different levels of regulation (e.g. transcription regulation by a signal cascade involving plasma iron and hepcidin, or translation of mRNA into protein regulated by the IRP machinery) are integrated into these two overall rates. Figs. 2.4a and 2.4b illustrate how the aggregation of the mRNA and protein level together with a qualitatively equivalent transformation of the regulatory levels was modelled.

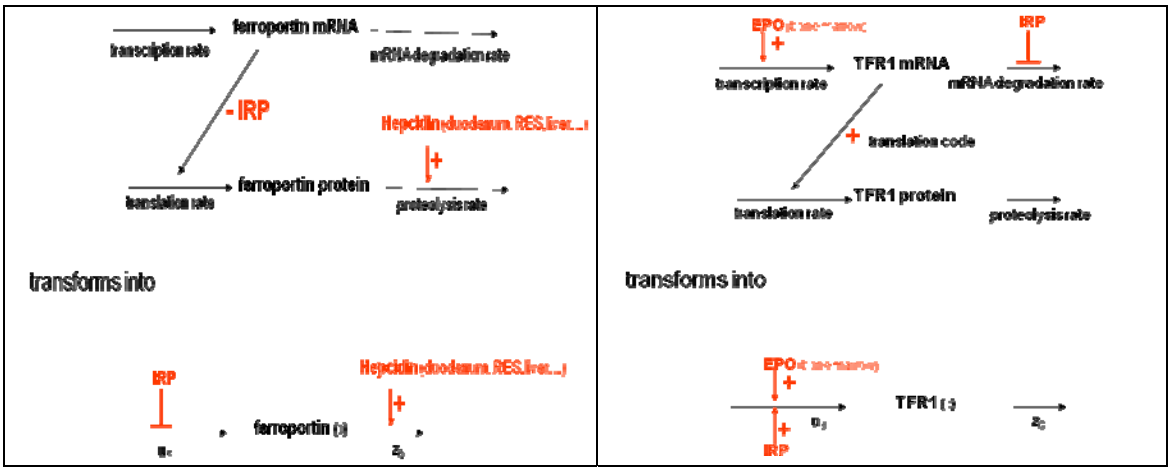

Fig. 2.4: a) EPO increases transcription of TFR1-mRNA in bone marrow; IRP stabilizes mRNA and thereby indirectly increases TFR1 expression level. b) Hepcidin increases degradation of ferroportin protein; IRP inhibits translation of ferroportin mRNA, so indirectly decreasing ferroportin expression level

Figure 2.5 shows the cellular processes of steady macromolecular synthesis and steady decay that were implemented in this model. The “u” arrow stands for the integrated rate of translation and translation of a certain protein, whereas “z” represents the rate of degradation of a given protein.

Included in this schematic picture is the IRP regulation. In the case of TfR1 and DMT1 the IRP proteins inhibit m-RNA degradation and hence enhance protein synthesis indirectly by the increased level of the mRNA.

In the case of ferroportin, apoferritin and other cellular iron proteins the IRP system inhibits the translation of mRNA, thereby reducing the rate of synthesis of the respective protein in the cell. The Labile Iron Pool (LIP) plays a significant regulatory role as intracellular signal of the iron status. The exact nature of the iron signal is not known, but there is evidence that the LIP is correlated with it. The key regulator IRP1 protein has two states: active and inactive. The LIP has a stimulatory effect in the transition of the IRP1 protein from active to inactive state. When there is plenty of iron in the cell the synthesized Fe-S clusters bind to the IRP1 protein and convert it to a cytosolic aconitase which is not able to exert its role as an iron regulatory protein (reviewed in [40]).
In the case of the second regulator IRP2 it is not a conversion between states that is regulated but rather the degradation rate of this protein in the cell. Therefore in our model LIP has a positive effect on the degradation of IRP2.
One important aspect of our model concerns the descriptive combination of the IRP1 and IRP2 proteins in order to formulate an indicator variable “IRP effective”. The “division of labor” between these two closely related versions of intracellular iron regulation is not completely clear. We represent the two proteins here as a “pool” of IRP and posit a combined effect of the IRP´s, represented by a simple formula:

$IRP = IRP1_{act} / IRP1_{reference} + IRP2 / IRP2_{reference}$

where $IRP1_{act}$ stands for the active part of the expression level of IRP1, and IRP2 stands for the total expression level of the protein. The reference parameters allow for different activities of the two versions, the empirical basis of which is the fact that knockouts of IRP1 in mice are lethal and those of IRP2 are not lethal, but lead instead to an iron storage disorder [42]. The transition for active IRP1 into its inactive aconitase form is taken into consideration as rapid equilibrium, whose position is influenced by the level of the labile cellular iron pool (as well as by other physiological parameters like oxygen level, H_2O_2 and NO levels). [43, 44].

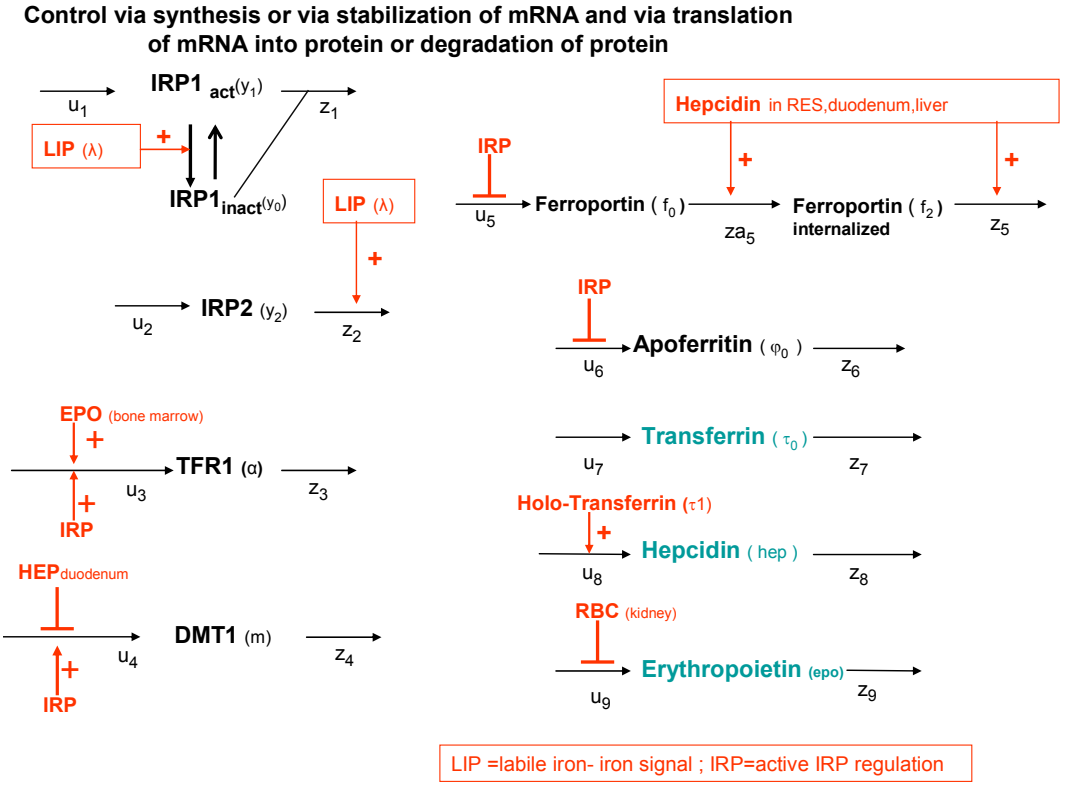

Fig. 2.5: This is a simplified scheme of the turnover of the iron-processing proteins in the generic cell. The transcription/translation process is represented in aggregated form by arrows and fluxes dubbed u (with index) and the decay process by arrows and rate variables z. The latter refer either to proteases or RNAses that remove the respective iron-processing proteins or their mRNA precursors. The lower-case letters at the macromolecules refer to the variable names of the differential equation system.

Some processes are subject to global regulation by hepcidin. Hepcidin expression is regulated by the iron saturation level of plasma transferrin (symbolized as a direct stimulation of hepcidin synthesis). Hepcidin enhances the degradation of ferroportin predominantly in RES and duodenum, also in liver. It leads to a rapid internalization of membrane-resident ferroportin (f_0 into f_2) with slower proteolytic degradation afterwards.

EPO has a positive stimulatory effect on the synthesis of TfR1 in bone marrow. The synthesis of EPO is negatively regulated by the levels of RBC: when the RBC level is high, there is no need for EPO, when RBC level diminishes, more EPO is synthesized to stimulate erythropoiesis.

All these processes tend towards a steady state (u = z) which is reached after a characteristic time set by the ratio of ambient protein level / cellular degradation rate.

2.12 Nomenclature: variables and rates

Table 2.1 summarizes the molecular elements and table 2.2 describes the fluxes in the model. Every organ has the same basic set of fluxes and the same set of differential equations; what distinguish them are the kinetic parameter values relating to the expression level and its regulation. There is only one transferrin synthesis and degradation term for the whole system (table 2.3), because the carrier protein transferrin is mainly synthesized in the liver and not in other cells.

Table 2.1: Species shared by all cell-types in the model. The exceptions are Hepcidin, EPO, RBC and transferrin (τ_0, τ_1), which are defined once for the whole system.

Symbol	Description
α	TFR1 on cell membrane surface
β	TFR1 / holoTF complex on cell membrane surface
γ	TFR1 / holoTF complex internalized
δ	TFR1 / apoTF complex in membrane
τ_0	apo TF in plasma
τ_1	holo TF in plasma
λ	LIP (labile intracellular iron pool)
φ_0	apoferritin
φ_1	holoferritin (with iron)
s	FeS cluster
f_0	free ferroportin exporter in cell membrane
f_1	iron-loaded ferroportin exporter in cell membrane
f_2	ferroportin in inactive form
h	heme level in cell
m_0	DMT1 as duodenal entry of iron, and as activator of holoTF/TFR1-processing in the lysosomes
m_1	iron-binding state of DMT1
y_0, y_1	IRP1 level, in active and inactive form
y_2	IRP2 level
EPO	Erythropoietin
Hep	Hepcidin level
RBC	Circulating red blood cells, iron content

Table 2.2: Model fluxes. This are the essential operations which involve transfer of ionic iron between different model parts, e.g. from outside the cell to inside or from LIP to apotransferrin. They are depicted in figure 2.3.

Flux	Description
y_{eff}	effective activity of IRP system
w_1	uploading LIP iron on apoferritin
w_2	mobilization of ferritin iron into LIP
w_3	synthesis of FeS cluster
w_4	decay of FeS cluster protein, liberation of iron into LIP
w_5	uploading LIP iron onto ferroportin
w_6	export of iron onto apotransferrin (via FP)
w_9	heme synthesis
w_{10}	heme degradation
w_{11}	flow of iron between the bone marrow and RES (ineffective erythropoiesis
w_{12}	Return of iron from heme to LIP (catabolism)
w_{13}	iron loss due epithelial cell desquamation (skin / intestine)
v_1	binding of holoTF (plasma) onto TFR1 (membrane)
v_2	internalization of TFR1 / holoTF complex
v_3	release of iron into LIP from TFR1
v_4	return of apoTF into plasma & TFR1 onto membrane surface
v_5	TFR1-independent inflow of iron into certain cells
v_7	Non-transferrin or DMT1-mediated iron uptake

Table 2.3 summarizes the turnover rates of macromolecules (synthesis and degradation). It should be noted that the elements in this table also contain the index "i" which refers to the different cell types (tissue types).

Symbol	Description
u_{i1}	translation of IRP1-mRNA
u_{i2}	translation of IRP2 –mRNA
u_{i3}	translation of TFR1 –mRNA
u_{i4}	translation of DMT1-lyso – mRNA
u_{i5}	translation of ferroportin mRNA
u_{i6}	translation of apoferritin-mRNA (in liver)
u_{i7}	synthesis of apo-transferrin
z_{i1}	Decay of IRP1-mRNA
z_{i2}	Decay of IRP2 –mRNA
z_{i3}	Decay of TFR1 –mRNA
z_{i4}	Decay of DMT1– mRNA
z_{i5}	Decay of ferroportin mRNA
z_{i6}	Decay of apoferritin-mRNA
zi_7	Decay of plasma transferrin

2.13 Balance equations

We derive the kinetics of iron interaction within and between cell types of the body according to the following general concept:

- stoichiometric structure of the main reactions in the form of balance equations describing the iron transfer between biochemically defined entities
- aggregation of quantitatively minor biochemical reactions of the same type (e.g. cellular heme protein)
- bilinear kinetics of iron binding to iron carrier proteins and translocators
- signalling superstructure by effector terms in rate equations
- formulation of dynamics in terms of ordinary differential equation systems

These is a kinetic "hybrid" model (in the spirit and wording of [45]). For practicability purposes we combine simplified rate laws as basis of the model and insert special terms for signalling effects.

2.13.1 Balance equations in the plasma compartment

In the central compartment the transferrin-bound iron and the hormones hepcidin and erythropoietin are dispatched to their effector locus.

$d\tau_0/dt = u_7 - z_7 + \Sigma_i (v_{i4} - w_{i6})$ apo-transferrin
$d\tau_1/dt = v_0 + \Sigma_i (w_{i6} - v_{i1})$ holo-transferrin

The indexed fluxes have the following meaning:
v_{i1} - entry of holo-transferrin into the endocytotic cycle
v_{i4} – release of apo-transferrin after endocytotic deloading of iron
w_{i6} - transfer of cellular iron onto apo-transferrin (ferroportin-mediated)

The index i applies to the cell/tissue types:
i=1: bone marrow,
i=2: liver
i=3: RES
i=4: muscle
i=5: integument
i=6: intestine
i=7: duodenum

and the sum Σ is defined for the w_6 and v_1 of the respective cell type or tissue.

$dHEP / dt = u_8 - z_8$ hepcidin
$dEPO / dt = u_9 - z_9$ erythropoetin

Balance equations in the blood cell compartment

$dRBC / dt = w_{10} - w_{RBC}$

2.13.2 Balance equations in the cell, with cell type parameter specification

Fig. 2.2 symbolizes the events within the generic cell and its borders. We now write down the balance equations pertinent to this scheme. The individual rate equations for special cell types will be derived below, but we indicate in bracket if a flux applies only to certain cell types (i.e. has a non-zero value only for the cell types indicated in bracket). The designations are defined in tables 2.1-2.3 (apo- and holo- applies to free and iron-loaded entities, respectively).

$d\varphi_0 / dt$	=	$w_2 - w_1 + u_6 - z_6$	apo-ferritin
$d\varphi_1 / dt$	=	$w_1 - w_2$	holo-ferritin
df_0 / dt	=	$u_5 - za_5 - w_5 + w_6$	apo-ferroportin
df_1 / dt	=	$w_5 - w_6$	holo-ferroportin
df_2 / dt	=	$za_5 - z_5$	ferroportin for degradation (phosphorylated)
dm_0 / dt	=	$u_4 - z_4 + v_6 - v_5$	apo-DMT1
dm_1 / dt	=	$v_5 - v_6$	holo-DMT1
$d\alpha / dt$	=	$u_3 - z_3 + v_4 - v_1$	TFR1 in membrane
$d\beta / dt$	=	$v_1 - v_2$	holo-TF-TFR1 in membrane
$d\gamma / dt$	=	$v_2 - v_3$	holo-TF/TFR1 internalized
$d\delta / dt$	=	$v_3 - v_4$	apo-TF/TFR1 in membrane
dy_1 / dt	=	$u_1 - z_1$	IRP1
dy_2 / dt	=	$u_2 - z_2$	IRP2
ds / dt	=	$w_3 - w_4$	
dh / dt	=	$w_9 - w_{10}$ (bone marrow) $- w_{12} - w_{11}$	

The expression for cellular free iron (LIP) reads

$$d\lambda / dt = v_3 - w_1 + w_2 - w_3 + w_4 - w_5 + v_6 \text{ (duodenum only)} + v_7 \text{ (liver only)} - w_9 \text{ (bone marrow \& muscle)} - w_{11} \text{ (bone marrow)} + w_{12} \text{ (muscle only)} - w_{13} \text{ (integument \& intestine)} + (w_{shunt} + w_{RBC}) \text{ (RES only)}$$

2.14 Rate equations of iron transfer between iron-processing proteins

Kinetic theory of biochemical catalysis in aqueous dilution is not applicable to iron metabolism. Iron occurs in coordinated states bound to carrier protein or in complex as component of prosthetic groups (e.g. heme). The kinetic description was therefore chosen in terms of on- and off- rate constants times the cellular content (“concentration”) of respective reactants of a transfer or binding reaction. For the transferrin-receptor-mediated endocytosis a kinetic theory was obtained from data on isolated cells [41]. We assume that the time characteristics of intra-cellular iron transfer is of the same range for all metabolically active cells. Variables are scaled to dimensionless quantities, setting them equal to unity in what we call the reference state of the organism (adult male mouse, 25 g, on adequate iron diet).

Tissue contents of ferritin (“non-heme iron”) were available from the literature and from measurements of Schümann et al. [27], as were flux rates between tissue compartments after analysis of ferrokinetic data. These quantitative data can be converted to tissue-specific kinetic rate parameters. We applied power-rate laws in some cases, when the subsystems of iron transfer or endocrine signalling to cells have a high logarithmic gain in vivo (i.e. small relative concentration changes lead to high relative effects).

2.15 Kinetic Description of Iron-Transfer and Regulatory Signals

The cell manages ferrous iron in bound form, attached to specialized carrier proteins, such as ferritin. Iron-containing prosthetic groups (such as heme group) are bound to protein carriers. Uptake and secretion of iron is also catalyzed by proteins which organize the transfer of iron into and out of the cells. Plasma iron is bound to the transport protein transferrin. All these processes take place in a cellular or membrane medium where the methodology of kinetic analysis in biochemistry with its concepts of “concentration” and “steady-state enzyme kinetics” are applicable at best by loose analogy. Well-known methods to achieve this are the methods of approximate kinetic formalisms [46, 47]**.** In effect, these concepts allow for a quantitative description of metabolic turnover that integrates the mechanistic molecular detail as black-box which is assumed to be in a dynamic steady state. [46-52]
Many of the iron-transfer reactions take place within a narrowly restricted range of “concentrations” of the partaking components. We introduce expansions (linear for protein turover, bilinear for iron processing, power law for reguatory signals) of the complex rate laws which are approximately valid in the neighborhood of a generic reference state, which is conceived as an idealized model of the “normal” healthy organism. All iron-processing proteins are assumed to exist in an iron-free and an iron-bound state (e.g. apoferritin and holoferritin), the sum of both being fixed at a given moment. This ensures that there are upper and lower constraints to the rates in the simplified kinetic description.

For convenience of controlling different simulation runs with systematic parameter variation we adopted a formulation of the bi-linear kinetics of reversible binding reactions as reversible rates with k_{on} and k_{off} as rate parameters:

Binding rate = k_{on} * substrate level * free protein carrier level

and

Release rate = k_{off} * occupied protein carrier level,

with

free protein carrier + occupied protein carrier = ambient expression level of protein carrier.

The signal cascades operating in iron metabolism involve a number of components to which the details of the accepted biochemical formalism cannot be specified. In contrast to the kinetic formalism of metabolic transfer the black-box formulation of the signaling cascades has to include an amplifier mechanism, because otherwise the operational gain of a signal (log final effect /log effector level) becomes very small at the end of a long and branched cascade. Regulatory cascades in vivo have inbuilt strong amplifier mechanisms (sometimes even to the extent of an all-or-none effect), but we will not produce this by meticulous formulation of details, but rather choose a general black-box formula in the form of a simple power rate law. For an activator signal we adopt the representation

activator signal = (activator level / K_{app}) ^{n}

and for an inhibitor signal:

inhibitory signal = $(K_{app}$ / effector level$))^n$

The effector levels and the signal strength are expressed in dimensionless form and included into the rate equations for the respective reaction. The term K_{app} (= apparent) refers the ambient effector level to that of the idealized (“normal”) reference state. The exponent n realizes the required amplifier gain. This particular form of signal kinetics was chosen for the sake of ensuring that the logarithmic gain of activator and inhibitor signals of different regulatory loops is symmetric and may be qualitatively related to each other by choice of the apparent kinetic parameter K_{app} and the logarithmic gain factor n. For illustration, consider the fate of a macromolecule x which is synthesized and degraded by a steady-state dynamics:

$\rightarrow x \rightarrow$

If there is an activator effect operative enhancing the expression level of x, this can be achieved either by an activator term (act) on the input reaction

dx/dt = 0 = U * act – Z * x with stationary x = U * act / Z

or, equivalently (when there is no information on the precise molecular mechanism) by an inhibitor term (inh) on the output reaction

dx/dt = 0 = U – Z * x * inh with stationary x = U / (Z * inh)

Equivalence of both effects is only given if

act = 1 / inh

With a logarithmic gain of n this requires that

act = $(\text{effector} / K_{app})^n$ and inh = $(K_{app} / \text{effector})^n$

Any of the usual Hill or allosteric equations for activation and inhibition cannot guarantee this equivalence. For the sake of comparison of interacting global and cellular signals we chose therefore this simple form. It guarantees that the reference state of the system (arranged to effector/K_{app}=1) does not change when different n-values are tested for efficiency. And it guarantees that activation of one partial reaction is symmetric to inhibition of the other partial reaction involving synthesis and decay of an effector, so that quantitative comparison of effector strength becomes possible, with K_{app} and n as modifying parameters. In numerical simulations one must take care of not falling into regions far from the reference state where the simple formula is no longer even qualitatively valid (e.g. approach of positive or negative infinity of the ratio).

2.16 Modelling the hepcidin effect on ferroportin expression

Hepcidin is being synthesized in the liver and reaches the locus of its signalling effect via plasma. Effector cells are mainly duodenum, macrophages of RES and hepatocytes. Hepcidin interacts with the membrane-resident ferroportin and causes its internalization, which is then followed by intracellular proteolytic degradation. From hepcidin injection experiments it is known that the internalization occurs rapidly (within a few hours [53, 54], whereas the ensuing proteolytic degradation has the general time characteristics of several days. This regulation was therefore modelled as depicted in fig. 6.

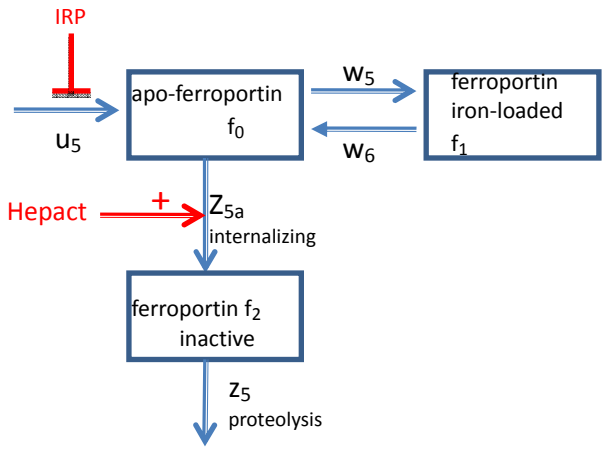

Fig. 6: Hepcidin increases degradation of ferroportin protein by binding and internalizing.

The balance equations of this subsystem read

$df_0/dt = u_5 - z_{5a} - w_5 + w_6$
$df_1/dt = w_5 - w_6$
$df_2/dt = z_{5a} - z_5$.

Assuming linear kinetics one gets

$z_{5a} = Z_{5a} * f_0 * hepact$
$z_5 = Z_5 * f_2$

(hepact is the kinetic activation term of hepcidin level)

and for the steady state
$f_0 = u_5 / (Z_{a5} * hepact)$
$f_2 = u_5 / Z_5$
f_1 is proportional to f_0 , depending on cellular iron and free plasma transferrin
(λ and $\{\tau_0 / (\tau_0+\tau_1)\}$

2.17 Rate equations of iron uptake and iron release by the cell

$v_1 = K_1 * \alpha * \tau_1$	(K_1 = 0.4; calculated from [41])
$v_2 = K_2 * \beta$	(K_2 = 0.1; calculated from [41])
$v_3 = K_3 * \gamma * m_1$	(K_3 = 0.05; calculated from [41])
$v_4 = K_4 * \delta$	(K_4 = 1.25; calculated from [41])
$v_5 = K_5 * m_0$	(K_5 = 2.5; iron in intestinal tract)
$v_6 = K_6 * m_1$	(K_6 = 2.5; iron uptake via DMT1)
$v_7 = K_7$	(K_7 = 0.5; parameter for non-TFR1 iron uptake by liver)

2.18 Rate equations of internal transfer

$w_1 = H_1 * \varphi_0 * \lambda$	($H_1 = 10$)
$w_2 = H_2 * \varphi_1$	($H_2 = 1$)
$w_3 = H_3 * \lambda * / Y_{eff} \wedge q_3$	($H_3 = 5$; $q_3 = 1$; signal Y_{eff} see below)
$w_4 = H_4 * s$	($H_4 = 5$)
$w_5 = H_5 * \lambda * f_0 \wedge 3$	($H_5 = 1.8$)
$w_6 = H_6 * f_1 * \tau_0$	($H_6 = 2.4$)
$w_9 = H_9 * \lambda / Y_{eff} \wedge n_9$	(H_9 = 20.1 in bone marrow; 2.22 in muscle else=0; n_9 =1)
$w_{10} = H_{10} * h$	(H_{10} = 18.1 bone marrow; else = 0)
$w_{11} = H_{11} * h$	(H_{11} = 2.0 bone marrow; else=0; w_{11} identical to w_{shunt})
$w_{12} = H_{12} * h$	(H_{12} = 2.2 in muscle heme turnover)
$w_{13} = H_{13} * \lambda$	(H_{13} = 1.65 in integument ; 1.35 in intestine)
$w_{RBC} = k_{RBC} * RBC / RBC_{ref}$	(k_{RBC} = 18.1; RBC_{ref} = 1)

The parameters of w_{RBC} were derived by normalization. The actual reference pool size of RBC is 301.7 µg per mouse, and the rate corresponds to a erythrocyte renewal rate of 0.06 per day.

2.19 Rate equations of combined transcription/translation (protein biosynthesis)

$u_1 = U_1$	($U_1 = 1$) expression of IRP1
$u_2 = U_2$	($U_2 = 1$) expression of IRP2
$u_3 = U_3 * epo \wedge n_{epo} * yeff \wedge n_3$	($n_3 = 1$, n_{epo}=5) expression of TFR1
Tissue	**U_3 Parameter value in different cell types**
bone marrow	420
liver	70
RES	0
Muscle	44
Integument	34.4
intestine	28
duodenum	1

The EPO activation term is only valid for the bone marrow, for the other organs it is to be cancelled out. The U_3 values were calculated from ferrokinetic flux estimates (see below, results). RES does not receive iron over the TFR1-pathway, but rather by phagocytosis of erythrocyte hemoglobin. The U_3 values were calculated from ferrokinetic flux estimates (see below, results).

$u_4 = U_4 * yeff \wedge n_4$	($U_4 = 1$; n_4 =1) expression of DMT1
$u_5 = U_5 / yeff \wedge n_5$	($U_5 = 0.5$; n_5 =1) expression of ferroportin
$u_6 = U_6 / yeff \wedge n_6$	(n_6 =1) expression of apoferritin
Tissue	**U_6 Parameter value in different cell types**
bone marrow	1.63
liver	2.84
RES	6.5
muscle	1.45
integument	3.92
intestine	0.38
duodenum	0.02

$u_7 = U_7$	($U_7 = 1$) expression of transferrin
$u_8 = U8 * (\tau_1/(\tau_1+ \tau_0) / 0.15 - 1.0)$	($U_8 = 0.3$) expression of hepcidin, descriptive formula calculated from figure 1 of [55])
$u_9 = U_9 * (RBC_{ref} / RBC) \wedge n_9$	(U_9=1; RBC_{ref} =1; n_9 =4) (expression of erythropoietin is activated when RBC decreases)

2.20 Rate equations of protein degradation

$z_1 = Z_1 * y_1$	($Z_1 = 1$) degradation of IRP1
$z_2 = Z_2 * y_2 * \lambda \wedge n_2$	($Z_2 = 1$; $n_2 = 3$) degradation of IRP2
$z_3 = Z_3 * \alpha$	($Z_3 = 2$) degradation of IRP1
$z_4 = Z_4 * m_0$	($Z_4 = 1$) degradation of DMT1
$z_5 = Z_5 * f_2$	($Z_5 = 0.5$) degradation of ferroportin
$za_5 = Za_5 * f_0 *$ hepact	internalization of ferroportin
tissue	**Za_5 Parameter value in different cell types**
bone marrow	1
liver	0.225
RES	0.044
muscle	0.409
integument	12.857
intestine	18
duodenum	0.3529
$z_6 = Z_6 * \varphi 0$	($Z_6 = 1$) degradation of ferritin
$z_7 = Z_7 * \tau_0$	($Z_7 = 1.33$) degradation of transferrin
$z_8 = Z_8 *$ hep	($Z_8 = 0.2$) excretion of hepcidin
$z_9 = Z_9 *$ epo	($Z_9 = 1$) degradation of erythropoietin

2.21 Kinetics expressions for autocrine and endocrine signalling

Active IRP1: $Y_{1\_act} = Y_1 / \lambda \wedge 3$ (LIP inactivates IRP1)

Combined effect of IRP-system, with IRP2 dominating and the IRP1 equilibrium poised towards aconitase in the reference state; [56])

$Yeff = Y_{\_act}/ Y_{1reference} + Y_2 / Y_{2reference}$ ($Y_{1\_reference} = 20$;$Y_{2\_reference} = 1.0526$)

Erythropoetin signalling to bone marrow:

epoact = epo $\wedge$ n_{epo} ($n_{epo} = 5$)

Hepcidin signalling to RES, liver, duodenum, activating ferroportin degradation:

hepact = hep $\wedge$ n_{hep} ($n_{hep} = 3$)

2.22 Parameter portrait to simulate physiological or pathological deviation

Parameter portraits plot the steady-state value of system variables against systematic changes of one or several of the parameters. This simulates physiological challenge or genetic perturbation of the basic reference state. The dynamic stability of the steady-state was checked as return to it after a series of random-perturbations of variables and, in critical cases, by evaluating the eigen-system around the steady-state.

2.23 Numerical solution of dynamic systems (ordinary differential equations)

With parameter values and the initial state of variables specified the dynamics of approach to steady-state was calculated using MatLab integration routines, mainly a Runge-Kutta algorithm.
The attainment of steady-state was checked by calculating the absolute values of right-hand sides of the differential equations divided by the level of the corresponding variable. A steady-state criterion was a level below 10^{-8} of this indicator.

Chapter 3

3 - Results

3.1 Plasma Iron Pool

The iron pool in blood plasma, despite its importance as the main iron exchange medium in the vertebrate body, has a small size compared to other pools (1-2 µg Fe per mouse) and is renewed several times per day (table 3.1).
The table shows that the transferrin-bound plasma iron concentration varies according to the iron status in the body. It tends to be lower under an iron deficient diet and higher in iron loaded conditions. It is in the range of 80-150 µg/dL and is similar to other mammalian species [57-61]. In rats, iron deficiency does not seem to lower plasma iron concentration.

TABLE 3.1: 1) Molecular weight of iron 55.847 2) 1.36 ml plasma per 25 mg mouse (see table 2.1) 3) Rounded value of row 4 * 55.847 / 1000 *1.36 ml (body plasma volume)

	Fe-Deficient	**Fe-Adequate**	**Fe-Loaded**
Plasma iron concentration [µM]	15.2 ± 5.5	19.8 ± 1.4	25.8 ± 1.0
scaled t [µg/dL] [1]	84.0	110.5	144.1
Plasma pool size [µg per mouse] [2]	1.15	1.50	1.96
Plasma iron turnover rate [µM/day] (PIT)	139	185	245
Scaled to µg per mouse[3]	11	14	19
Total clearance rate [d^{-1}]	17.2	18.1	18.8
Plasma half-life time of iron [min]	58	55	53

The Plasma Iron Turnover rate is an indicator of how much iron is cleared from plasma per day. Iron molecules leave the plasma and go to peripheral organs and in our model iron molecules either slowly return to plasma to be again distributed through the organism or are lost due mucosal or skin desquamation. The Plasma Iron Turnover is calculated as follows:

PIT = 10 [per day] * plasma concentration [µM] – 13 [µM per day].

the slope of 10 and the intercept of -13 were estimated from fig. 5 of [33]. Like the plasma iron concentration, the PIT increases in an iron-loaded diet and diminishes under iron-deficient conditions.

The total clearance rate from table 3.1 is calculated by the plasma turnover rate and plasma iron concentration, taken from fig. 5 of [33]. In their study turnover was measured at 2 h after administration assuming that the exponential clearance rate constant is given by

-24/2 * ln {1 - (turnover rate) / (plasma concentration) * 2/ 24}

This estimate is probably somewhat too low due the influence of tracer reflux. For parameter estimation we therefore rounded this preset value to maximum of 20 per day. To assess the precise total clearance rate would be necessary to perform measurements in groups of mice in a short period right after radioiron injection. This was not done in our experiments, since it

is not feasible in mice. Our first measurement was performed at 12h, when most part of injected radioiron was already cleared from plasma. Cavill et al. have summarized the corresponding problems in humans [62, 63].
With the calculated turnover rate constants it is possible to estimate the half-life of transferrin-bound plasma iron as follows:

Half-life = ln (2) / turnover rate constant [per day] * 24 * 60 [min])

The half-life of transferrin-bound plasma iron is somewhat slower for the iron deficient diet (58 minutes) and somewhat faster for iron-loaded diet (53 minutes). These values are in the same range from other species like dogs and rats [10, 59, 60] and in accordance with other studies [33, 64].

3.1.1 Tracer uptake into murine Organs

Schümann´s tracer data [27] (see appendix A) allow to estimate clearance parameters of their compartment representation, see table 3.2. These parameters can be used to understand what proportion of the initial injected radioiron dose is absorbed by the organs and later returned to plasma. As mentioned previously, for our optimization purposes it was established that the sum of the fractional rates leaving the plasma was set to 20 per day. Figure 3.1 depicts how many percent of this fixed value is distributed among organs of mice under different dietary conditions.

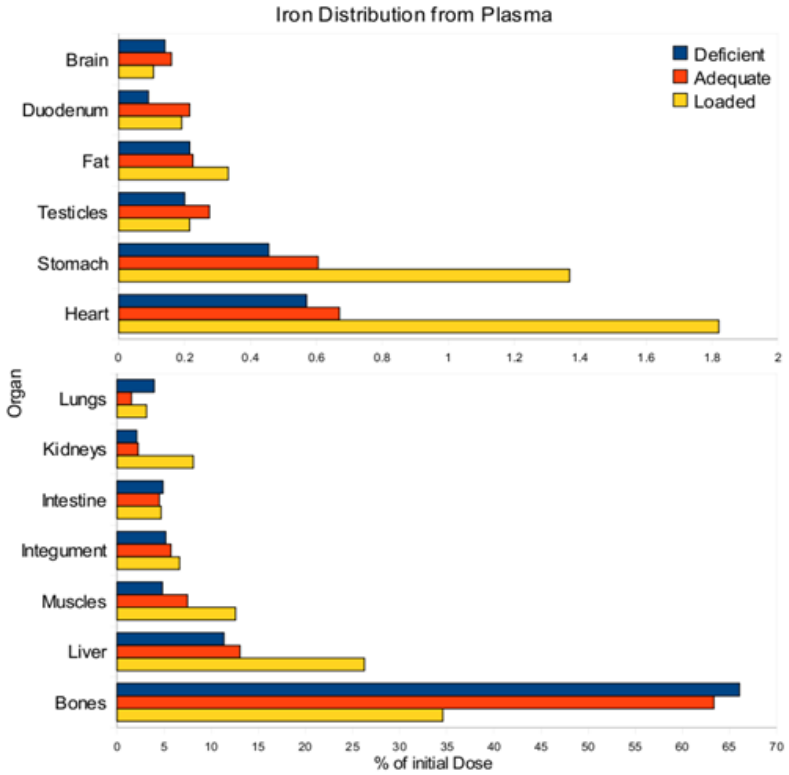

Figure 3.1: distribution of radioactive plasma iron between organs. There are two different scales: one for the organs known to have a high iron storage or demand like liver and bone marrow and a second scale with peripherical organs like the testicles, heart and brain. The percentage values depicted were calculated as follows: The best-fit clearance parameters for flux plasma-organ for the respective diet were divided by the total (=20) and multiplied by 100.

TABLE 3.2: Clearance parameter rates for the best fit and also the upper and lower limits obtained after Monte Carlo perturbations of the measurement values followed by the curve-fit procedure. This sequence was performed 100 times. The dimension of the data is day^{-1}. The + and – indicate statistically valid change compared to iron-adequate diet (bracketed if only slight).

	Fe-Deficient				Fe-Adequate			Fe-Loaded			
Parameter	**Best Fit**	**Lower Limit**	**Upper Limit**		**Best Fit**	**Lower Limit**	**Upper Limit**	**Best Fit**	**Lower Limit**	**Upper Limit**	
1kp_bon	**13.22**	12.47	13.63		**12.67**	12.01	13.26	**6.92**	6.01	7.09	+
2kp_kid	**0.42**	0.28	0.54		**0.45**	0.36	0.51	**1.62**	1.18	1.82	+
3kp_int	**0.98**	0.77	1.06		**0.9**	0.63	1.1	**0.93**	0.66	1.01	
4kp_liv	**2.27**	1.83	2.54		**2.61**	2.28	2.9	**5.25**	4.25	5.73	+
5kp_sto	**0.09**	0.06	0.18		**0.12**	0.08	0.17	**0.27**	0.21	0.37	+
6kp_intg	**1.04**	0.89	1.32		**1.14**	0.96	1.35	**1.33**	1.05	1.50	
7kp_fat	**0.04**	0.03	0.05		**0.05**	0.04	0.05	**0.066**	0.051	0.075	(+)
8kp_mus	**0.96**	0.8	1.23	-	**1.49**	1.31	1.8	**2.52**	2.06	2.75	+
9kp_lun	**0.79**	0.64	1.06	+	**0.31**	0.22	0.44	**0.63**	0.56	0.75	+
10kp_duo	**0.02**	0.01	0.15		**0.04**	0.03	0.06	**0.038**	0.027	0.050	
11kp_bra	**0.03**	0.03	0.03		**0.03**	0.03	0.04	**0.021**	0.019	0.022	-
12kp_hea	**0.11**	0.1	0.14		**0.13**	0.12	0.15	**0.36**	0.31	0.38	+
13kp_tes	**0.04**	0.04	0.05		**0.06**	0.05	0.06	**0.043**	0.037	2.68	
14kkid_p	**0.2**	0.11	0.32		**0.2**	0.14	0.25	**0.23**	0.16	0.32	
15kliv_p	**0.25**	0.21	0.32	+	**0.14**	0.11	0.16	**0.10**	0.073	0.12	(-)
16ksto_out	**0.18**	0.09	1.72		**0.37**	0.27	0.49	**0.29**	0.20	0.40	
17kfat_p	**0.1**	0.06	0.19		**0.13**	0.1	0.15	**0.099**	0.079	0.12	
18kmus_p	**0.03**	0.02	0.05	-	**0.15**	0.12	0.21	**0.14**	0.11	0.17	
19klun_p	**0.41**	0.37	0.52	+	**0.19**	0.11	0.3	**0.086**	0.065	0.12	(-)
20kbra_p	**0.02**	0.02	0.03	-	**0.06**	0.05	0.07	**0.028**	0.022	0.034	-
21khea_p	**0.06**	0.03	0.08	(-)	**0.08**	0.06	0.09	**0.17**	0.14	0.19	+
22ktes_p	**0.05**	0.03	0.07	-	**0.09**	0.07	0.12	**0.067**	0.044	7.16	
23kspl_p	**14.61**	13.86	15	-	**7.29**	5.53	9.15	**1.91**	1.52	2.33	-
24kintg_out	**0.03**	0.02	0.05		**0.04**	0.03	0.06	**0.072**	0.057	0.102	(+)
25kint_out	**0.3**	0.22	0.4		**0.36**	0.26	0.42	**0.22**	0.16	0.26	-
26kduo_p	**0.17**	0.12	2.55		**0.42**	0.32	0.55	**0.24**	0.18	0.34	
27kbon_rbc	**1.85**	1.74	1.92	+	**1.07**	0.93	1.26	**0.50**	0.48	0.57	-
28kbon_spl	**0.56**	0.4	0.83	+	**0.1**	0.08	0.13	**0.046**	0.033	0.058	-
29krbc_spl	**0.03**	0.02	0.04	-	**0.06**	0.05	0.07	**0.032**	0.027	0.047	-
fval chi_sqr	0.58				0.72			1.05			
sq root of mean weighted squared dev	0.07				0.08			0.07			

-

Considering the two different scales of figure 3.1 (0-2% and 0-70%) we observe that there were organs which did not demonstrate a strong difference in terms of tracer iron uptake between the diets: brain, fat, testicles, intestine and integument. In the case of duodenum, stomach and lungs it is not possible to affirm that there is a representative difference on the iron uptake levels. This can be attributed to technical difficulties associated to the organ size (duodenum, stomach) or the lack of cellular homogeneity of the organ itself (lungs).
On the other hand, it is visible that other organs have a great difference in tracer uptake levels when the mice were held under different diets. The heart and the muscles absorb around 2 times more iron under loading scenarios. In contrast, in the iron-loaded diet the bone marrow absorbs around 30% less in comparison to iron-deficient or -adequate. This difference in absorption in the bone marrow, liver and muscles reflects a “switch” to a storage mode that occurs in the organism when there is iron repletion.

Figures 3.2, 3.3 and 3.4 show the tracer distribution among organs during the study period under the three different diets. We can observe from the figures and numerically assess from tables 1-3 in Appendix A that at the time when the first measurement was performed (12h) the plasma radioiron clearance was already complete. The tracer had been already absorbed by the organs and the tracer level in plasma was very small and remained practically constant.

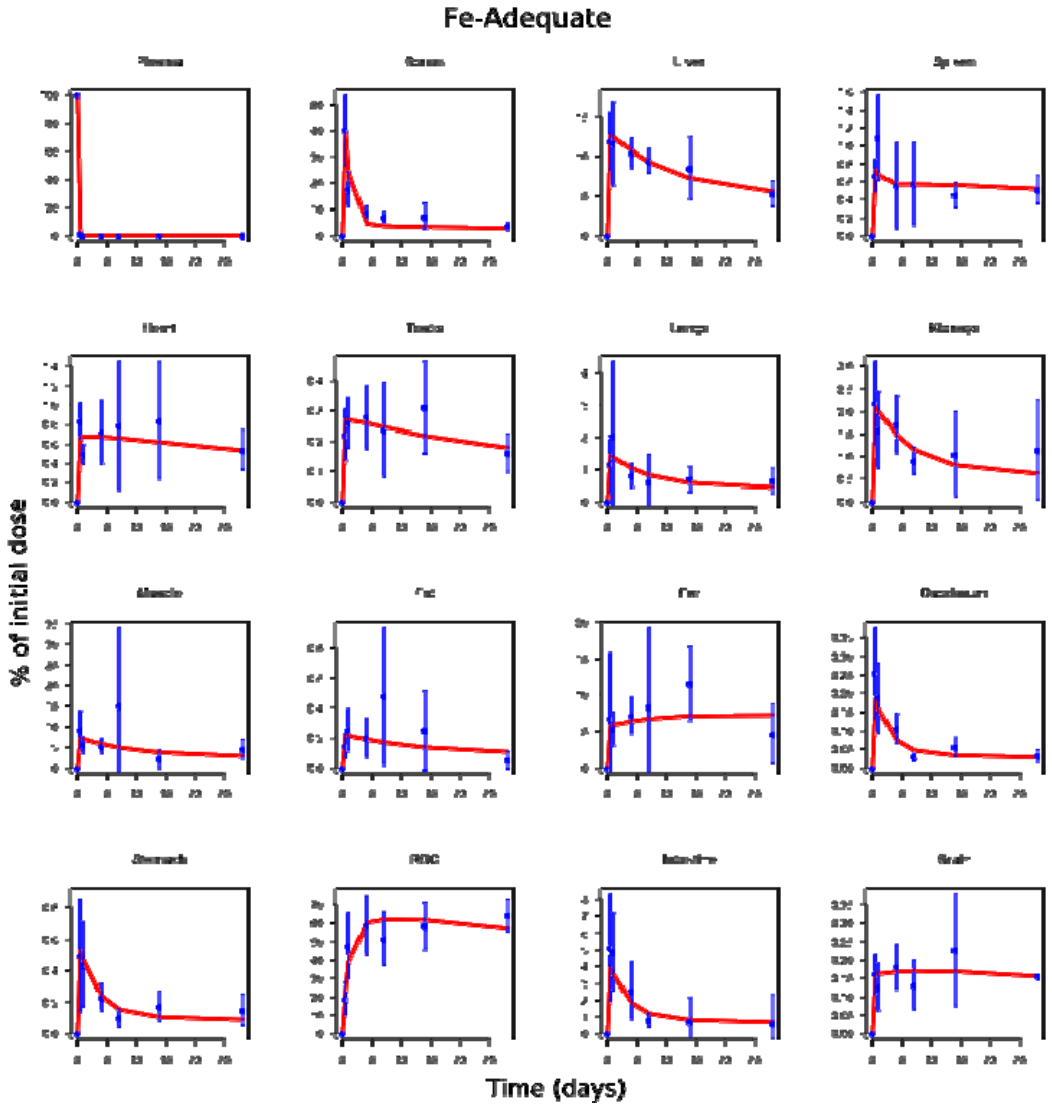

Figure 3.2: The best fit of our model to the measured data of mice held under iron adequate diet. The blue dots with standard deviation are the measurements and the red line of the curve produced by our model.

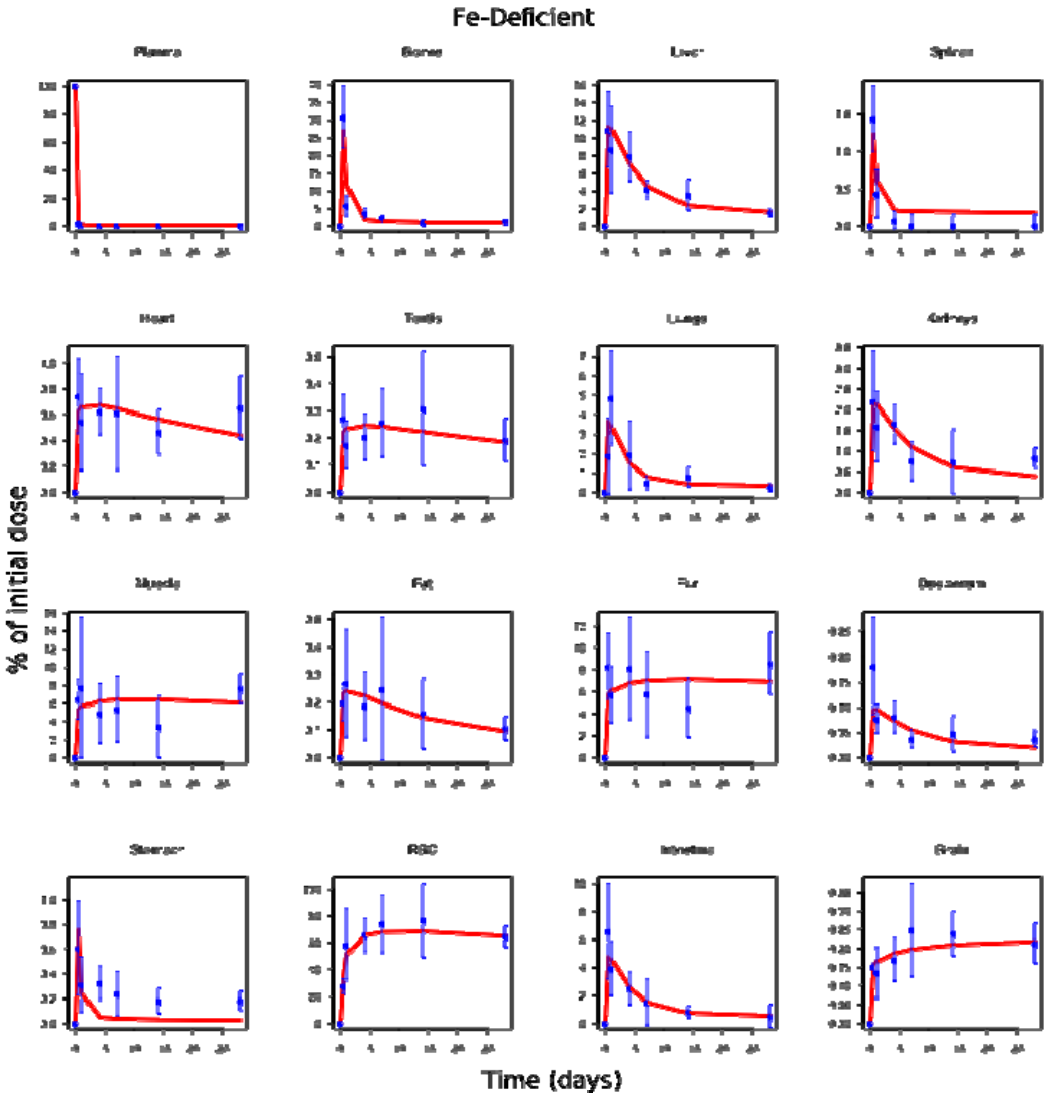

Figure 3.3: The best fit of our model to the measured data of mice held under iron deficient diet. The blue dots with standard deviation are the measurements and the red line of the curve produced by our model.

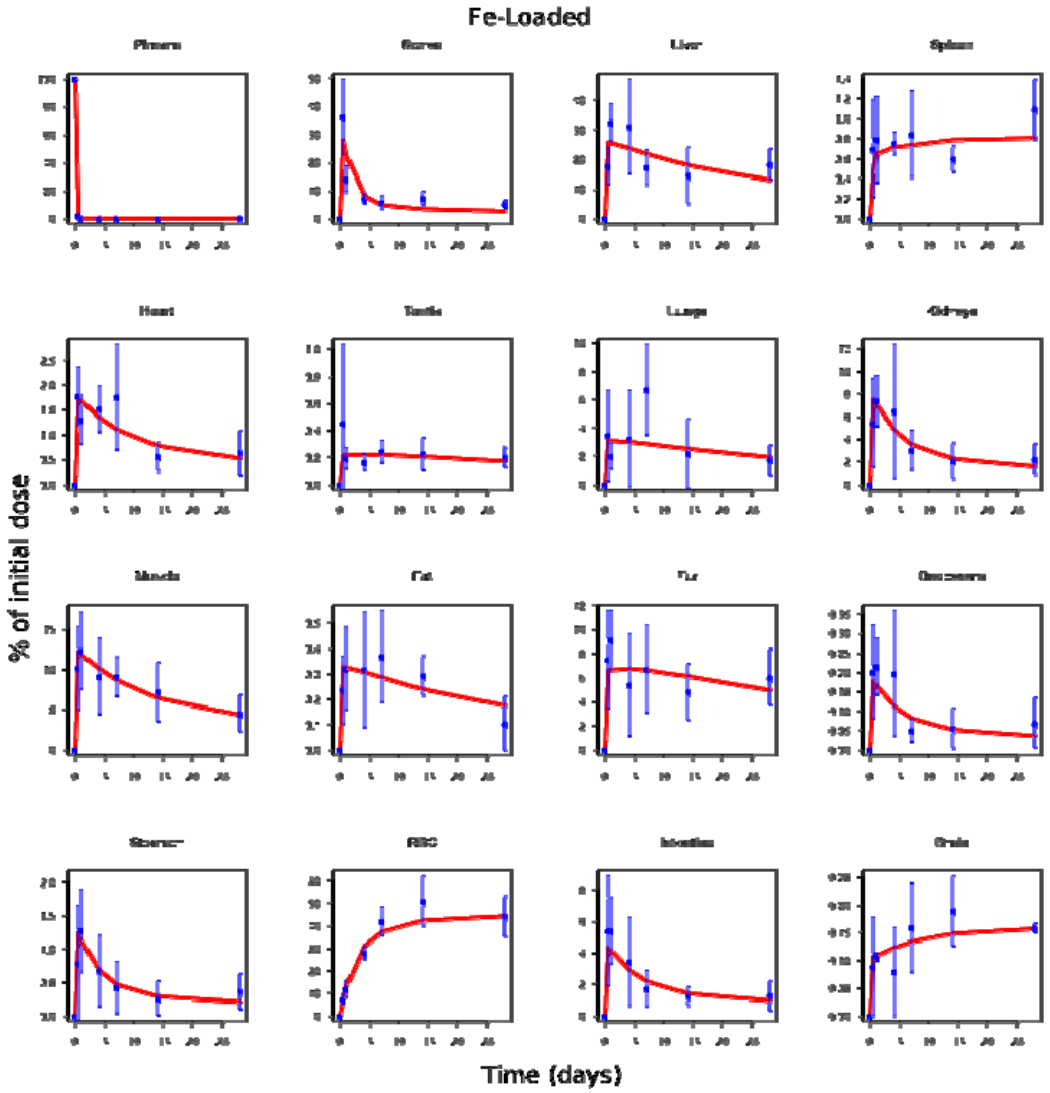

Figure 3.4: The best fit of our model to the measured data of mice held under iron loaded diet. The blue dots with standard deviation are the measurements and the red line of the curve produced by our model.

The two components in the plasma curve (first exponential decay and later a small tracer level close to zero) can be attributed to i) the first clearance phase (which happens approximately within one hour [33] and ii) to a reflux of iron from the organs to the plasma.
Inspection of the organ curves demonstrate that after 12-24 hours the reflux into plasma starts to take place and follows until the end of the study. In addition, from the same figures it is possible to verify that the organs receive radioiron and store for biosynthetic functions, return it to plasma to be redistributed among other organs or looses it by desquamation, as is the case of intestine and integument.
In addition, the influx and outflux of radioiron from the organs obviously take place simultaneously, in accordance with the steady-state experienced during the development of this study.
The results presented so far related to iron uptake by the organs were expressed as percent of the injected tracer dose. To have a more precise quantitative description of the amounts exchanged by the organs and present the results in units that can be further used for comparison among species, one should use absolute flux rates.
To calculate the absolute flux rates it is necessary to have the fractional clearance rates (table 3.2) and the iron content of plasma plus the extracellular fluid (table 3.1).
We calculate the flux rates ($\mathbf{v}_{plasma\_i}$) as:

$\mathbf{v}_{i\_plasma} = \mathbf{k}_{i\_plasma} * \mathbf{C}_{plasma/ECF}$

where $\mathbf{k}_{i\_plasma}$ is the fractional clearance rate between plasma into the organ i and $\mathbf{C}_{plasma/ECF}$ is the iron content in plasma plus extracellular fluid.
We can observe in figure 3.5 and table 3.3 that three sets of flux rates may be distinguished:

- flux through the erythron (range of 10 to 20 µg / day per mouse)
- flux through peripheral compartments with storage function (liver, muscle, integument, intestinal tract, kidneys, lungs, heart: 0.5 to 4 µg / day per mouse)
- flux through organs with slow iron turnover (testicles, fat, brain: 0.05-0.08 µg per day per mouse).

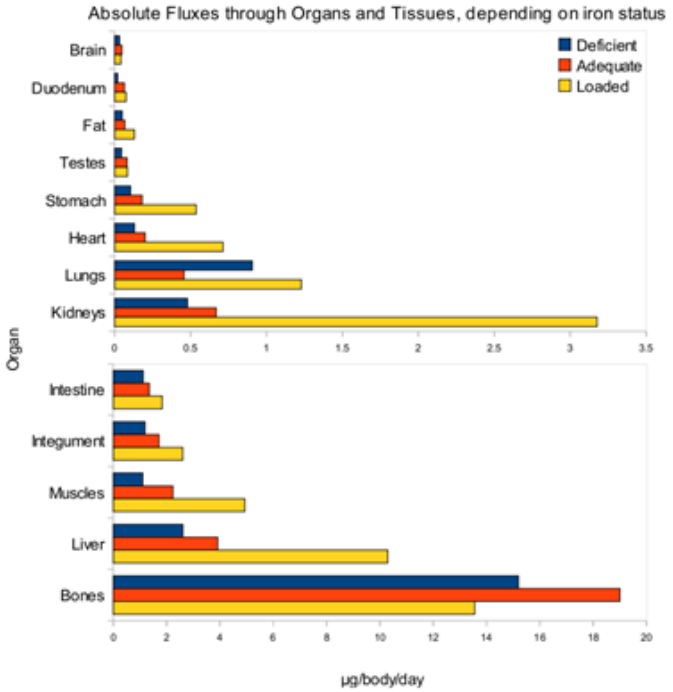

Figure 3.5: The calculated radioiron fluxes from plasma into organs. Data obtained from

Table 3.3. The calculations were done for the "best-fit" parameters.

	Absolute Flux Rates (µg/body/day)		
Parameter	**Fe-Deficient**	**Fe-Adequate**	**Fe-Loaded**
1kp_bon	15.19	19.007	13.55
2kp_kid	0.48	0.66	3.17
3kp_int	1.12	1.34	1.83
4kp_liv	2.61	3.92	10.29
5kp_sto	0.105	0.18	0.53
6kp_intg	1.19	1.71	2.602
7kp_fat	0.05	0.067	0.13
8kp_mus	1.106	2.24	4.93
9kp_lun	0.907	0.45	1.22
10kp_duo	0.021	0.064	0.075
11kp_bra	0.032	0.048	0.041
12kp_hea	0.132	0.202	0.71
13kp_tes	0.046	0.082	0.084
14kkid_p	0.48	0.66	3.17
15kliv_p	2.61	3.92	10.29
16ksto_out	0.105	0.182	0.53
17kfat_p	0.05	0.067	0.13
18kmus_p	1.106	2.24	4.93
19klun_p	0.907	0.457	1.22
20kbra_p	0.032	0.048	0.041
21khea_p	0.132	0.202	0.71
22ktes_p	0.046	0.082	0.084
23kspl_p	15.19	19.007	13.55
24kintg_out	1.19	1.71	2.602
25kint_out	1.12	1.34	1.83
26kduo_p	not calculated	not calculated	not calculated
27kbon_rbc	11.66	17.36	12.42
28kbon_spl	3.53	1.63	1.13
29krbc_spl	11.66	17.36	12.42

3.1.2 The Erythropoietic System

The injected radioiron in plasma is cleared after approximately 1 hour and most part of its molecules is routed to the bone marrow. Due the intensive production of hemoglobin, the erythrocyte production path represents the greatest iron demand [20, 21]. According to figures 3.1, 3.5 around 63% of iron is taken up by the bone marrow under normal conditions and 66% under iron deficiency. The value obtained here seems to be lower than in other species [6, 21, 65].

Under iron-loaded diet the uptake by the bone marrow is decreased to just 35%, that is about half of normal uptake. In figures 3.1, 3.5 it is possible to see a switch of the system into a storage mode [66]. This increases the amount of iron absorbed initially by the liver and muscles and diminishes the iron to be used in the erythrocyte forming pathway. A corresponding, but slight, decrease in hemoglobin synthesis was observed under this iron loaded condition [27].

Some days after injection, for all three conditions, saturation behavior can be observed on the red blood cell curves (figures 3.2, 3.3 and 3.4). In iron-deficient and iron-adequate mice, around 60% of the injected radioiron dose is present as hemoglobin in the red blood cells,

and in iron-loaded mice, just 40%.
This saturation behaviour instead of a continuously increasing curve suggestsrandom elimination of red blood cells (independent of cell age), in addition to the normal lifespan removal. The bone marrow receives daily an influx of 15;19;14 µg iron (table 3.3). Without this random destruction component, radioiron that returned from other organs would be continuously further incorporated into red cells.
Horký et al. [67] studied the red cell lifespan and developed an age independent linear component of cell destruction. This linear element in combination with a life-span determined component produced a rate of red cell elimination of 0.012 per day. Our value is higher: between 0.03 and 0.06 per day. However, these values rely on estimated pool sizes, therefore they are not totally reliable.

After about 30 days the red blood cells are senescent or damaged and need to be removed from circulation, so their iron molecules are liberated and used in the synthesis of new healthy erythrocytes. The murine spleen has a dual role: both removing red cells and colloidal iron from circulation [9, 68] or as an erythropoietic organ [64].
The spleen contains 5% of the total macrophage population and depending on body iron status the spleen either releases or stores iron originated from the red cell destruction. Table 3.2 shows that under iron deficient diet the spleen releases back to plasma approximately 14.6 splenic pools per day while under iron loaded conditions, this amount decreases to just 1.91 pool units per day.
Another source of iron for the spleen is provided by ineffective erythropoiesis, especially under iron deficiency, when the demand for iron increases. Under iron scarcity many erythrocytes are synthesized in the bone marrow receiving less than the appropriate amount of iron to be functional [68]. These red cells do not reach the final stage of maturation and are cleaned from blood by the macrophage system. Table 3.2 shows that the rate of transfer between the bone marrow and spleen increases 10 times between iron-deficient and iron-loaded and 5 times between iron-deficient and iron- adequate conditions. This is evidence that the spleen releases iron based on body status or stores it either as ferritin or hemosiderin [69].
It is important to mention that in our model there is no distinction between the macrophage populations and therefore RES is mentioned interchangeably with spleen (figure 2.1). To understand the precise role of macrophage population in each organ would be necessary to carry a cell separation, which is known to be technically very difficult [68].
The erythropoietic contribution of the spleen is a minor factor in terms of body iron turnover and erythropoesis. From tables in 1-3 in Appendix A it can be observed that the amount of iron absorbed by the spleen after 12 hours is not high. The ratio between the tracer content of bone marrow and spleen after 12 hours is respectively 50, 60 and 20 in iron-adequate, -loaded and -deficient mice.

3.1.3 Compartment size of Tracer-Accessible Peripheral Pools

The compartment sizes in our model were estimated inorder to calculate the size of the “tracer-accessible pools”. This should reflect the behavior of newly absorbed molecules whichcan be either stored, used for cellular functions of returned to plasma.
Under steady state assumption, to calculate the tracer accessible pool sizes we need to be aware of:

- the fractional clearance rates from plasma into a compartment (k_{i_plasma}) and also from that compartment back to plasma (k_{plasma_i}).
- the plasma/ECF iron concentration ($C_{plasma/ECF}$).

With these values, we use equation (7).
Comparing the diets, it can be observed in table 3.4 and figure 3.6 that under iron-loaded diet the amount of absorbed and possibly stored radioiron is increased in every organ considered.

We can see from table 3.4 (and depicted in fig. 3.6) that the pool sizes can be group mainly into three groups:

- The red blood cells, composing the biggest iron pool in the body (280-390 µg iron)
- The organs that exert storage function: liver, muscle, integument (10-100 µg iron)
- The peripherical organs of the organism: kidneys, heart, brain, stomach (0.2-3 µg iron)

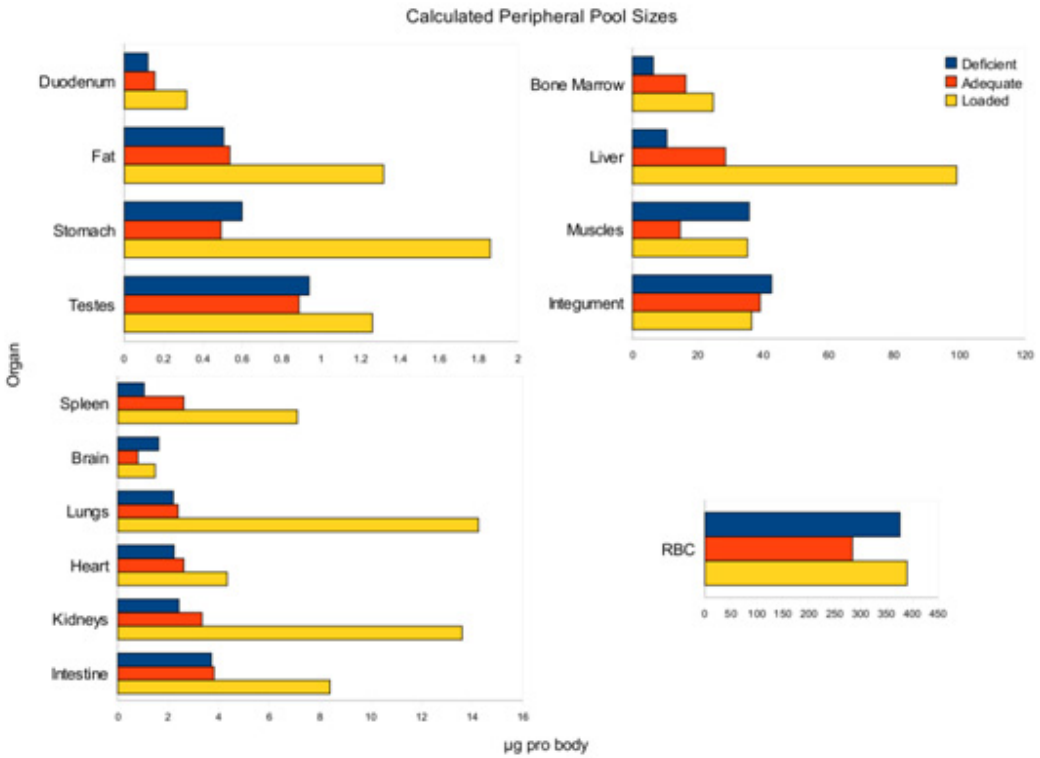

Figure 3.6: The calculated pool sizes for the different organs under three diets. Data obtained from table 3.4.

TABLE 3.4: The calculated pool sizes for the three dietary regimes.

Compartment size	Fe-Deficient	Fe-Adequate	Fe-Loaded
Red blood cells	**380**	**284**	**390**
Integument	**42.2**	**39.2**	**36.4**
Liver	**10.4**	**28.4**	**99.1**
Bone marrow	**6.3**	**16.3**	**24.7**
Muscles	**35.5**	**14.5**	**35.1**
Intestinal tract	**3.7**	**3.8**	**8.4**
Kidneys	**2.4**	**3.3**	**13.6**
Spleen	**1.0**	**2.6**	**7.1**
Heart	**2.2**	**2.6**	**4.3**
Lungs	**2.2**	**2.4**	**14.3**
Brain	**1.6**	**0.8**	**1.5**
Testicles	**0.9**	**0.9**	**1.3**
Fat	**0.5**	**0.5**	**1.3**
Stomach	**0.6**	**0.5**	**1.9**

3.1.4 Hierarchy of Iron Residence Times in Different Organs

To understand how the organs deal with the injected iron molecules – whether they store it for biochemical processes of return it to plasma – is necessary to asses the time scale of the system. In addition, this provides a realistic idea about the stiffness of the system that is being modeled.
Using the fractional clearance rates from table 3.2 we can calculate the residence time of radioiron molecules in different compartments by equation (4), see methods. Table 3.5 shows that there is a rapid circulation between the plasma, bone marrow and spleen (characteristic time below 1 day), intestinal tract (~2-3 days), an average circulation time in liver, fat, muscles and other inner organs (~5-13 days) and a longer residence time in red cells, brain and integument (greater than 16 days).

Table 3.5: The calculated residence time that iron molecules spend in the organs of mice held under different diets.

	Fe-Deficient	**Fe-Adequate**	**Fe-Loaded**		**expressed in hours**	
Plasma TF-bound*	0.05	0.05	0.05	1.2	1.2	1.2
Spleen	0.07	0.14	0.52	1.6	3.3	12.6
Bone marrow	0.4	0.9	1.8	9.9	20.5	43.7
Intestinal tract	4.2	2.8	3.9			
Stomach	5.7	2.7	3.5			
Lungs	2.4	5.2	11.6			
Kidneys	5.0	5.0	4.3			
Muscles	32.1	6.5	7.1			
Liver	4.0	7.3	9.6			
Fat	10.3	7.9	10.1			
Testicles	20.5	10.8	15.0			
Heart	16.8	13.0	6.1			
Red blood cells	32.6	16.4	31.4			
Brain	49.7	16.4	35.7			
Integument	35.4	22.8	14.0			

It is also possible to see from table 3.5 that there is a hierarchy of time scales in the system. The following five groups of time periods are in accordance with literature data [23, 24, 33] and can be described as:

- Rapid mixing of radioiron with transferrin pool/ECF: below 1 hour
- Initial clearance of iron due absorption by the bone marrow, liver and muscle: ~1 hour
- Reflux of tracer from the organs to plasma: ~2 days for intestinal tract and ~8 days for parenchymal organs.
- Incorporation into iron storage or carrying proteins (red cells, muscles, integument and fat): ~1 month.
- Complete excretion of the tracer from the body: ~200 days.

It should be noted that the last aspect, the iron excretion, differs from humans. Miceloose around 0.5 % per day of their iron [23, 24], while humans loose less (only about 0.1% [24,58,72,73]). A characteristic time of 200 days means a considerable part of murine life-expectancy. So the mouse has an iron depot for its whole life, by contrast to humans.
Another fact that can be observed for a number of organs is that for the most part of organs, the time-hierarchy does not change significantly between the three dietary regimes, also in accordance with the conclusion of [33]. However, exceptions are bone marrow, liver, spleen

and muscles, where the different diets have an impact on the residence time of iron molecules in the organs.
It is also noteworthy from table 3.5 and table 3.4 that there seems to be two kinetically distinct iron pools in mice: one which comprises about 20% of total body iron and has a residence time between 5 and 25 days and the second which comprises the other ~80% and has a residence time of ~200 days. The first pool type resides in liver, integument, fat and muscles, while the second compartment comprises the brain and especially the red cells compartment.

3.1.5 Comparison of Tracer-accessible pools with unlabelled non-heme

It is useful to understand how well the newly injected tracer iron mixes with the pre-existing iron in tissues. This gives an idea about how the organ's storage and absorption capacity changes under different dietary regimes. It is assumed that the tracer-accessible pool is a fraction of the total non-heme pool of the organs. To identify the pools that become quickly labelled we rely on the dynamics revealed by the tracer molecules. Table 3.6 provides the amount of non-heme iron for some organs under the different diets in this study.
Table 3.6 shows that the amount of non-heme iron increases from 106 to 1600 µg iron (~ 15 fold-changes) in liver of iron-loaded and -adequate diets. On the other hand, under iron-deficiency the pool is reduced to about half of normal non-heme levels (from 106 to 59.5 µg iron).
A dramatic change also happens in spleen, which under iron-loaded diet accumulates more than 120 µg iron (compared to 17.8 µg and 9.9 µg for iron-adequate and -deficient mice - ~ 7 and 12 fold-change, respectively).

Table 3.6: Non-heme iron content of mouse (C57B6/L) organs in different dietary regimes. Frazer et al. [70] give 56 **µg/g wwt. Vácha et al. [71] report 257 µg/g wwt. he concentration (µg non-heme iron per g of organ) data are unpublished data (K.Schümann for liver, kidneys, spleen and heart) and Vujic-Spasic & Muckenthaler for duodenum, lung, brain and muscle. The whole organ data were calculated as concentration times organ mass. The standard deviation was estimated from that of both sets of measurements (see methods). Note that liver, kidney and spleen store iron (ferritin) with increasing supply, whereas heart does not.**

Diet	**Fe-Deficient**	**Fe-Deficient**	**Fe-Adequate**	**Fe-Adequate**	**Fe-Loaded**	**Fe-Loaded**
	Content	**Whole organ**	Content	**Whole organ**	Content	**Whole organ**
Organ	µg/g wwt	**µg**	µg/ g wwt	**µg**	µg/g wwt	**µg**
Liver*	48.8 ± 5.1	**59.5 ± 7.9**	86.7 ± 14.9	**106 ± 20**	1310 ± 90	**1600 ± 170**
Kidneys	36.9 ± 2.3	**14.0 ± 2.0**	60.8 ± 2.4	**23.1 ± 3.2**	88.1 ± 7.1	**33.5 ± 5.2**
Spleen	141 ± 46	**9.9 ± 3.5**	254 ± 99	**17.8 ± 7.4**	1760 ± 240	**123 ± 24**
Heart	71.2 ± 2.4	**10.0 ± 1.5**	68.2 ± 7.9	**9.5 ± 1.8**	81.8 ± 10.5	**11.5 ± 2.2**
Duodenum				**2.9 ± 0.3**		
Lung				**9.5 ± 0.8**		
Brain				**13.4 ± 1.7**		
Muscle				**142 ± 29**		

In kidneys there is a decrease of 10 µg iron (~2 fold-change) between non-heme iron in iron-adequate and -deficient mice; and an increase of ~105 µg iron (~7 fold-change) between iron-adequate and -loaded conditions).
Table 3.7 shows how the tracer-accessible pools relate to non-heme iron pools under the three different diets. The calculation used the values of table 3.4, which contain the estimated tracer-accessible pool sizes.

We can see that the percentage of the liver compartment accessible to the tracer drops from 27 to 6% when comparing iron-adequate with -loaded condition. The spleen also undergoes a reduction from 15 to 6%.
Furthermore, comparing iron-adequate and -loaded conditions, we can see that the kidneys the heart has an increase in the percentage of compartment size occupied by tracer: from 14 to 41% and from 27 to 27% for kidneys and heart, respectively.
Analyzing the difference between iron-adequate and -deficient conditions, we can verify that the percentage occupied by tracer-accessible pools in some organs decrease (liver: 10%, spleen: 5%, heart: 5%) and in kidneys an increase of 3%.

Table 3.7: Tracer-accessible Iron Pools compared with non-heme Iron in different dietary Regimes. The tracer-accessible pool sizes were calculated as described in the text. For the "cold" non-heme iron content refer to table 3.6. It may be noted that upon iron loading non-heme iron in liver and spleen is less accessible to tracer uptake, whereas in kidneys and heart the tracer-reachable fraction increases.

Diet	Fe-Deficient	Fe-Deficient	Fe-Adequate	Fe-Adequate	Fe-Loaded	Fe-Loaded
	Content	% of non-heme iron	Content	% of non-heme iron	Content	% of non-heme iron
Organ	µg per mouse		µg per mouse		µg per mouse	
Liver	10.4	17	28.4	27	99.1	6
Kidneys	2.4	17	3.3	14	13.6	41
Spleen	1.0	10	2.6	15	7.1	6
Heart	2.2	22	2.6	27	4.3	37

3.1.6 Iron Excretion from the body

Iron, as mentioned before, enters the body by the duodenum and to a lesser extent from other parts of the small intestine. Iron is lost from the body via mucosal exfoliation, skin desquamation and also via bile und urine [72]. The iron lost by mice is about 2-5 times greater than in other animals and man [24, 34, 58, 72-74]. Therefore, it may be hard to develop an iron-overload scenario in mice without a severe mutation.
Table 3.3 shows that the losses through skin and intestine desquamation appear to be in the same range. The amount of iron leaving the body through skin desquamation in iron-deficient, adequate and loaded mice are respectively 1.19; 1.71 and 2.6 µg iron per day. The iron losses due intestinal mucosal exfoliation (intestine + stomach) are 1.22; 1.5; 2.3 µg iron per day for iron-deficient, -adequate and -loaded, respectively.

3.2 Simulation Studies with the Cellular Model

The kinetic model of iron metabolism that we have sketched in the methodical section needs the assignment of suitable values for the numerous parameters. We achieved this by applying the pool sizes and flux rates as calculated from tracer data in the previous section. The source of these estimated parameters are the tracer data of Schümann et al. (2007) [27], complemented by quantitative statements obtained from the physiological literature on iron metabolism. The flux values and pool sizes are stated in fig. 3.5 and 3.6. They define the quantitative range of the major fluxes in all cell types and tissues and set therefore parameters for input, throughput and output of iron, together with the equilibration of ferritin stores and heme synthesis. Other internal events are of minor quantitative importance, and it is therefore possible to set the parameters in a dimensionless form derived from the reference state of an adult, healthy and well-fed (also in terms of iron supply) mouse.

In this part we report findings of simulations performed for several physiological and pathological conditions: i) to see the effect of considerable blood losses by bleeding, ii) to assess the cellular and physiological changes to the organism under iron deficient or loaded diet, iii) to study the role played by hepcidin and IRP system in iron regulation. All results are obtained as parameter portraits (section 2.22). We present extracts here as percentage changes of certain salient parameter jumps.

3.2.1 Simulation of Chronic Blood Loss

In our simulations we established a daily blood loss with different degrees of severity. In model terms, a leakage of iron was introduced in the RBC pool. Instead of a complete route of RBC to the RES compartment, there is then a parameter characterizing loss of blood iron from the RBC pool to outside the body.

3.2.2 Erythropoiesis

The constant loss of red blood cells has a strong effect on the erythropoietic mechanism of the body (fig. 3.7). The change in the daily blood loss by 1% of the formation rate causes a parallel decrease of serum iron (transferrin saturation) by a factor of 40%. The consequence of lower transferrin saturation levels is that less iron is circulating and available for heme synthesis in the bone marrow. In this organ, the flux v1 (iron uptake by transferrin receptor 1, TFR1, also shares a parallel decrease and for each percent increased of the daily blood loss v1 level is reduced by 14%.
It can also be observed that the heme export (w10) is reduced in parallel under chronic blood loss: 1% increase in the daily loss of iron reduces the export of heme by 12%. It can be observed in the figure 3.7 that the level of RBC is also reduced in parallel and with 1% blood loss per day, it causes a reduction of 23% in the final level of RBC, where a new steady state is reached.
The reserve of iron in the bone marrow (Phi1 and Lambda) is also reduced under constant blood loss: 1% increase of the daily loss of iron reduces the levels of ferritin and free iron by 12 and 10% respectively.
The presence of the main receptor of iron in the bone marrow (TFR1) is increased when there is a chronic blood loss. For each percent of iron lost in red blood cells, the expression of this receptor increases by 16%. This happens due the stimulatory effect exerted by Erythropoietin (EPO). This hormone is produced at high levels in hypoxia situations, and in our model for each percent of blood lost on a daily basis, there is an increase of 40% in the level of EPO. And due to this increase, the production of TFR1 is also elevated. This is interpretable as a feedback loop in order to bind and internalize as much circulating serum iron as possible.

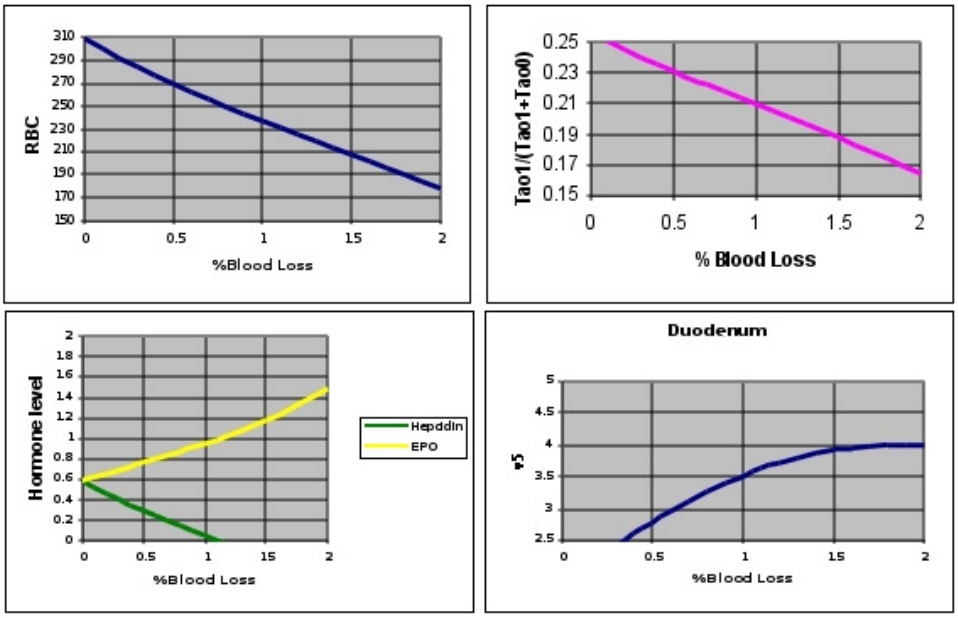

Figure 3.7: Blood loss and its relation to body iron status indicators. RBC, hepcidin and transferrin saturation fall in parallel with increases in the daily percentage of red cell loss. On the other hand, EPO increases almost linearly, due the demand for new erythrocytes and the duodenal iron absorption also increases until it reaches a plateau after 1.8% daily loss.

3.2.3 Recycling of iron

Under normal conditions, the major source of iron for the blood plasma is the Reticulo Endothelial System (RES). The iron released from the macrophages consists of molecules that were recycled from senescent red blood cells and ineffective erythropoiesis. In a chronic blood loss scenario, there is a constant decay in the level of the major source of iron molecules (RBC) that would be recycled and released into circulation.
In our simulations we observed that the v7 flux into RES (sum of iron intake from the two above mentioned sources) decreases in parallel with the constant blood loss: 25% less flux for each percent of blood lost daily. Since the system is in a steady-state, even with the constant blood loss, the same happens with the flux w6, which is the export of iron into circulation.
The iron stores in the macrophages also suffer a decrease (not shown as parameter portrait), For each percent of iron lost daily, the levels of Phi1 (ferritin bound iron) and Lambda (Labile Iron Pool) decrease by 70% and 84% respectively.

3.2.4 Storage

The iron uptake, storage and the eventual export from the liver decreases with blood loss. It can be observed from our simulations that 1% increase in the daily loss of red blood cells implies almost 20% lesser iron uptake by TFR1(v1 flux). As in the bone marrow, in the liver the expression of TFR1 is also increased . However, this increase in liver cells is much less pronounced than in bone marrow. In the liver the expression of this receptor in the cell membrane increases by around 1% for 1% daily blood loss.
The iron stored in ferritin form (Phi 1) and the cellular labile iron pool (Lambda) are reduced aby bout 18% for each percentual increase in the daily blood loss.
The iron export from the liver cells through ferroportin is also reduced by 20% for one

percent loss of red cells. It was also observed that the level of ferroportin loaded with iron molecules (Fpn1) is reduced; even on simultaneous decrease in the expression of hepcidin, which is known to reduce the expression of ferroportin.
A parallel reduction can also be observed in muscle cells. Ferritin iron (Phi 1) and the labile iron pool (LIP) are reduced by 20% for each percentual increase in the daily blood loss. In addition, the absorption through Transferrin receptor 1 (v1) and export through ferroportin (w6) are also reduced as the same proportion as the iron storage pools (figure 3.8).

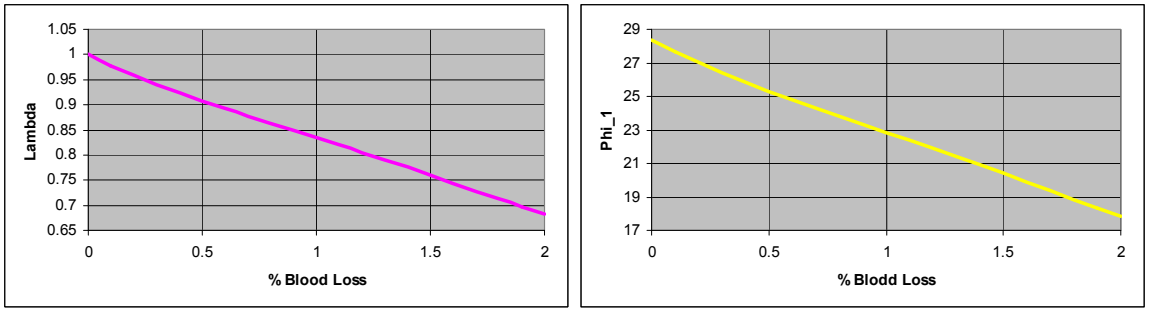

Figure 3.8: The reserves of iron are linearly depleted with increases in the daily loss of iron. Both forms, ferritin and free iron (Phi 1 and Lambda) have their levels decreased with increased loss of red cells.

3.2.5 Absorption

The absorption of dietary iron in the duodenum is mediated through DMT1 (m0 and m1 variables in our model). Its flux, termed v5 as panel in fig. 3.7, increases with a saturation-like curve witzh the daily loss of red cells, reaching a plateau after 1.8% daily blood loss. With 1% daily blood loss, v5 increases 68% and its plateau is achieved after 80% increase in the dietary absorption.
Due this high increase in dietary iron absorption, the iron stores in ferritin form (Phi1) and the labile iron pool (Lambda) also increase correspondingly with increases in blood loss. For a 1% increase in blood loss, we observe an increase of 50% in Phi1 and Lambda. However, they also reach a plateau after about 1.8% daily blood losses.
The iron export to the plasma is also increased in this blood loss scenario. It was observed that with 1% increase in blood loss there is a 68% increase in iron export from the cell.

3.2.6 Excretion

The excretion of iron from the body happens through 2 distinct mechanisms: by loss of intestinal mucosa cells and by skin desquamation (integument).
From our simulations we observed that with increases in the daily loss of red blood cells (and consequently less iron circulating in the body), the excretion of iron is diminished. This decrease in iron excretion can be observed in equal proportions both in intestine and in the integument. For a percentual increase in blood loss, the flow of iron from the body to outside (flux w13) is reduced by about 20%.
In addition, it can be observed that the iron stores in the intestine and in the skin are also reduced. Both ferritin iron (Phi 1) and the labile iron pool (Lambda) decrease by more than 20% for each percent of daily loss of red cells.

3.2.7 The new steady state

The new steady state in our simulations, after a slow ultimate drift, would be reached after many days from the beginning of the daily blood loss.
The half-time necessary to achieve the steady state with a 1% blood loss would be around

29 days. With a greater daily loss (2%), the half-time necessary to achieve the steady state would be around 89 days (figure 3.9). This new steady state has different levels of red cells, well below the reference values.

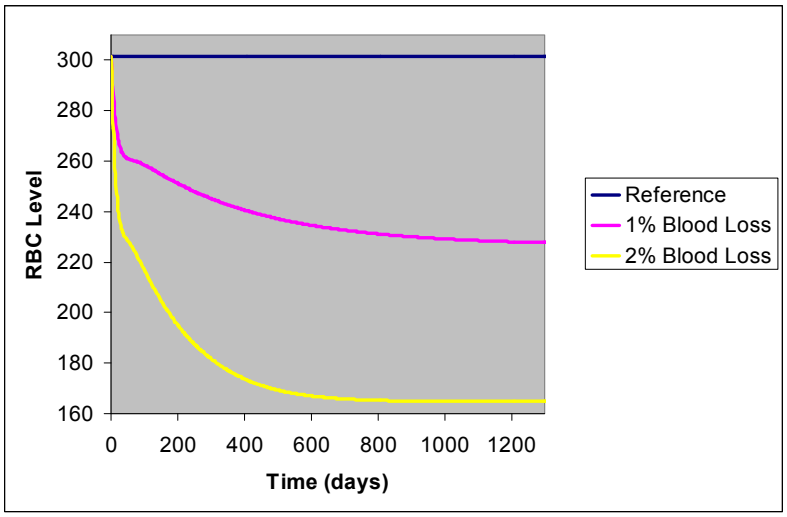

Figure 3.9: Time necessary for the model to establish a new steady state with a daily loss of iron. As was demonstrated in the previous sections, the dietary uptake to compensate for this new daily loss is increased but does not overcome totally the demand for new red cells. Therefore, a new state exists were there is less circulating red cells than the reference levels.

3.3 Analysis of changes in dietary iron supply

3.3.1 Absorption

With changes to parameter K5 of our model, the flux v5 (absorption of dietary iron via DMT1) is either increased or decreased. It can be observed that the value of v5 increases exponentially with changes in K5. Increasing or decreasing the value of K5 by 50% causes a change of 20% (figure 3.10).
The iron stores in the cell, either in ferritin form (Phi 1) or in the labile iron pool (LIP) are also increased or decreased according to the amount of dietary iron absorbed by the intestinal cells. Doubling or reducing the amount of available dietary iron causes an increase by 12% of Lambda and Phi 1.
The export of iron from intestinal cells is also increased or decreased by 20% respectively for higher or lower values of K5.
While the stores and the iron export from the cells increase with greater values of K5, the opposite happens with the amount of active IRP in the cell (Yeff, representing a sum of IRP1 and IRP2). It can be observed that with lower dietary iron supply, the amount of Yeff is more than linearly increased. This happens because with less iron available in the intestinal cells two processes related to IRP are reduced: first, the conversion of IRP1 from its active form into cytosolic aconitase and second, the degradation of IRP2, which happen with iron levels above a certain limit (figure 3.10).

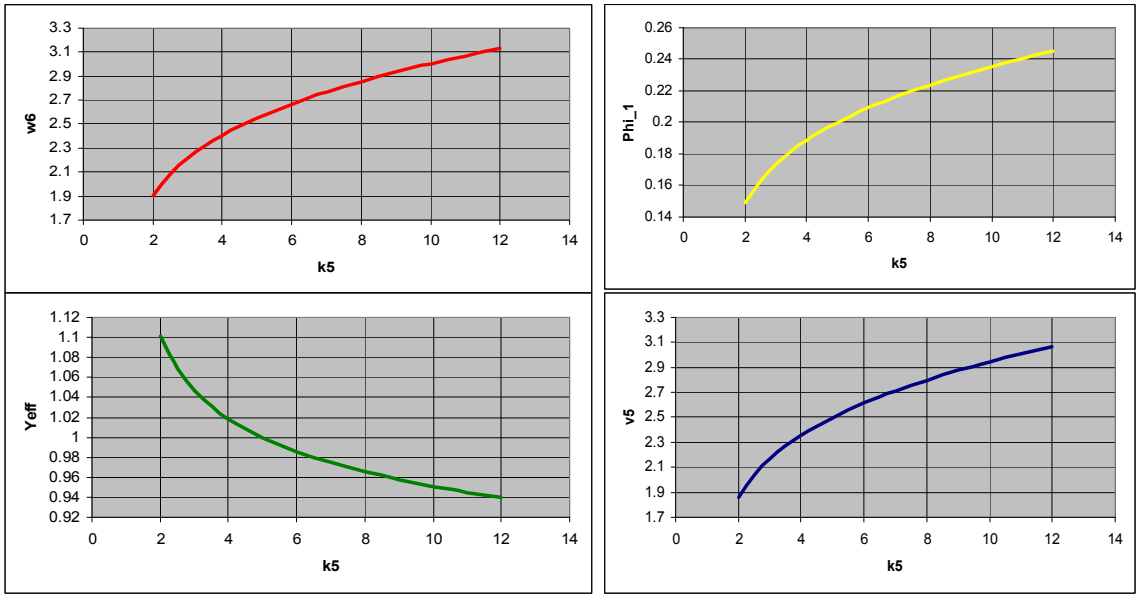

Figure 3.10: Relation of changes in the dietary iron supply (flux v5, controlles by parameter K5) and iron fluxes/storage/regulation. With increased iron supply, the levels of ferritin iron and iron export through ferroportin are increased. Meanwhile, the activity of the IRP system decreases due degradation of IRP2 and conversion of IRP1 to its aconitase form. Note that the reference level of the model is at K5=5.

3.3.2 Erythropoiesis

The increased transfer of iron from the duodenum into the circulation is accompanied by greater transferrin saturation. The opposite also holds, decrease in dietary iron supply leads to lower transferrin saturation. In quantitative terms, in both directions, either increasing or reducing the dietary availability of iron by 50% changes the ratio tao1 / (tao1 + tao0) by 12% (Figure 3.11).
It was observed that with decreased iron supply from the diet there is a rise in the EPO levels. This increase results in more TFR1being expressed in the bone marrow. However, even with increased levels of this receptor, the supply of transferrin iron from the circulation is decreased, since the level of transferrin iron is reduced under lower dietary iron supply.
The storage of iron in its ferritin form and in the labile iron pool is also reduced in bone marrow in the case of lower dietary iron supply. This decrease is not drastic, since the reserve of iron in the bone marrow is relatively small by comparison with other organs like liver or spleen (figure 3.11).
Ultimately, the production of heme in the bone marrow is increased or decreased in the case of higher or lower dietary iron supply, respectively. The change leads to higher production of red blood cells, which are increased or reduced in 10% for 50% more or less dietary supply, respectively (figure 3.11). This tendency would be damped by a higher cooperativity (exponent of power law) of the EPO-loop as so far assumed in the model.

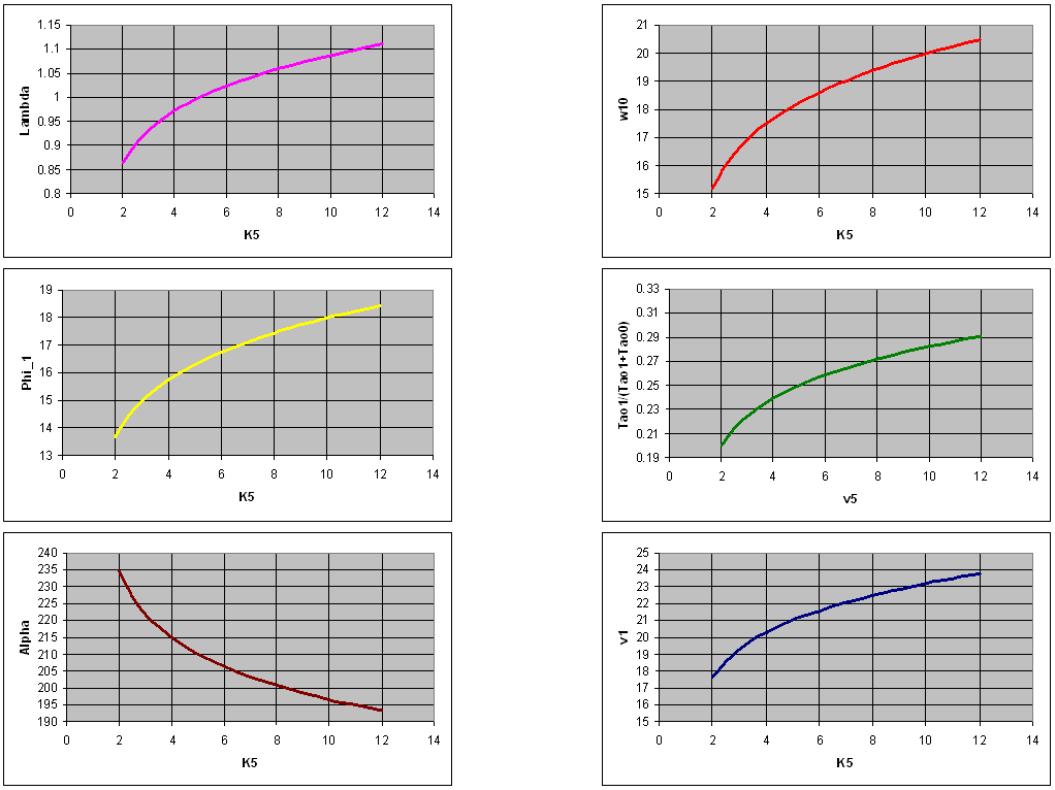

Figure 3.11: With increases in duodenal iron supply, there is an increase in the iron absorption in the bone marrow through TfR1, its ferritin stores also increases and consequently the RBC levels are also increased. However, the expression level of TfR1 (alpha) at the cell membrane is diminished due the decrease in the EPO levels. In addition, the transferrin saturation is also increased, providing more iron to every organ in the model with exception of RES (which receives more, but indirectly). Note that the reference level of the model is at K5=5.

3.3.3 Recycling

With increased or decreased iron supply by the diet, the absorption of iron by the RES macrophages is also either increased or decreased. The flux v7, which represents the sum of RES iron uptake from senescent red cells and from bone marrow, due toineffective erythropoiesis follows the same trend as the flux v5 from duodenum (figures 3.10 and 3.12). In addition, the stores in the RES are also reduced in case of lower iron supply in the diet. This reduction in both forms of cellular iron (ferritin and labile iron pool) is very strong: changing the iron supply by 50% causes changes in Phi 1 and Lambda by 66 and 40% respectively.
It can also be observed that the release of iron from RES is also decreased in case of reduced iron supply by the diet. However, for a change of 50% in the dietary supply, there is a change of just 10% in the level of iron export from the RES.

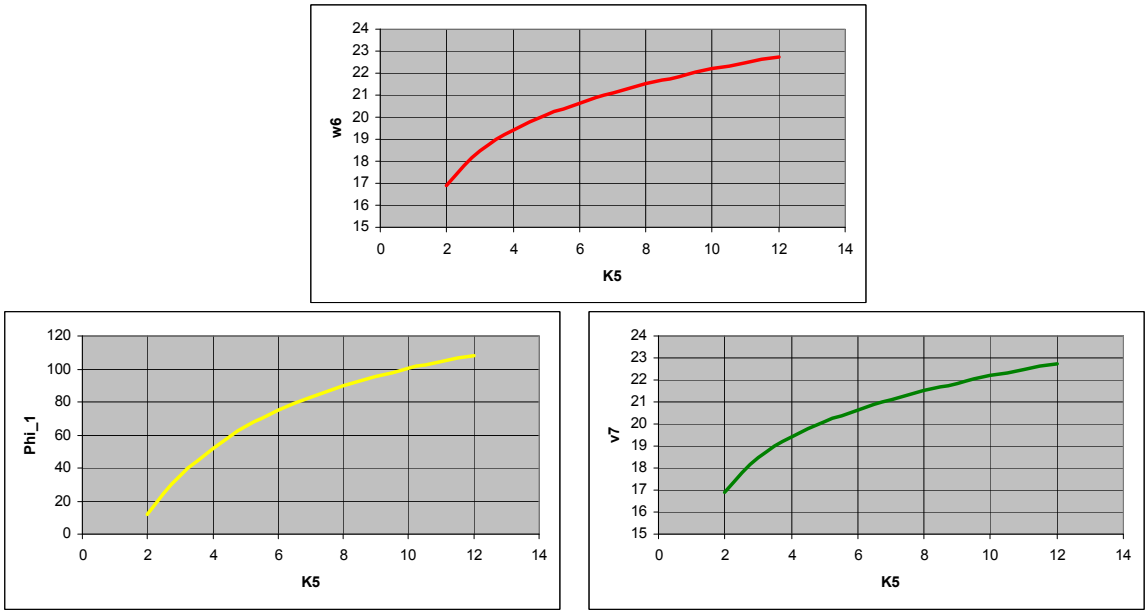

Figure 3.12: With increased duodenal absorption there is an increase in the iron supply in the RES, due ineffective erythropoiesis. It can also be observed that the ferritin level in the RES system is also increased. The same happens with the export of iron to blood plasma, it follows the same trend as the two other previous indicators. Note that the reference level of the model is at K5=5.

3.3.4 Storage

In a scenario of reduced iron supply from the diet, the body stores present mainly in the liver will also be depleted. Both forms of iron, in its ferritin form and also as labile iron pool are reduced according to the decrease in iron supply in the intestinal cells. Changing the dietary iron supply in 50% causes a change in lambda and Phi 1 by 10 and 14% respectively.
In addition, the export of iron from liver cells is also reduced in the case of lower duodenal iron supply as can be observed in figure (figure 3.13).

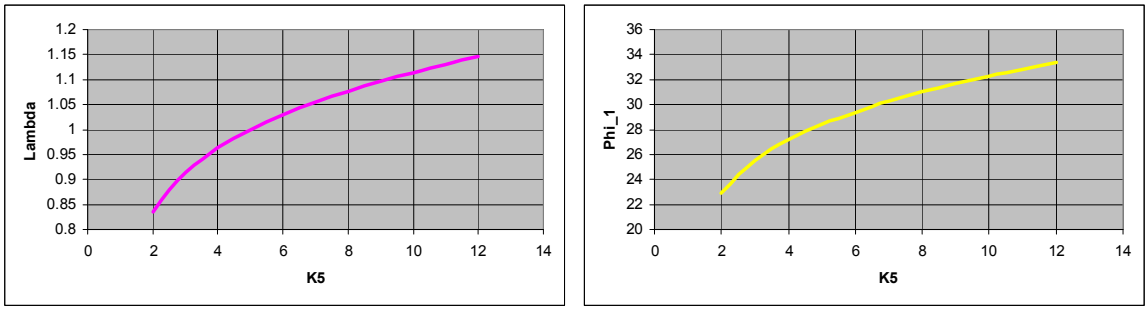

Figure 3.13: The reserved in the liver and muscles are increased with higher duodenal iron absorption. Iron in its two forms present in our model, ferritin and the labile iron pool have higher values after changes to the duodenal iron supply. Note that the reference level of the model is at K5=5.

3.3.5 Excretion

Iron losses from the body are also reduced or increased according to the amount of iron absorbed from the diet. In organs like the intestine or the skin (integument), the iron stores in ferritin form or the labile iron pool are either increased or decreased, following the same trend of the flux v5 in the duodenum (figure 3.14).
In our model, we can observe that the iron excretion from the body, represented by the flux

w13, is also increased or decreased on higher or lower dietary iron absorption. Changing by 50% the amount of iron absorbed in the duodenum causes a change of 18 and 14% in the rate of iron loss in the integument and intestine, respectively (figure 3.14).

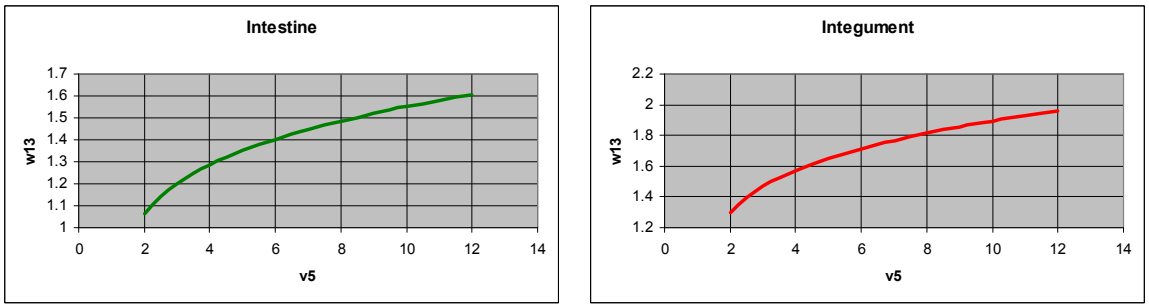

Figure 3.14: With increased iron levels in the body, the excretion level through skin desquamation and mucosal exfoliation are also raised. Note that the reference level of the model is at K5=5.

3.4 Hepcidin Studies

3.4.1 Hepcidin seems not to be active in Liver Hepatocytes

Ramey and collaborators [75], have published experiments. where hepcidin targeted ferroportin for degradation in liver hepatocytes. If this would be operative in our model, then a hepcidin knock-down should lead to higher expression of liver ferroportin and consequently to lower iron levels in this organ. This would not explain , however, the observed in crease [76-78] of iron in hepcidin hemochromatosis. The paper [79], on the other hand, suggests that the hepcidin effect is different dependent on the target organ. In our model it can be shown (fig. 3.15) that with hepcidin acting in liver hepatocytes, there is no increase in stored liver iron, compared with the implementation where hepcidin acts only in RES and duodenum.

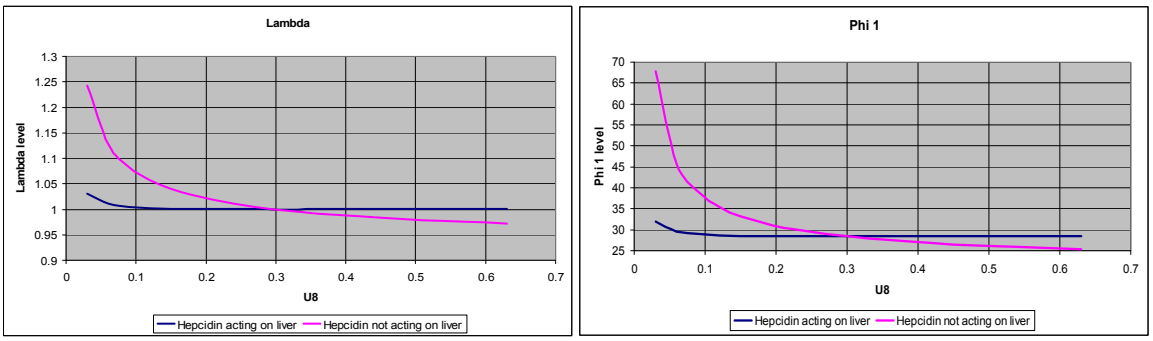

Figure 3.15: Comparison of different model configurations. If hepcidin also targeted ferroportin in hepatocytes for degradation, there would be not enough iron accumulation to characterize the iron overload reported in several studies [76-78]. Note that the reference (normal) level of hepcidin expression is at U8=0.3.

3.4.2 DMT1 and ferroportin expression changes

As demonstrated in two different studies [53, 79], the increase in hepcidin levels leads to a decrease in the expression level of DMT1. It can be observed that with increased levels of hepcidin, the level of DMT1 is reduced by about 10% and with steps toward a hepcidin knock-out mouse there is an increase in the level of DMT1 by up to 50% of its original value (figure 3.16).
The level of ferroportin in the duodenum is also inversely correlated with the level of

hepcidin in the organism [53]. “Level of hepcidin” in the organism is ambiguous, when related to blood or urine measurements [80, 81]. It probably refers to the total production in a given time period, and therefore a measure of the turnover rate. Changing the expression levels of hepcidin in our model we obtained the same as their study: reducing hepcidin we observe an increase in the expression level of ferroportin (figure 3.16). This increase in iron transported was also confirmed experimentally by [77].
Reducing the level of hepcidin we observe an increase in the expression of ferroportin, leading to an increase in the iron transport from the basolateral membrane to the plasma (figure 3.17).

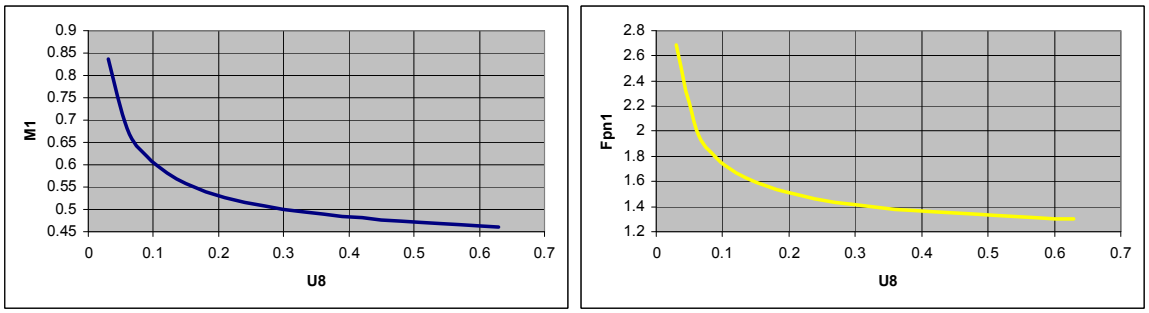

Figure 3.16: the increase and decrease in hepcidin expression is inversely followed by expression levels of DMT1 and ferroportin in duodenum. Near an absolute lack of hepcidin there is an exponential increase in the expression of those two proteins. Note that the normal level of hepcidin expression is at U8=0.3.

3.4.3 Iron in Spleen

According to [78] and [77] in case of lack of hepcidin it can be observed that the iron level in the spleen is decreased. In our simulations we could observe the same effect (figure 3.17), decreasing the hepcidin levels there is a correlated decrease in the ferritin iron stores in spleen (Phi1).
This decrease in the iron stores in the RES can be explained by the increase in ferroportin levels and consequently the efflux of iron from the spleen macrophages. This was also confirmed experimentally by [78] and [77] and can be seen in (figure 3.17). However, these results are in conflict with the findings of [76] who observed no changes in the RES iron stores of mice not expressing hepcidin as consequence of the ablation of the HFE gene.

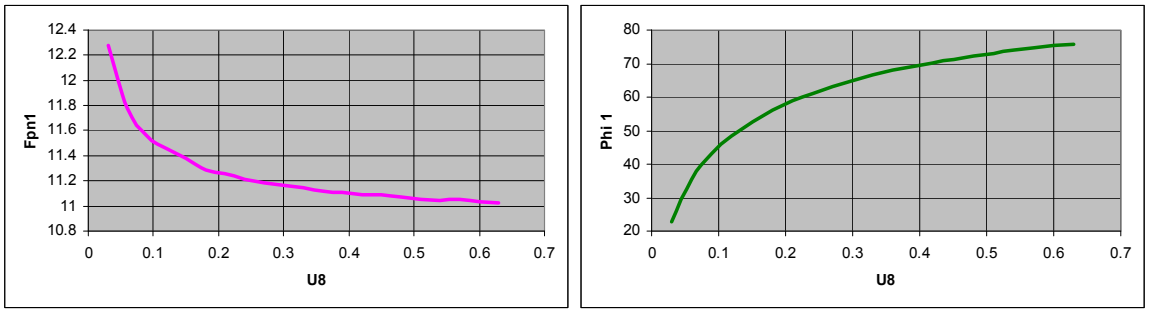

Figure 3.17: with lack of hepcidin there is an increase in the levels of the membrane iron transporter ferroportin. Consequently the ferritin iron stores in the RES are decreased. Note that the normal level of hepcidin expression is at U8=0.3.

3.4.4 Transferrin Saturation and Erythropoiesis

It was reported [78]) [76] that the transferrin level of mice lacking hepcidin expression is increased. This could be observed in our simulations where the level of transferrin saturation (Tao1 / (Tao 0 + Tao 1) in our model) increased according to the reduction of hepcidin in the organism (figure 3.18). This is a characteristic of hemochromatosis and an indicator used to diagnose this disorder.
However, those same studies reported that there were no changes in the level of RBC in mice lacking hepcidin expression. In our model that there is an increase in the level of RBC in mice lacking hepcidin. However, the increase is not very high until the level of hepcidin is extremely low, a most severe condition where other factors not included here may interfere. Therefore, from (figure 3.18) we may conclude that the problem could be solved in future versions of the models by adapting the cooperativity parameters of EPO signaling or changing the kinetic equations in the expression of TfR1 in bone marrow.

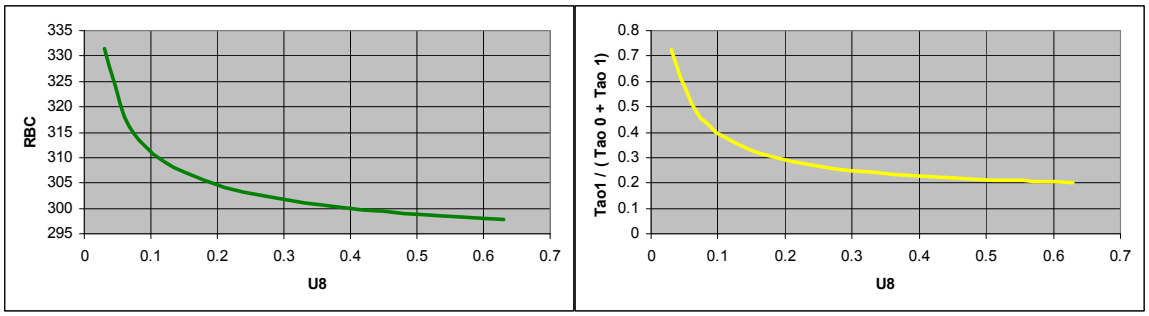

Figure 3.18: at very low values of hepcidin expression we can observe an increase in the erythrocytes and in the transferrin saturation. These two events are related since with higher serum iron there is more uptake by the bone marrow, which produces an increased number of red cells.

3.5 IRP Studies

According to several studies [44, 82], IRP 2 dominates the intracellular iron homestasis in mammals. The mentioned studies performed IRP 1 and IRP 2 ablations and concluded that in most part of tissues IRP 2 expression can be increased in order to compensate the lack of IRP 1. However, the opposite is not true: in absence of IRP 2, IRP alone is not able to maintain alone the control of TfR1, DMT1 and ferritin levels [44].
This feature was implemented and tested in our model. In the reference state IRP1 exerted an effecte that was responsible for 5% of all IRP activity in the cells, while IRP 2 was responsible for the other 95%, in agreement with [56].
With those values we were able to simulate and observe most of the results reported in the literature. Below is a summary of our observations and comparison with the literature.

3.5.1 Transferrin Saturation and Erythropoiesis

The transferrin saturation in our model expressed by (Tao1 / (Tao 0 + Tao 1)) was not changed when we changed the expression of IRP 1 or IRP 2 to either lower or higher values (figure 3.19). This observation is accordance with the studies of [83] and [42].
In addition the RBC levels are reduced when there is a decrease in IRP 2 expression (figure 3.19). This observation was also reported by [83] but not by [42], who mentioned that there the RBC levels were unchanged in IRP2-/- mice.

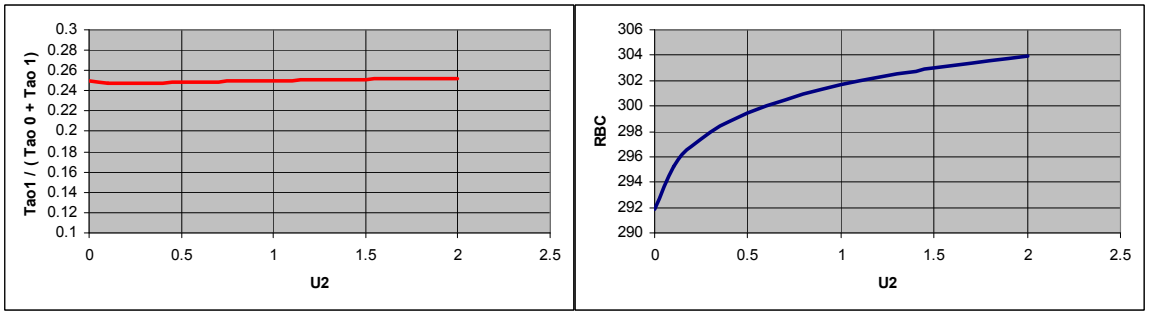

Figure 3.19: with lack of IRP2 expression in tissues there is a decrease of RBC despite the fact that no change can be observed in the transferrin saturation. Please note that the normal level of IRP2 expression is at U2=1.0.

3.5.2 Duodenum

In the study of [83] it was observed that the level of ferritin heavy and light chains change when there is a lack of IRP 2 expression. But we do not differentiate in our model the two different isoforms of ferritin, we could observe that there is a decrease of this protein when we simulate an ablation of IRP 2 (figure 3.20).
Two differences between our model and the experimental results published by [83] refer to the levels of DMT1 and ferroportin. In their paper, they report that in the IRP2-/- mice, the level of DMT1 and ferroportin is unchanged. However in our model we observed that the level of DMT1 is decreased with lower expression levels of IRP 2 (figure 3.20). This difference can be due the different isoforms of DMT1 (with or without IRE, alternative splicing. [84]). In addition, in a different study where a conditional knock-out targeting only the IRP system in the intestine was made [85], it was observed that DMT1 is decreased, in accordance with our simulaion.
The same happens with ferroportin level, where [83] report that it is unchanged and in our simulation we found it to be decreased with lower IRP 2 levels (figure 3.20).
These differences confirm the point of view of [44] who pointed out that there are important characteristics that are not totally understood regarding the role of IRP1 and IRP2 in different cell types.

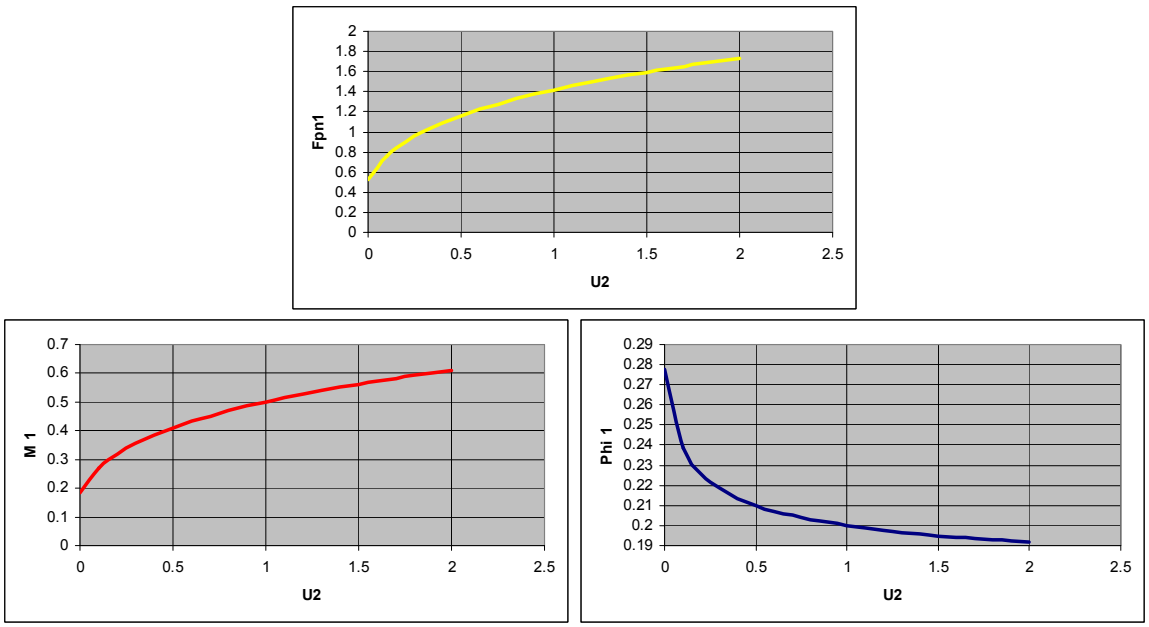

Figure 3.20: with lack of IRP2 expression there is a decrease in ferroportin and DMT1, however, there is an increase in the level of ferritin iron which corresponds to the observations of [83]. Note that the normal level of IRP2 expression is at U2=1.0.

3.5.3 Liver

Simulating the ablation of IRP 2 gene in the whole organism we observed in our model an increase in the level of ferritin in the liver (figure 3.21). This observation is in accordance to the experimental studies of [83] and [44].
In the study of [83] it was also reported that the level of TfR1 in liver hepatocytes is reduced under lower expression of IRP2. This characteristic could be also observed in our model (figure 3.21). Since IRP2 exerts a protective role in the mRNA of TfR1, it is expected that there is a decrease in the protein level of this transporter.
The hepcidin levels in our model and in the experimental model of [83] are also in accordance. In their work they reported that there is a slight increase in the expression level of hepcidin, but it was not high enough to be statistically significant. In our model we have the same: there is an increase but not enough to be considered important (figure 3.21).
The only divergence between our model and the experimental work published by the above-mentioned authors refers to the ferroportin level. They report that there is no difference in the expression level of ferroportin in the liver of IRP2 ablated mice, while our theoretical simulations show that the level of ferroportin would be severely reduced under lower expression of IRP 2 (figure 3.21). Since the IRP system has a protective role over the mRNA of ferroportin it would be expected that the level of this protein would be reduced. This discrepancy sugggests the existence of a modified biological mechanism for the regulation of ferroportin in hepatocytes. This mechanism was not yet found. It may involve different preferences for IRP 1 in this molecule and cell-type.

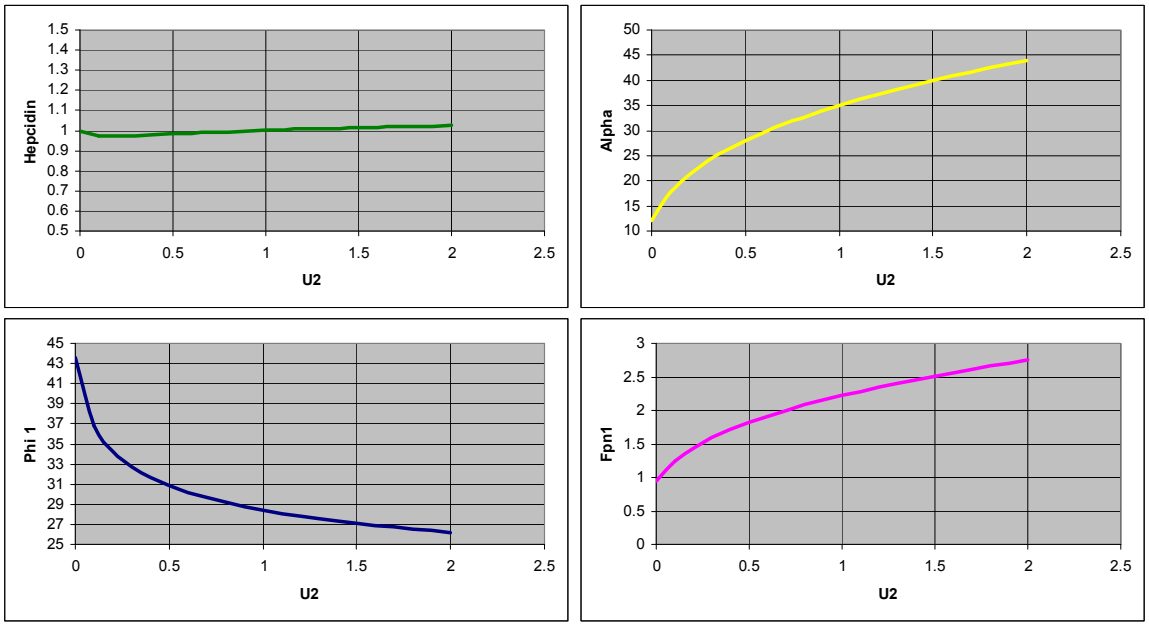

Figure 3.21: with lack of IRP2 expression there is a decrease in ferroportin and TfR1, since the IRP system provides protection of the mRNA of those genes against degradation. However, just the decrease of TfR1 is in accordance with [83]. There is an increase in the level of ferritin iron, in accordance to the experimental work of the same author. In addition, there is no change in the hepcidin level. Note that the normal level of IRP2 expression is at U2=1.0.

3.5.4 Spleen

There is some divergence between the observations in the spleen compartment of our model and the measurements on spleen reported by [83]. They reported that the level of ferritin iron in the spleen decreases under IRP 2 ablation. In our model the opposite effect obtained: the level of ferritin increased. In addition, the same authors report that the level of ferroportin is also decreased under this mouse construct, while in our simulations we

observed that the level of ferroportin is not changed with lower IRP 2 expression values (figure 3.22).
The only agreement between our model and the experimental data concerns the iron acquisition by the spleen. In our model this originates as “ineffective erythropoiesis”. Galy and collaborators [83] report that this acquisition is reduced in IRP 2 ablated animals and the same observation was made in our simulations (figure 3.22).
Again, these differences direct us to the conclusions of [44] who pointed out that there are characteristics that are not understood the IRP system in different organs.

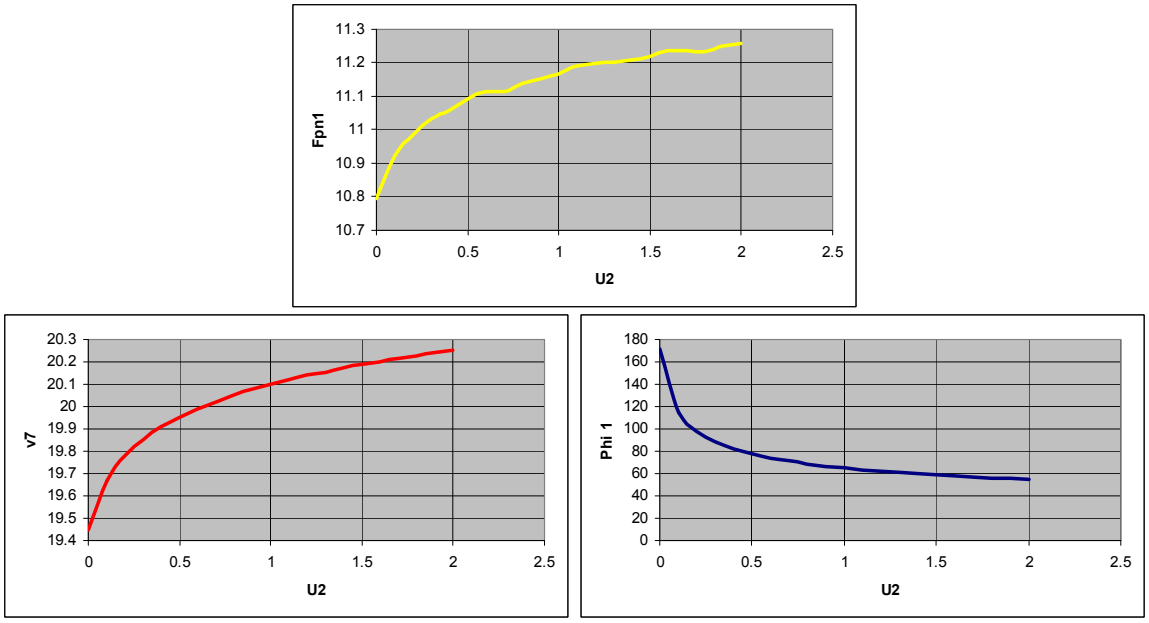

Figure 3.22: with lack of IRP2 expression there is a decrease in ferroportin and in the iron acquisition. It can also be observed an increase in the ferritin levels in the spleen macrophages which is not in accordance to the literature. Note that the normal level of IRP2 expression is at U2=1.0.

3.5.5 Bone marrow

In the studies of [83] and [42] there is one point of agreement and one of divergence. Both reported that in erythroid precursors the level of TfR1 is reduced in mice with IRP 2 ablation. This is also in accordance with our simulations and can be explained by the fact that the IRP system prevents the mRNA of TfR1 of getting degraded (figure 3.23).
The observed fact that is different between the two papers deals with the level of ferritin protein: while [42] reports that the level of this protein increases, [83] observes that its level did not change with IRP 2 ablation. Our simulations are in accordance with [83], since we observed no change in the level of this protein (figure 3.23).

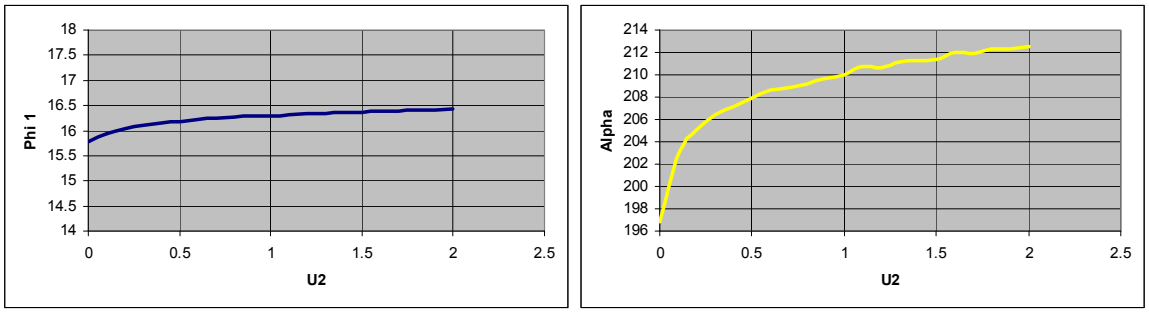

Figure 3.23: In IRP 2 knock-out mice there is no change in the level of ferritin iron in the bone marrow. However, there is a strong reduction in the level of TfR1. Both observations are in accordance to the study of [83]. Note that the normal level of IRP2 expression is at U2=1.0.

3.6 IRP and Hemochromatosis

In the study of [82] it was reported some interesting characteristic was reported between the interaction of the IRP system and the lack of hepcidin expression in patients suffering from hereditary hemochromatosis.
The first is that in macrophages and monocytes of HH patients there is an increase in the level of IRP 1 and IRP 2. In our model the effect of both IRPs is summarized in the term Yeff. We can observe in (figure 3.24) that with lower expression of hepcidin there is an increase in the level of effective IRP in spleen macrophages, observation which is in agreement with the experiment.
The second fact reported by [82] is that in the duodenum of both anemia and hemochromatosis patients there is an increase in the level of IRP activity. In our simulations we could also observe the same effect. Reducing the expression of hepcidin or reducing the intake of iron from the diets caused the pathological effects and could explaion the values of IRP activity in duodenum (figure 3.24).

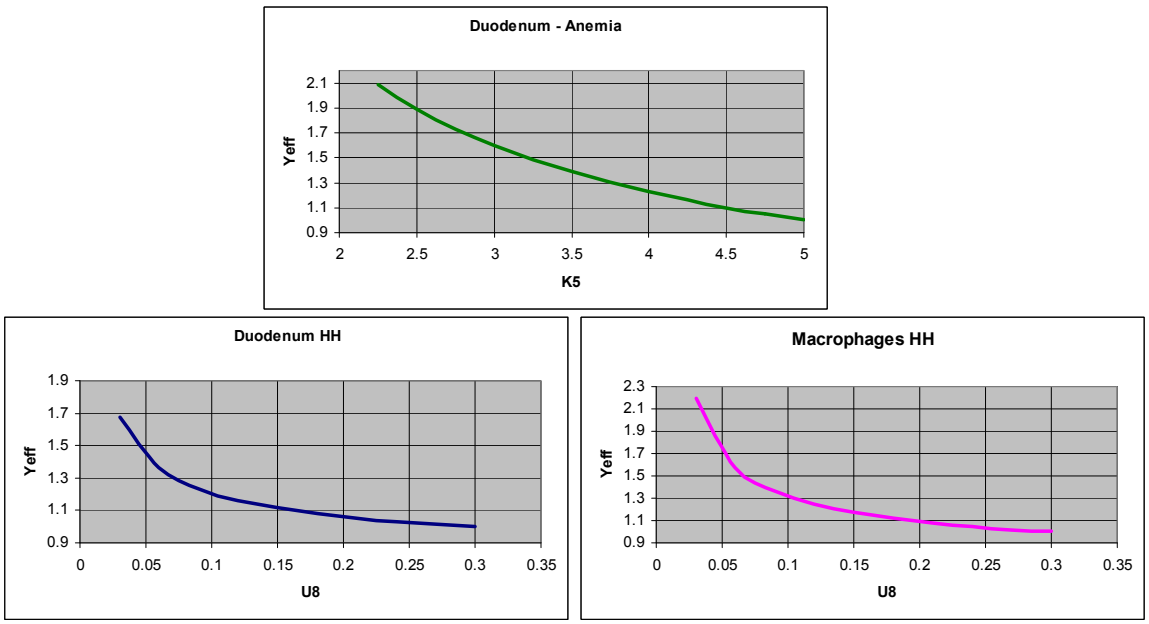

Figure 3.24: In the duodenum of hereditary hemochromatosis or anemic patients there is increased activity of IRP activity. The same happens in the macrophages of patients with hemochromatosis. Please note that the normal hepcidin level occurs with U8=0.3 and the normal daily food intake is settled at K5 = 5;

4 - Discussion

4.1 Mathematical Model of Iron Metabolism – General Structure

The vital importance of iron for redox catalysis and oxygen handling and its strong toxic potential of its radical-forming capacity require a very carefully fine-tuned regulation of absorption, excretion and inter-tissue distribution as well as of cellular balance and intracellular deployment for biosynthesis and storage. A systems biological approach to understanding this complexity requires the application of a mathematical model which integrates the molecular and cell-biological detail in a way that makes the regulatory structure transparent. Ingenious interpreting work has so far been done on a qualitative level, but a full quantitative description of the cellular and organismal hierarchy is still missing. In the work presented here a first such model is presented for the iron metabolism of the mouse strain C57BL6. This is the most widespread and best characterized model animal for studying organismal status and transgenically constructed pathology of iron metabolism.

From a technical point of view the model presented here follows a standard methodology of systems biology. We envisage the organism as an aggregate of organs and tissues, each of which represented as an idealized compartment, consisting of a given number (or volume) of cells. Transport into and out of a compartment and the interconversion of its elements is described as a network of metabolites and reactions, characterized by well-defined biochemical and biophysical status and interconversion descriptors. Metabolites are quantified by content (or “concentration”), and the dynamics of transfer of “substrate” into “product” is quantified by a reaction rate. The reaction rate is a function of the content in partaking metabolites and contains parameters of the catalysts and the signals (inhibitory or activatory) that influence the interconversion. The whole system´s dynamics is then described by a balance sheet of differential equations which usually are linear combinations of the reaction rates according to the stoichiometric matrix of the system.

This theory has envisaged metabolic systems as a kind of “well-stirred” biochemical reactor. It has been applied to holistic descriptions of E. coli, yeast cells and erythrocytes [86] [87-89]. For more complex eukaryotic cells the basic tenets of the theory, especially compartment and reactant homogeneity, are not given, and the description has to introduce subcompartments or has to integrate over the whole cell. In a cell with multiple subspaces embedded in a membranous structure filled with organelles and a certain content in macromolecules the description is bound to become phenomenological, assuming that a system can be quantitatively described in the conceptual framework of a cellular reactor, where the compartments, the variables and the parameter definitions and their numerical values are valid as a weighted average over the object considered.

Iron metabolism has some special properties that render such an idealized description applicable, and it has other features which introduce specific restrictions. The typical iron content of a cell, when expressed as if it were a homogenous water solution, is in the millimolar range (for instance 120 mg non-heme iron per kg liver, or, for that matter, 3 mg iron for 50 l water of a 70 kg human body [90]), but the cytosolic “concentration” of LIP (labile or transit iron pool) is in the micromolar range at most [26]. The bulk of iron is bound to specific protein carriers (below the micromolecular range), most of them containing per molecule only one or a few iron molecules (such as transferrin or myoglobin). Only ferritin and hemosiderin are able to corral up to 4500 iron atoms per macromolecule fold. It is evident that a kinetic description in classical terms does not apply in such situations, and only a phenomenological “quasi”-description is possible that has to justify itself by the criterion of “producing the global phenomena”.

However, there are features that greatly simplify an adequate systemic description. One point in case is that fact that iron is inorganic and therefore alien in the ocean of bioorganic matter. So only few specific proteins or translocators of iron (and other metals) need to be considered. A second point is that iron is as Fe (II) or Fe(III) always in electrostatic coordination rather than in covalent bond, so the number of kinetically relevant biochemical states, although as prosthetic group present in multifarious protein entities (more than 100 species coded for in the whole genome [91], is limited in terms of metabolic turnover. Most of the states of iron bound to specific proteins are now well known and easily traceable by physical measurement. A further point is the residence time of most iron atoms in active cells is longer than the life-time of the carrier molecules (e.g. about 7 days vs. 1 day in liver), so one can assume that the binding/releasing cycle as well as the renewal of protein carriers is close to steady-state.

4.2 Structural and Kinetic Hierarchy of the Model

The structure of the model is a set of peripheral organ and tissue compartments connected via a central compartment. The relative organ weight is the factor that integrates the compartments to a whole system. Each cell type is contains three levels of intertwined kinetic representation: material transfer of iron, synthesis and decay of the protein arsenal, and the regulatory superstructure (mainly IRP/IRE system). On the organismal scale there is the exchange flux into and out of the central compartment and the global absorption (via duodenum) and loss of iron (several organs), the turnover of the transferrin carrier and the regulatory superstructure (hepcidin for the iron household, and erythropoietin for the erythron). Hepcidin as a hormone has a similar function for global homeostasis of iron as has insulin for carbohydrate homeostasis. Both act as a feedback signal produced by a sensor cell reporting a high level (hepatocyte and pancreas ß-cell, respectively), and both exert their main effect via a membrane receptor in certain cell types (ferroportin vs. insulin receptor).

Compartment content and within- and inter-compartment transfers and fluxes are the main kinetic elements of the system. Simple linear kinetics has been installed for the turnover of the protein arsenal. The elementary kinetic formalism for material iron transfer is a rate law bilinear in iron content and in protein acceptor level for iron binding and a linear rate of iron release. Where regulatory signals have been experimentally demonstrated to be operative the basic rate law is multiplied by a simple signal expression (power law). Since the hormonal signals are triggered and exert their effect with a considerable gain we chose the exponent of the power law greater than unity. For the cellular IRP/IRE a value of unity was sufficient, since the experimental background was only qualitative. Anyway, the effect of a high exponent in a steady-state system is mainly the swiftness of concentration jump in order to trigger an effect. As is well known, high non-linearity introduced by steep signals in metabolic systems may produce alternative states or oscillations, but our system has only one potential positive feedback loop (i.e. back effect of hepcidin on the liver), but there is no indication so far that the system may run over a bifurcation surface (i.e. over a structure in the parameter space where the qualitative behaviour makes a sudden jump).

The quantitative domain in which each cell metabolism is operating is set by the experimentally measurable content of the major iron fraction as well as the distribution of radioactive tracer into the organs and back into the central compartment. For the non-transferrin part of iron transport (haptoglobin- and haemopexin-borne) there were not enough quantitative data available, and it had to be modelled therefore only cursorily. The intracellular steady-state structure of most iron-related pathways, due to the nanomolar content level of the individual iron-carrying proteins, made it possible to apply the integrative

assumptions, i.e. aggregation of kinetically similar reactions into one component (e.g. haemo- and myoglobin synthesis, mitochondrial iron uptake, iron-sulfur biogenesis), and normalization of contents and fluxes to a common reference state (adult healthy mouse on adequate iron food). Any further specification of the model must await corresponding quantitative determination as experimental input.

What can be expected and what cannot be achieved with a kinetic model as presented here?
The answer is:

- a quantitative representation of the iron status, globally as well as for specific cell types,
- a quantitative representation of the major iron fluxes into and out of the major tissues,
- a qualitative evaluation of the regulatory structure within and between cell types, in particular the interaction of local and global feedback signals,
- and certain global switches (e.g. between iron supply for the erythron and into the parenchymal iron stores.

This can be done for the reference state of the normal mouse, but also for certain perturbational variations:

- different iron supply,
- acute and chronic blood loss, application of chelating therapy)
- structural changes (e.g. brought about by genetic mutation, spontaneous or experimentally constructed).

This can be studied either by variation of the boundary conditions (e.g. acute loss from the RBC compartment) or of the parameter structure of the model. Parameters may be varied as a jump (as if by a gene knock-out) or by continuous variation that makes it possible to adapt the model structure to realistic measurements. The parameters of the models belong to three classes:

- of kinetic property (e.g. to simulate a mutation in an iron-carrier or transporter),
- of gene expression (e.g. to simulate a knock-out or knock-in), and
- of regulatory power (e.g. to simulate interference into a signalling chain).

In what follows we discuss the results that we have obtained for establishing parameters from flux and content measurements *in vivo*, of physiological inferences that can be made from such estimates, and of computer experiments of acute and chronic changes of the model structure compared with explorative simple simulations.

4.3 Model Parameterization from Experimental Data: Iron Status and Fluxes

From the viewpoint of systems analysis, iron metabolism of the body is an open black-box with input, internal processing and output. Absorption fluxes and losses are relatively slow compared to internal iron circulation [90, 92]. The most relevant internal dynamic events occur within the first few days after tracer injection. They involve the plasma iron turnover and the turnover of the erythron. On this time scale the system is nearly closed, with input (absorption) and output (excretion, desquamation) being slow compared to the dominant rates of inner metabolism. Iron absorption from guts is in the range of 0.5 µg per day (calculated to whole-body scale from the data of Bahram et al. [93] and Lebeau et al. [35], whereas the rate of total plasma iron exchange with the body periphery, as shown in table 3.2, is in the range 20 – 30 µg per day. Such a system will approach an inner steady-state with slowly drifting concentrations and fluxes.

To study such a steady-state one can measure stationary content variables and inject a tiny dose of Fe^{59}, preferentially bound to its transferrin carrier [94], into the central compartment of radioactive iron. In the initial hours after mixing of the injected iron, when the periphery does not appreciably return tracer, the flow of blood into the organs is proportional to the flow of tracer. This initiates distribution dynamics of the tracer in conformity with the pools and stationary rates of the unlabelled bulk of iron in the steady-state, which is not disturbed by the addition of trace amounts. The time course of the ensuing run-off of tracer distribution obeys a system of ordinary differential equations with constant coefficients.

4.4 Iron status of the adult mice on different dietary regimes

The experimental data which form the basis for the model calculations presented here are derived in adult mice that were on different dietary regimes during growth. The adult animal develops a steady-state which is maintained during its further adult life, i.e. for approximately 1-2 years. This assumption is prerequisite for the ferrokinetic model. The empirical background for the model consists of the static iron status and of tracer dynamic data.

4.5 Modelling iron fluxes by the Fe^{59} tracer method

The literature contains numerous papers (e.g.[6, 7, 10-12]) which measured the dynamics of iron metabolism on the intact organism with the help of the tracer Fe^{59}. The basic rationale is that the tracer, while being always measurable as radioactivity, due to its tiny relative amount does not perturb appreciably the iron status of the body. Most of the mathematical models derived from such measurements were obtained for humans, dogs and rats. Only the paper by Vácha et al. [13] derived a whole-body model for the normal mouse , collected from measurements in blood, liver and spleen, without systematic control of dietary regime. The model was based on a number of ad-hoc assumptions of fluxes, which partly could not be substantiated by cellular mechanisms, and the parameters were in part estimated without a whole-model statistical fitting procedure (computer capacity-limited). We can confirm, with the experimental evidence now available, that their ingenious model, in spite of some speculative elements due to limited molecular knowledge, gives a remarkably adequate description of the global dynamic structure of murine iron metabolism

4.6 Iron status

This is defined as the iron content of the iron fractions in the different organs and tissues. It reflects the expression of protein carriers to which iron is bound (transferrin, ferritin, heme proteins etc.). We can assume that this status is stable during the ferrokinetic observation period.

4.7 Dynamic fluxes

The second data type is the time course of iron flow through body organs after administration of a radioactive tracer. The data base stems from partly published measurements of Prof. Schümann´s lab [27] and from studies done elsewhere under a comparable experimental design. The aim is to integrate the entire data set into an integrative model, thereby displaying the systemic structure which is not obvious from inspection of raw data.

4.8 Kinematic model of iron flux steady-state

The crucial supposition for a representative model is that iron fluxes in the body are (approximately) balanced and cellular pools do not fluctuate violently during the experimental period. Tracer injection permits to collect data on internal fluxes without upsetting the steady-state. Analysis of the fate of tracer-Fe^{59} in the tissues in terms of a linear system of differential equations describing influx, outflux and internal metabolism of the system gives a picture of the prevailing “kinematics” of the system, i.e. it describes what happens, not the causes and controlling mechanisms. Such a phenomenology is the prerequisite for any in-depth systemic description.

4.9 Inhomogeneity of compartments

For some important tissues under consideration the assumption of homogeneity is not valid. This applies to liver, which consists of parenchymal cells (hepatocytes) and cells of the RES (Kupffer-cells). Both types have different iron regulation. Similarly, the murine spleen has subcompartments, of erythropoietic and of macrophage cells. Muscle tissue contains a large fraction of iron in myoglobin, the turnover of which is different from that of the macrophages in muscle. On the whole, the macrophages of RES are spread over a multiplicity of organs and change their distribution in inflammation. For the sake of model calculation, nevertheless, we treated these organs as compartments.

4.10 Numerical parameter estimation

Tracer motion in a steady-state system of homogenous pools (like fig. 2.1) can be modelled by ordinary linear differential equations. In theory, the concentration of tracer in these pools follows a time course described by superimposed exponentials. In the initially labelled central compartment (plasma) the tracer content falls monotonously. In all the other compartments, initially void of tracer, the concentration rises to a maximum and then turns into a monotonously decreasing phase of recycling into plasma together with outflux out of the body. The parameter values of the interconnected system can be obtained as “best fit” according to a suitable distance criterion. In practice this estimation process may run into two types of difficulty: statistical scatter and redundancy of the parameter space.

The scatter of measured data in most biological systems is considerable and cannot be avoided. The reason is individual variation between subjects and the impossibility to exactly repeat the same experiment. A statistical model of this situation can, at best, be a close approximation to the measured data in the form of an idealized curve. We repeated the estimation procedure on sets of artificially generated data which keep the error structure of the observed data. The range of parameter variation was revealed in this way.

4.11 Interdependence (correlation) of parameter estimates

This is an unavoidable problem of complex biological models. It became clear from the ACE analysis (see methods) that our data contained two causes of parameter interdependence: insufficient resolution at very early time after tracer injection, and cases of double output of tracer back into plasma and out of the body. We overcame these problems by prescribing an approximate value of the total plasma clearance calculated from the data of Trinder et al. [33]. Furthermore, we replaced double outfluxes by a single lumped one, thus not specifying the precise fractional contribution of each pathway (see dotted outflux arrows in fig. 2.1). In

this way we obtained parameter estimates with a reasonable range of scatter avoiding strong intercorrelation.

4.12 Further parameters of the model

The set of clearance- and rate-parameters resulting from the parameterization is given in table 3.1. The quality of the fit is satisfactory, as demonstrated in figs. 3.2-3.4. Table 3.1 contains the most compact representation of the information content of the empirical data. It can be used to calculate flux rates 3.3, pool sizes 3.4 and as well as a characteristic temporal structure of the system 3.5. Figures 3.5 and 3.6 visualize these quantitative estimates. These indirectly derived data indicate ranges (not precise values) of system-relevant parameters. Their totality is amenable to physiological interpretation of the static and dynamic state of the iron system in the mouse in the different “lifestyle” regimes studied.

4.13 Physiological interpretation of the flux model

4.14 Systemic iron metabolism can be described as a closed compartment system.

The quasi-closed state of the iron system together with the ensuing internal steady-state makes into possible to simplify the non-linear structure to a system of ordinary linear differential equations. The dynamics of tracer motion depicts the statics of the underlying stationary flux-and-pool network. We could build on a number of previous attempts to model iron metabolism in this way [9-12, 95], reviews in [6, 7]. The novel aspect here is the detailed reversible balance in a network of peripheral tissues that were previously combined *ad hoc* to black boxes.

4.15 Iron metabolism is organized as temporal hierarchy on five time scales

The importance of time structure has been emphasized by Klipp [96]. We adopted the simple time scale defined in eq. 4 (methods section). Analysis of the clearance parameters of our experiments (table 3.1, transformed into residence times – table 3.5) and of literature data [23, 24, 33] lead to the following grouping of characteristic time periods:

- Rapid mixing time of the transferrin-bound plasma/ECF pool: below 1 h
- Total clearance time of plasma iron due mainly to flux into bone marrow, liver and muscle: ~ 1 hour.
- Clearance time of compartments that return tracer into plasma (descending branches in figs. 3-4): between ~2 days in the intestinal tract and ~8 days in parenchymal organs.
- Incorporation time into iron-carrying proteins in red blood cells, muscles, integument or fat: ~ 1 month.
- Characteristic life-time of iron molecules in the whole body: approaches 200 days in the adult mouse, i.e. its life expectation provided that it had the opportunity to acquire a store in the adolescent stage (adequate diet). It is therefore difficult to induce iron-depletion anemia in the mouse (contrast to humans).

The time hierarchy does not change appreciably between different iron statuses in normal mice (confirming the conclusion in [33]).

4.16 Iron turnover in the plasma compartment depends on the iron status

The concentration of transferrin-bound plasma iron in plasma is in the range of 100 -200 µg/dL in the mouse. This is similar to other mammalian species (e.g. [19, 58-61]). The iron concentration tends to lower values in iron-deficient and to higher values in iron-loaded mice. The iron clearance from plasma defines a half-time of renewal in the range of 1-2 hours, again similar for species otherwise as different as *Mus musculus* and *Homo sapiens.* Rats [61] and dogs [10, 60] are also in the same range. In rats, however, iron deficiency does not lower the plasma concentration [61].

4.17 Iron distribution into body periphery is a three-level hierarchy of flux rates

The initial tracer concentration in plasma becomes rapidly cleared within a few hours after administration and stays at a low, but steady value afterwards. This coincides with the ascending tracer curves in the peripheral compartments (figs. 3.2-3.4). The initial distribution is complete at the first time of measurement (12 h). The position of the maximum fixes the time point when plasma tracer is nearly washed out and the periphery begins to return some of the previously accumulated tracer iron into the plasma. The continuous decrease of organ tracer content begins after 12-24 hours. It is an expression of the fact that “fresh” cellular iron is not only stored or channelled into biosynthesis, but also shows an appreciable back-flow into the plasma.
The descending branch of the peripheral tracer curves show that all tissues return the radioactivity into the plasma, unless they lose it by desquamation, which is the case for intestine and integument. This characteristic pattern proves that iron flux into the periphery and reflux into plasma take place simultaneously.
The quantitative level of all the superimposed fluxes can result only from a deeper analysis of the corresponding mathematical model. This analysis yields a set of fractional clearance parameters (table 3.2). From these values and by application of the steady-state assumption all iron fluxes can be estimated when the iron content of the central compartment is available. Data by Trinder et al. [33] contribute an estimate of the total plasma turnover clearance rate (table 3.1).
Three clusters of flux rates may be distinguished (fig. 3.5):

- flux through the erythron (range of 10 to 20 µg / day per mouse)
- flux through peripheral compartments with storage function (liver, muscle, integument, intestinal tract, kidneys, lungs, heart: 0.5 to 4 µg / day per mouse)
- flux through organs with slow iron turn-over (testicles, fat, brain) – 0.05-0.08 µg per day per mouse.

4.18 Share of flux into tissues mirrors transferrin receptor expression

The clearance time of plasma iron is in the range of 1 h, largely independent of the plasma iron content and hence the state of the animal’s iron supply. This linear kinetics suggests that the total population of TFR1 receptor molecules (responsible for most of the iron uptake) works far below its maximal capacity in all cells. The share of radioiron going into the body organs reflects this tissue-specific transferrin receptor expression. In contrast to the rather stable total clearance time the share of radioiron is dependent on the

physiological state. In the states of iron depletion and of normal iron supply more than two thirds of the plasma iron turnover is directed to the erythropoietic bone marrow and is rapidly incorporated into hemoglobin. This is, again, similar to other species [6, 20, 21, 65]. The corresponding fraction of tracer iron passes through the immature cells of the erythropoietic lineage until it reaches the erythrocyte compartment.

4.19 Tracer distribution iron-rich condition reflects the switch-over to the storage mode

The flux through the storage pathway into parenchymal organs increases from 25% to 49% of plasma turnover (table 3.2; visualized in figures 3.1 and 3.5). Stores are filled up in liver, kidney, spleen/RES, to a lesser extent also heart and skeletal muscle, but not integument and brain.

4.20 Tissue cells equilibrate influx and reflux of iron to maintain the iron pool

An adult mouse does not grow much during its life-time of ~2 years (if not killed before). Iron is taken up by cells with a time characteristic of a few days and must, therefore, be balanced by corresponding iron-release. Muscle, fat, heart, lungs, brain and testicles excrete iron into plasma or extravascular fluid. The influx of tracer is mediated by transferrin receptor. It is not clear from tracer data whether the export is mediated only by the ferroportin channel [18], or also via catabolism of heme-bound iron. Ferroportin is dominantly expressed in liver, duodenum, and macrophages, and to a lesser extent also in other tissues [97]. Ferroportin is not involved in the case of catabolism of whole cells (erythrocytes, intestine, and integument). The tracer data as used here cannot distinguish between export of iron and loss of whole cells. They yield only an estimate of the total flux out of the compartment.

4.21 Intracellular residence time of iron is longer than the life time of its protein “carriers"

The life-time of the iron-storage proteins (such as apoferritin/holoferritin) is in the range of one day in the liver [98]. Up to 4500 iron ions can be stored in one ferritin molecule [69], and become released on proteolytic ferritin degradation. The residence time of iron in the liver cell, however, is much longer - in the range of 1-2 weeks (table 3.5). This shows that iron released into the very small labile iron pool does not leave the cell, but is re-utilized. This slow export conforms to well-known data showing how slowly iron is mobilized from ferritin stores to replace iron losses, e.g. after phlebotomy (in men: [66, 99]). Intracellular iron stores are no inert long-term reserves, but are continuously turned over within the cell and may therefore be directed, in accordance with changing requirements, into the three competing pathways (biosynthesis, storage, export).

4.22 Readily accessible tissue iron pools are a fraction of the non-heme iron

These iron pools are stored in different subcompartments, mainly in non-heme form. The iron-loaded liver stores ferritin in the hepatocytes and a less mobilizable (hemosiderin?) form in the Kupffer cell [100-102]. The labelled and unlabelled iron data from whole organs do not permit to differentiate quantitatively between parenchymal and macrophage iron in

such mixed cases. Tracer dynamics identifies iron pools that become quickly labelled. Their pool sizes have been estimated from the fractional plasma iron turnover and the tissue clearance rates (table 3.1 and 3.2). Three groups may be distinguished. Red blood cells contain as hemoglobin the largest readily labelled iron pool (~ 300 µg Fe per mouse, about 50% of total haemoglobin-iron, see calculation in table 3.1). There is a second cluster of pools (integument, liver, bone marrow, skeletal muscles, skin), each containing about 20-40µg Fe. In particular the hepatic iron pool is expandable in iron overload to reach a kinetic pool level of ~ 100µg Fe, presumably in ferritin form. A still larger store can possibly accumulate on a longer time scale, which is not covered here. There are additional pools with an iron content (lungs, kidneys, intestine, heart, and spleen) of about 3µg Fe, which can moderately expand up to 4-14µg. Other organs, such as fat, testicles or brain, are not able to store more iron in overload. Table 3.7 shows that in some tissues the readily accessible pools are only a fraction (6 to 40%) of cellular non-heme iron.

4.23 There are two kinetically distinct major iron pools in the mouse body

The total tracer-accessible iron amounts to ~400 µg table 3.6. The residence time in the main compartments excluding intestine (table 3.5) is between 5 and 25 days. This comprises about 20% of the total iron (i.e. of ~2 mg per 25 g body [24]). The reminder is not readily accessible. The residence time of molecules here is ~200 days [23, 24].

4.24 Iron turnover occurs at similar rate in intestine and skin, but assignment to iron loss vs. iron reflux is only indirectly estimable

Physiologically iron enters the body via duodenal and (less) small-intestinal absorption in a tightly controlled way. It leaves the body by desquamation, exfoliation of epithelial cells, by blood losses, and to a lesser extent via bile and urine [103]. The relative amount leaving the murine body is, according to literature references, 2 to 5 times larger than in other animals and man [24, 34, 58, 73, 74, 103]. A consequence of this higher excretion is that heavy iron-load is sometimes difficult to attain in mouse models.
Net iron losses cannot be measured by the tracer method as applied here. However, the fractional clearance rates (table 3.2) yield indirect information on iron fluxes through intestine and integument (table 3.3). Iron clearance of the epidermis integument is about 5% per day and that of the stomach-intestinal epithelium ca. 36% per day (calculated from table 3.2). From the fractional uptake from plasma one can calculate influx rates of ~1.7 µg per day into epidermis, and a sum of ~1.5 µg per day into intestine plus stomach (all for iron-adequate mouse, see table 3.3). These values are about 39% lower and higher in iron deficient and iron-load regimes, respectively. The data do not support a calculation of the rate of net iron loss through these compartments, because there may be a fraction that is recycled into plasma. The iron residence times for intestine are similar to the known exfoliation times of epithelium (both 3-5 days), which suggests that the main fraction goes into loss. For skin integument (iron residence about 40 days) such external information was not available.

4.25 Murine erythrocyte iron turnover has a random elimination component together with a lifespan-determined removal component

During one month after administration 60% of the tracer (40% in iron-loaded state) accumulates in the red blood cell compartment (figs. 3.2-3.4). The first quick uptake of Fe^{59} reflects passage through bone marrow and incorporation into hemoglobin at a steady rate.

The uptake reaches a saturation phase which is clearly visible in the RBC curve of figs. 3.2 to 3.4. This behaviour proves the existence of a reflux caused by a random component of erythrocyte catabolism independent of the cell age. Without reflux iron would be further incorporated even at a very low plasma radioactivity. The erythron cycle transports (table 3.3) 15;19;14 µg Fe/d into bone marrow in iron-deficient, -adequate, and -loaded animals, respectively, of which 12;17;12 µg Fe/d pass through the RBC compartment back via into RES into plasma. This turnover rate is quantitatively analogous to ~ 25 mg Fe/d per 70 kg in iron-adequate humans [87].

The life span of mouse erythrocytes has been studied in mathematical detail by Horký et al. [67]. They also formulated an age-independent linear elimination component acting simultaneously with a lifespan-determined senescence process. Our elimination rate (between 0.03 and 0.06 d^{-1}) is somewhat higher than obtained in [67] (0.012d^{-1}). However, our estimates are not very reliable, as they stem from an indirect deduction. This applies also to the size of the “readily accessible” iron pool in red blood cells (300 µg instead of the 568 µg calculated from the hemoglobin pool of the mouse, see table 3.1).

4.26 The spleen is a mixed indicator of erythropoiesis and RES activity

The murine spleen is an erythropoietic organ [64]. Therefore, one subcompartment of iron in the spleen is expected to behave similar to iron in the bone marrow. Figs. 3.2 - 3.4 show a quick uptake phase in both bone marrow and spleen. The ratio of tracer iron content between both organs after 12 h is about 50 to 60 in adequate and iron-rich mice, and 20 in iron-deficient animals. Thus, the quantitative contribution of the spleen to total murine erythropoiesis is not high. Furthermore, the iron-deficient spleen loses iron as quickly as the bone marrow, reflecting the rapid flow into “iron-deficient” erythropoiesis. In contrast to the bone marrow, the iron-adequate, and even more so the iron-loaded spleen retains Fe^{59} for long periods. This reflects a storage behaviour which is similar to that of RES cells in the liver and elsewhere. The spleen contains 5% and the liver 16% of the whole population of macrophages [30]. The RES system serves as scavenger to remove senescent erythrocytes together with their hemoglobin and colloidal iron from the circulation [9, 68]. Part of this RES iron is rapidly recirculated into plasma, thereby completing the iron-recirculation back to the erythrocyte pool. Except in iron deficiency, another part of the RES iron is stored as ferritin or hemosiderin [69].

The quantitative contribution of both spleen compartments to whole body iron turnover is low. The spleen is therefore an indicator, but not the main quantitative locus of the total erythropoietic and macrophage activity. In iron-deficiency splenic iron clearance is very rapid (15 % d^{-1}, see table 3.2), while it is distinctly slower (down to 1.9 % d^{-1}) in iron loaded mice. This may reflect distinct differences in the role of the spleen depending on the state of iron-repletion. A precise quantitative partition of splenic iron fluxes into a RES- and an erythron-fraction would require separation of the cells.

4.27 Experimental design for characterizing the iron status and the dynamic turnover of the C57BL6 mouse strain.

The C57BL6 mouse is a widely used strain for genetic modifications to address the regulatory networks of iron metabolism. Any such transgenic strain needs a characterization of its iron kinetics (examples in [104, 105]). This includes a survey of static and dynamic characteristics of iron metabolism under the limitations set by thrifty experimental expense. The turnover model developed here permits to derive diagnostic requirements for healthy or diseased mice, after a steady-state has been established and maintained for the time of at

least one red blood cell turnover. The following data should be scaled up to the total body level:

- plasma iron steady state, measured by transferrin level and its iron saturation
- liver and spleen total iron and non-heme iron (may be replaced by plasma ferritin as indicator)
- hemoglobin iron content, if possible red blood cell turnover (as indirect control of iron turnover
- hepcidin and erythropoietin levels
- plasma iron clearance rate constant (only possible with tracer injection and several measurements during the first 12 h)
- percentage uptake of tracer from duodenum (after a bolus dose into the stomach)
- organ content of tracer iron, blood-corrected, by several measurements between 12 and 72 h at least in liver, spleen, red blood cell compartment and bone marrow
- long-term rate of iron loss.

The biochemical parameters yield a survey of the static of iron metabolism and its steady-state level. Ferrokinetics yields the fluxes. This full programme can be reduced, if in a particular situation preliminary analysis of data and their comparison with the mathematical model indicate that certain features of the iron status are not changed or are negligible.

4.28 Simulated Experiments – Perturbation and Transgenic Reconstruction

Given knowledge on the stoichiometric network structure, the most important regulatory signal (IRP/IRE system), hepcidin and erythropoetin) and the flux parameters estimated from the distribution dynamics of radioactive iron in the mouse body, it is possible to draft a kinetic model of cellular metabolism integrated to the whole organism. The important parameters of this system have been chosen as to reproduce the flux pattern into and out of the periphery of the body. The intracellular parameters that are not available have been set at normalized standard values, relative to the normal state of the adult mouse.

We have done simulation runs on the resulting system of balance equations. Extracts of calibration experiments *in silico* have been presented and discussed in the “results” section. Studies are at present under way to built a specified model version that takes into account the results of ongoing transgenic cpmstructions in the labos of Profs. Hentze, Muckenthaler and Schümann.

4.29 Conclusion and Outlook

This mathematical model presented a comprehensive physiological picture of mice under three different diets with varying iron contents. We could assess which parameters will change under dietary perturbations and study in quantitative terms when those changes take place. We have devised a simulation model of the iron metabolism of the mouse that integrates the various tissues and cell types in the form of a system of differential equations. We chose the parameters of this model, partly by fitting to ferrokinetic tracer data, partly by adopting biochemical data, and partly by formulating black boxes of kinetic behavior and of regulatory signals, using the established general theory of metabolism as source of first principles. This is a different from the recent review paper of Hower et al. [106] where they explained many known molecular mechanisms of iron metabolism and finished offering a SBML layout, but without equations or simulations.The kinetic model of the reference state reproduces in a semi-quantitative way the main features of the iron status of the mouse in

several conditions, including transgenic constructs.

Future studies could profit from the model and the results presented here. One idea would be to perform the same type of ferrokinetic studies in genetically constructed mice, either knock-out, knock-in or conditional knock-out mice. Adapting the parameter structure of our model to these artificial conditions and carrying out biochemical measurements of the iron status of these animals one will obtain a still more precise quantitative description of the system.

An obvious extension of the work would be an attempt to transform the model to the human organism. This can of course not been a simple up-scaling everything by a factor of 3000 or so. There is ample literature data on the iron metabolism of man and its physiological and pathological perturbations. There is hope that such a quantified global computer model could be of great help in the diagnostics and therapy planning of iron disorders.

Appendix A

Table 1: Iron-adequate Diet in healthy Mice - Tracer Iron Content of Body Organs after intravenous Injection

Organ / Time	0.5 Day	1 Day	4 Days	7 Days	14 Days	28 Days
Duodenum	0.555 ± 0.222	0.349 ± 0.148	0.207 ± 0.055	0.052 ± 0.002	0.085 ± 0.032	0.047 ± 0.019
Liver	0.849 ± 0.249	0.706 ± 0.317	0.664 ± 0.105	0.547 ± 0.076	0.432 ± 0.199	0.258 ± 0.075
Spleen	0.831 ± 0.196	1.153 ± 0.471	0.619 ± 0.517	0.582 ± 0.452	0.398 ± 0.111	0.438 ± 0.114
Bones	1.937 ± 0.587	0.720 ± 0.247	0.381 ± 0.085	0.282 ± 0.083	0.251 ± 0.163	0.124 ± 0.031
Heart	0.520 ± 0.090	0.260 ± 0.040	0.400 ± 0.170	0.400 ± 0.330	0.370 ± 0.260	0.230 ± 0.080
Kidneys	0.500 ± 0.200	0.310 ± 0.160	0.350 ± 0.120	0.170 ± 0.050	0.170 ± 0.150	0.180 ± 0.170
Lungs	0.780 ± 0.480	1.170 ± 1.160	0.490 ± 0.110	0.330 ± 0.420	0.330 ± 0.120	0.300 ± 0.120
Stomach	0.240 ± 0.160	0.180 ± 0.100	0.100 ± 0.030	0.040 ± 0.020	0.060 ± 0.030	0.050 ± 0.030
Integument	0.150 ± 0.190	0.100 ± 0.040	0.140 ± 0.040	0.150 ± 0.190	0.180 ± 0.070	0.070 ± 0.060
Fat	0.040 ± 0.020	0.060 ± 0.030	0.050 ± 0.030	0.110 ± 0.100	0.050 ± 0.050	0.010 ± 0.010
Muscle	0.060 ± 0.030	0.030 ± 0.010	0.030 ± 0.010	0.080 ± 0.100	0.010 ± 0.010	0.020 ± 0.010
Brain	0.030 ± 0.010	0.020 ± 0.010	0.030 ± 0.010	0.020 ± 0.100	0.030 ± 0.020	0.020 ± 0.000
Testes	0.080 ± 0.020	0.080 ± 0.010	0.090 ± 0.020	0.070 ± 0.040	0.080 ± 0.030	0.040 ± 0.010
Plasma	0.087 ± 0.048	0.015 ± 0.007	0.011 ± 0.007	0.005 ± 0.001	0.013 ± 0.001	0.016 ± 0.011
Blood	0.860 ± 0.380	1.730 ± 0.640	2.220 ± 0.600	1.780 ± 0.490	1.760 ± 0.380	1.880 ± 0.240
Intestine	0.370 ± 0.220	0.300 ± 0.130	0.160 ± 0.100	0.050 ± 0.020	0.040 ± 0.070	0.030 ± 0.080
Ileum	0.490 ± 0.280	0.350 ± 0.120	0.140 ± 0.040	0.040 ± 0.010	0.040 ± 0.120	0.030 ± 0.100
Caecum	0.310 ± 0.170	0.320 ± 0.140	0.230 ± 0.170	0.040 ± 0.020	0.030 ± 0.010	0.020 ± 0.100
Colon	0.300 ± 0.190	0.220 ± 0.130	0.120 ± 0.040	0.060 ± 0.030	0.040 ± 0.020	0.040 ± 0.020

Data (nmoles Fe^{59} per g wet weight after an intravenous injection of tracer) are from tables 3 and 4 of [27]. They apply to organ content after correction for residual blood content not removed by perfusion.

The intestinal content was calculated as mean **±** standard deviation (rounded to 2 digits) from the values of ileum/caecum/colon (standard deviation of intestine: root of the mean of the three variances).

For plasma and whole blood data were taken from fig. 2 of [27].
The tracer content in the original data was normalized to the iron concentration in the initial dose of administered radioactivity.

Table 2: Iron-deficient Diet in healthy Mice - Tracer Iron Content of Body Organs after intravenous Injection

Organ / Time	0.5 DAY	1 DAY	4 DAYS	7 DAYS	14 DAYS	28 DAYS
Duodenum	0.282 ± 0.130	0.133 ± 0.036	0.167 ± 0.046	0.069 ± 0.028	0.093 ± 0.064	0.081 ± 0.030
Liver	0.559 ± 0.214	0.494 ± 0.276	0.539 ± 0.184	0.259 ± 0.056	0.230 ± 0.110	0.108 ± 0.027
Spleen	1.279 ± 0.346	0.431 ± 0.303	0.085 ± 0.143	**-0.064** ± 0.105	**-0.151** ± 0.165	**-0.062** ± 0.077
Bones	1.053 ± 0.265	0.221 ± 0.101	0.165 ± 0.062	0.096 ± 0.028	0.041 ± 0.026	0.064 ± 0.012
Heart	0.330 ± 0.120	0.270 ± 0.180	0.370 ± 0.090	0.330 ± 0.230	0.260 ± 0.090	0.410 ± 0.140
Kidneys	0.360 ± 0.190	0.290 ± 0.150	0.360 ± 0.090	0.150 ± 0.090	0.150 ± 0.160	0.190 ± 0.050
Lungs	0.890 ± 0.820	2.600 ± 0.750	1.220 ± 0.950	0.280 ± 0.140	0.480 ± 0.240	0.160 ± 0.090
Stomach	0.210 ± 0.120	0.120 ± 0.080	0.150 ± 0.050	0.100 ± 0.070	0.080 ± 0.040	0.090 ± 0.030
Integument	0.130 ± 0.040	0.100 ± 0.040	0.170 ± 0.090	0.110 ± 0.070	0.090 ± 0.050	0.190 ± 0.050
Fat	0.040 ± 0.010	0.060 ± 0.040	0.050 ± 0.030	0.060 ± 0.060	0.040 ± 0.030	0.030 ± 0.010
Muscle	0.030 ± 0.010	0.040 ± 0.040	0.030 ± 0.020	0.030 ± 0.020	0.020 ± 0.020	0.050 ± 0.010
Brain	0.020 ± 0.001	0.020 ± 0.010	0.030 ± 0.010	0.040 ± 0.020	0.040 ± 0.010	0.040 ± 0.010
Testes	0.070 ± 0.010	0.050 ± 0.020	0.070 ± 0.020	0.080 ± 0.030	0.100 ± 0.060	0.070 ± 0.020
Plasma	0.080 ± 0.046	0.041 ± 0.030	0.017 ± 0.004	0.017 ± 0.019	0.012 ± 0.008	0.017 ± 0.015
Blood	0.880 ± 0.160	2.000 ± 0.890	2.640 ± 0.500	2.720 ± 0.780	2.920 ± 1.040	2.760 ± 0.320
Intestine	0.337 ± 0.167	0.223 ± 0.104	0.170 ± 0.072	0.093 ± 0.098	0.053 ± 0.027	0.037 ± 0.060
Ileum	0.360 ± 0.180	0.270 ± 0.050	0.140 ± 0.090	0.060 ± 0.060	0.050 ± 0.020	0.040 ± 0.020
Caecum	0.360 ± 0.160	0.260 ± 0.170	0.210 ± 0.070	0.090 ± 0.050	0.050 ± 0.030	0.020 ± 0.100

For plasma and whole blood data were taken from fig. 2 of [27].
The tracer content in the original data was normalized to the iron concentration in the initial dose of administered radioactivity.

Three values (spleen, iron-deficient at 7, 14, 28 days) were slightly lower than zero within a standard deviation interval covering the zero value. This is due to over-correction of blood-content (see methods section “Organ mass of the whole body”) in the original publication.

Table 3: Iron-loaded Diet in healthy Mice - Tracer Iron Content of Body Organs after intravenous Injection

Organ / Time	0.5 Day	1 Day	4 Days	7 Days	14 Days	28 Days
Duodenum	0.266 ± 0.140	0.469 ± 0.103	0.291 ± 0.221	0.074 ± 0.038	0.105 ± 0.092	0.103 ± 0.090
Liver	0.769 ± 0.257	2.332 ± 0.406	1.505 ± 0.763	0.840 ± 0.276	0.895 ± 0.586	0.898 ± 0.238
Spleen	0.526 ± 0.352	0.986 ± 0.511	0.633 ± 0.007	0.709 ± 0.344	0.632 ± 0.102	0.928 ± 0.217
Bones	1.062 ± 0.368	0.686 ± 0.203	0.234 ± 0.047	0.191 ± 0.066	0.304 ± 0.094	0.176 ± 0.034
Heart	0.670 ± 0.200	0.810 ± 0.280	0.640 ± 0.170	0.740 ± 0.430	0.300 ± 0.150	0.270 ± 0.180
Kidneys	0.750 ± 0.530	1.700 ± 0.460	1.000 ± 0.900	0.470 ± 0.260	0.410 ± 0.300	0.350 ± 0.200
Lungs	1.410 ± 1.110	1.340 ± 0.320	1.460 ± 1.350	3.050 ± 0.800	1.260 ± 1.250	0.800 ± 0.340
Stomach	0.230 ± 0.240	0.620 ± 0.260	0.220 ± 0.160	0.140 ± 0.120	0.110 ± 0.100	0.120 ± 0.080
Integument	0.100 ± 0.050	0.200 ± 0.040	0.080 ± 0.060	0.100 ± 0.050	0.090 ± 0.040	0.090 ± 0.030
Fat	0.040 ± 0.020	0.090 ± 0.040	0.060 ± 0.040	0.070 ± 0.030	0.070 ± 0.010	0.020 ± 0.020
Muscle	0.040 ± 0.020	0.080 ± 0.030	0.040 ± 0.020	0.040 ± 0.010	0.040 ± 0.020	0.020 ± 0.010
Brain	0.010 ± 0.010	0.020 ± 0.001	0.010 ± 0.010	0.020 ± 0.010	0.030 ± 0.010	0.020 ± 0.001
Testes	0.100 ± 0.120	0.070 ± 0.020	0.040 ± 0.010	0.060 ± 0.010	0.070 ± 0.030	0.050 ± 0.010
Plasma	0.085 ± 0.024	0.026 ± 0.013	0.006 ± 0.002	0.004 ± 0.001	0.007 ± 0.005	0.013 ± 0.005
Blood	0.240 ± 0.052	0.520 ± 0.164	0.800 ± 0.080	1.200 ± 0.180	1.840 ± 0.400	1.280 ± 0.256
Intestine	0.233 ± 0.145	0.387 ± 0.137	0.167 ± 0.131	0.083 ± 0.054	0.077 ± 0.034	0.063 ± 0.044
Ileum	0.250 ± 0.160	0.360 ± 0.140	0.150 ± 0.110	0.060 ± 0.050	0.040 ± 0.010	0.040 ± 0.010
Caecum	0.220 ± 0.110	0.400 ± 0.140	0.170 ± 0.130	0.080 ± 0.050	0.080 ± 0.030	0.060 ± 0.030
Colon	0.230 ± 0.160	0.400 ± 0.130	0.180 ± 0.150	0.110 ± 0.060	0.110 ± 0.050	0.090 ± 0.070

Data (nmoles Fe^{59} per g wet weight after an intravenous injection of tracer) are from tables 3 and 4 of [27]. They apply to organ content after correction for residual blood content not removed by perfusion.

The intestinal content was calculated as mean **±** standard deviation (rounded to 2 digits) from the values of ileum/caecum/colon (standard deviation of intestine: root of the mean of the three variances).

For plasma and whole blood data were taken from fig. 2 of [27].
The tracer content in the original data was normalized to the iron concentration in the initial dose of administered radioactivity.

References

1. Ordway, G.A. and D.J. Garry, *Myoglobin: an essential hemoprotein in striated muscle.* J Exp Biol, 2004. **207**(Pt 20): p. 3441-6.
2. Denic, S. and M.M. Agarwal, *Nutritional iron deficiency: an evolutionary perspective.* Nutrition, 2007. **23**(7-8): p. 603-14.
3. Koeppen, A.H., *The history of iron in the brain.* J Neurol Sci, 1995. **134 Suppl**: p. 1-9.
4. Moos, T. and E.H. Morgan, *The metabolism of neuronal iron and its pathogenic role in neurological disease: review.* Ann N Y Acad Sci, 2004. **1012**: p. 14-26.
5. Zecca, L., et al., *Iron, brain ageing and neurodegenerative disorders.* Nat Rev Neurosci, 2004. **5**(11): p. 863-73.
6. Finch, C.A., et al., *Ferrokinetics in man.* Medicine (Baltimore), 1970. **49**(1): p. 17-53.
7. Cavill, I. and C. Ricketts, *Human iron kinetics*, in *Iron in biochemistry and medicine*, J.A.a.W. M., Editor 1974, Academic Press: London. p. 769.
8. Hosain, F., G. Marsaglia, and C.A. Finch, *Blood ferrokinetics in normal man.* J Clin Invest, 1967. **46**(1): p. 1-9.
9. Pollycove, M. and R. Mortimer, *The quantitative determination of iron kinetics and hemoglobin synthesis in human subjects.* J Clin Invest, 1961. **40**: p. 753-82.
10. Nathanson, M.H., A. Muir, and G.D. McLaren, *Iron absorption in normal and iron-deficient beagle dogs: mucosal iron kinetics.* Am J Physiol, 1985. **249**(4 Pt 1): p. G439-48.
11. Berzuini, C., et al., *Iron kinetics: modelling and parameter estimation in normal and anemic states.* Comput Biomed Res, 1978. **11**(3): p. 209-27.
12. Stefanelli, M., et al., *Quantitation of reticuloendothelial iron kinetics in humans.* Am J Physiol, 1984. **247**(5 Pt 2): p. R842-9.
13. Vacha, J., et al., ***The Internal Iron Kinetics in Mice***. ACTA VET. BRNO, 1982. **51**: p. 3-22.
14. Lao, B.J. and D.T. Kamei, *A compartmental model of iron regulation in the mouse.* J Theor Biol, 2006. **243**(4): p. 542-54.
15. Bothwell, T.H. and C.A. Finch, *Iron Metabolism in Man*1962: Boston: Little, Brown and Co.
16. Jacobs, A. and M. Worwood, *Iron in Biochemistry and Medicine*1974, London and New York: Academic Press.
17. Crichton, R., *Iron Metabolism: From Molecular Mechanisms to Clinical Consequences*2009: John Wiley & Sons.
18. Ganz, T., *Cellular iron: ferroportin is the only way out.* Cell Metab, 2005. **1**(3): p. 155-7.
19. Morgan, E.H., *Transferrin and transferrin iron*, in *Iron in Biochemistry and Medicine*, A.J.a.M. Worwood, Editor 1974, Academic Press: London and New York. p. 29-71.
20. Allen, D.W. and J.H. Jandl, *Kinetics of intracellular iron in rabbit reticulocytes.* Blood, 1960. **15**: p. 71-81.
21. Noyes, W.D., F. Hosain, and C.A. Finch, *Incorporation of Radioiron into Marrow Heme.* J Lab Clin Med, 1964. **64**: p. 574-80.
22. Ricketts, C., A. Jacobs, and I. Cavill, *Ferrokinetics and erythropoiesis in man: the measurement of effective erythropoiesis, ineffective erythropoiesis and red cell lifespan using 59Fe.* Br J Haematol, 1975. **31**(1): p. 65-75.
23. Stevens, A.R., Jr., et al., *Iron excretion in the mouse.* J Biol Chem, 1953. **203**(1): p. 161-5.
24. Chappelle, E., et al., *Regulation of body iron content through excretion in the mouse.* Am J Physiol, 1955. **182**(2): p. 390-2.
25. Kakhlon, O. and Z.I. Cabantchik, *The labile iron pool: characterization, measurement, and participation in cellular processes(1).* Free Radic Biol Med, 2002. **33**(8): p. 1037-46.
26. Zanninelli, G., et al., *The labile iron pool of hepatocytes in chronic and acute iron*

overload and chelator-induced iron deprivation. J Hepatol, 2002. **36**(1): p. 39-46.
27. Schumann, K., et al., *A method to assess 59Fe in residual tissue blood content in mice and its use to correct 59Fe-distribution kinetics accordingly.* Toxicology, 2007. **241**(1-2): p. 19-32.
28. Vacha, J., *Blood volume in inbred strain BALB/c, CBA/J and C57BL/10 mice determined by means of 59Fe-labelled red cells and 59Fe bound to transferrin.* Physiol Bohemoslov, 1975. **24**(5): p. 413-9.
29. Barbee, R.W., et al., *Microsphere and dilution techniques for the determination of blood flows and volumes in conscious mice.* Am J Physiol, 1992. **263**(3 Pt 2): p. R728-33.
30. Lee, S.H., P.M. Starkey, and S. Gordon, *Quantitative analysis of total macrophage content in adult mouse tissues. Immunochemical studies with monoclonal antibody F4/80.* J Exp Med, 1985. **161**(3): p. 475-89.
31. Blumenfeld, D., *Operations Research Calculations Handbook*. 1 ed2001, Boca Raton, London, New York, Washington: CRC Press.
32. Bates, G.W., C. Billups, and P. Saltman, *The kinetics and mechanism of iron (3) exchange between chelates and transferrin. I. The complexes of citrate and nitrilotriacetic acid.* J Biol Chem, 1967. **242**(12): p. 2810-5.
33. Trinder, D., et al., *Iron uptake from plasma transferrin by the duodenum is impaired in the Hfe knockout mouse.* Proc Natl Acad Sci U S A, 2002. **99**(8): p. 5622-6.
34. Bonnet, J.D., et al., *Rate of loss of radioiron from mouse and man.* Am J Physiol, 1960. **198**: p. 784-6.
35. Lebeau, A., et al., *Long-term sequelae of HFE deletion in C57BL/6 x 129/O1a mice, an animal model for hereditary haemochromatosis.* Eur J Clin Invest, 2002. **32**(8): p. 603-12.
36. Nathanson, M.H., G.M. Saidel, and G.D. Mclaren, *Analysis of Iron Kinetics - Identifiability, Experiment Design, and Deterministic Interpretations of a Stochastic-Model.* Mathematical Biosciences, 1984. **68**(1): p. 1-21.
37. Breiman, L. and J.H. Friedman, *Estimating Optimal Transformations for Multiple-Regression and Correlation - Rejoinder.* Journal of the American Statistical Association, 1985. **80**(391): p. 614-619.
38. Hengl, S., et al., *Data-based identifiability analysis of non-linear dynamical models.* Bioinformatics, 2007. **23**(19): p. 2612-8.
39. Maiwald, T. and J. Timmer, *Dynamical modeling and multi-experiment fitting with PottersWheel.* Bioinformatics, 2008. **24**(18): p. 2037-43.
40. Hentze, M.W., M.U. Muckenthaler, and N.C. Andrews, *Balancing acts: molecular control of mammalian iron metabolism.* Cell, 2004. **117**(3): p. 285-97.
41. Ciechanover, A., et al., *Kinetics of internalization and recycling of transferrin and the transferrin receptor in a human hepatoma cell line. Effect of lysosomotropic agents.* J Biol Chem, 1983. **258**(16): p. 9681-9.
42. Cooperman, S.S., et al., *Microcytic anemia, erythropoietic protoporphyria, and neurodegeneration in mice with targeted deletion of iron-regulatory protein 2.* Blood, 2005. **106**(3): p. 1084-91.
43. Hentze, M.W., et al., *Identification of the iron-responsive element for the translational regulation of human ferritin mRNA.* Science, 1987. **238**(4833): p. 1570-3.
44. Meyron-Holtz, E.G., et al., *Genetic ablations of iron regulatory proteins 1 and 2 reveal why iron regulatory protein 2 dominates iron homeostasis.* EMBO J, 2004. **23**(2): p. 386-95.
45. Bulik, S., et al., *Kinetic hybrid models composed of mechanistic and simplified enzymatic rate laws--a promising method for speeding up the kinetic modelling of complex metabolic networks.* FEBS J, 2009. **276**(2): p. 410-24.
46. Heijnen, J.J., *Approximative kinetic formats used in metabolic network modeling.* Biotechnol Bioeng, 2005. **91**(5): p. 534-45.

47. Westerhoff, H.V. and D.B. Kell, *Matrix method for determining steps most rate-limiting to metabolic fluxes in biotechnological processes.* Biotechnol Bioeng, 1987. **30**(1): p. 101-7.
48. Savageau, M.A., *Biochemical systems analysis. I. Some mathematical properties of the rate law for the component enzymatic reactions.* J Theor Biol, 1969. **25**(3): p. 365-9.
49. Voit, E.O. and T. Radivoyevitch, *Biochemical systems analysis of genome-wide expression data.* Bioinformatics, 2000. **16**(11): p. 1023-37.
50. Liebermeister, W., J. Uhlendorf, and E. Klipp, *Modular rate laws for enzymatic reactions: thermodynamics, elasticities, and implementation.* Bioinformatics, 2010.
51. Wilkinson, S.J., N. Benson, and D.B. Kell, *Proximate parameter tuning for biochemical networks with uncertain kinetic parameters.* Mol Biosyst, 2008. **4**(1): p. 74-97.
52. Nielsen, J., *Metabolic control analysis of biochemical pathways based on a thermokinetic description of reaction rates*. Biochem J, 1997. **321 (Pt 1)**: p. 133-8.
53. Frazer, D.M., et al., *Hepcidin expression inversely correlates with the expression of duodenal iron transporters and iron absorption in rats.* Gastroenterology, 2002. **123**(3): p. 835-44.
54. Ganz, T. and E. Nemeth, *Iron imports. IV. Hepcidin and regulation of body iron metabolism.* Am J Physiol Gastrointest Liver Physiol, 2006. **290**(2): p. G199-203.
55. Lin, L., et al., *Iron transferrin regulates hepcidin synthesis in primary hepatocyte culture through hemojuvelin and BMP2/4.* Blood, 2007. **110**(6): p. 2182-9.
56. Rouault, T.A., *The role of iron regulatory proteins in mammalian iron homeostasis and disease.* Nat Chem Biol, 2006. **2**(8): p. 406-14.
57. Morgan, E.H. and E. Baker, *The interaction between transferrin and rabbit reticulocyte ghosts.* Biochim Biophys Acta, 1974. **363**(2): p. 240-8.
58. Kaufman, R.M., et al., *Effect of Hemolysis on Excretion and Accumulation of Iron in the Rat.* Am J Physiol, 1964. **207**: p. 1041-3.
59. Wick M., P.W., Lehmann P., *Clinical Aspects and Laboratory Iron Metabolism.* 2003.
60. Fillet, G., J.D. Cook, and C.A. Finch, *Storage iron kinetics. VII. A biologic model for reticuloendothelial iron transport.* J Clin Invest, 1974. **53**(6): p. 1527-33.
61. Kaufman, R.M., S. Pollack, and W.H. Crosby, *Iron-deficient diet: effects in rats and humans.* Blood, 1966. **28**(5): p. 726-37.
62. Cavill, I. and C. Ricketts, *Erythropoiesis and iron kinetics.* Br J Haematol, 1978. **38**(4): p. 433-7.
63. Cavill, I., et al., *The measurement of 59Fe clearance from the plasma.* Scand J Haematol, 1976. **17**(3): p. 160-6.
64. Brodsky, I., et al., *Normal mouse erythropoiesis. I. The role of the spleen in mouse erythropoiesis.* Cancer Res, 1966. **26**(2): p. 198-201.
65. Cavill, I., C. Ricketts, and A. Jacobs, *Radioiron and erythropoiesis: methods, interpretation and clinical application.* Clin Haematol, 1977. **6**(3): p. 583-99.
66. Finch, C., *Regulators of iron balance in humans.* Blood, 1994. **84**(6): p. 1697-702.
67. Horky, J., J. Vacha, and V. Znojil, *Comparison of life span of erythrocytes in some inbred strains of mouse using 14C-labelled glycine.* Physiol Bohemoslov, 1978. **27**(3): p. 209-17.
68. Knutson, M. and M. Wessling-Resnick, *Iron metabolism in the reticuloendothelial system.* Crit Rev Biochem Mol Biol, 2003. **38**(1): p. 61-88.
69. Harrison, P.M. and P. Arosio, *The ferritins: molecular properties, iron storage function and cellular regulation.* Biochim Biophys Acta, 1996. **1275**(3): p. 161-203.
70. Frazer, D.M., et al., *The role of duodenal cytochrome b in intestinal iron absorption remains unclear.* Blood, 2005. **106**(13): p. 4413; author reply 4414.
71. Vacha, J., J. Dungel, and V. Kleinwachter, *Determination of heme and non-heme iron content of mouse erythropoietic organs.* Exp Hematol, 1978. **6**(9): p. 718-24.
72. Hahn, P.F., et al., *Radioactive Iron and Its Excretion in Urine, Bile, and Feces.* J Exp

Med, 1939. **70**(5): p. 443-451.
73. Dubach, R., C.V. Moore, and S. Callender, *Studies in iron transportation and metabolism. IX. The excretion of iron as measured by the isotope technique.* J Lab Clin Med, 1955. **45**(4): p. 599-615.
74. Forrester, R.H., M.E. Conrad, Jr., and W.H. Crosby, *Measurement of total body iron in animals using whole-body liquid scintillation detectors.* Proc Soc Exp Biol Med, 1962. **111**: p. 115-9.
75. Ramey, G., et al., *Hepcidin targets ferroportin for degradation in hepatocytes.* Haematologica. **95**(3): p. 501-4.
76. Zhou, X.Y., et al., *HFE gene knockout produces mouse model of hereditary hemochromatosis.* Proc Natl Acad Sci U S A, 1998. **95**(5): p. 2492-7.
77. Huang, F.W., et al., *A mouse model of juvenile hemochromatosis.* J Clin Invest, 2005. **115**(8): p. 2187-91.
78. Nicolas, G., et al., *Lack of hepcidin gene expression and severe tissue iron overload in upstream stimulatory factor 2 (USF2) knockout mice.* Proc Natl Acad Sci U S A, 2001. **98**(15): p. 8780-5.
79. Yamaji, S., et al., *Inhibition of iron transport across human intestinal epithelial cells by hepcidin.* Blood, 2004. **104**(7): p. 2178-80.
80. Krause, A., et al., *LEAP-1, a novel highly disulfide-bonded human peptide, exhibits antimicrobial activity.* FEBS Lett, 2000. **480**(2-3): p. 147-50.
81. Park, C.H., et al., *Hepcidin, a urinary antimicrobial peptide synthesized in the liver.* J Biol Chem, 2001. **276**(11): p. 7806-10.
82. Recalcati, S., et al., *Iron regulatory proteins 1 and 2 in human monocytes, macrophages and duodenum: expression and regulation in hereditary hemochromatosis and iron deficiency.* Haematologica, 2006. **91**(3): p. 303-10.
83. Galy, B., et al., *Altered body iron distribution and microcytosis in mice deficient in iron regulatory protein 2 (IRP2).* Blood, 2005. **106**(7): p. 2580-9.
84. Hubert, N. and M.W. Hentze, *Previously uncharacterized isoforms of divalent metal transporter (DMT)-1: implications for regulation and cellular function.* Proc Natl Acad Sci U S A, 2002. **99**(19): p. 12345-50.
85. Galy, B., D. Ferring, and M.W. Hentze, *Generation of conditional alleles of the murine Iron Regulatory Protein (IRP)-1 and -2 genes.* Genesis, 2005. **43**(4): p. 181-8.
86. Pritchard, L. and D.B. Kell, *Schemes of flux control in a model of Saccharomyces cerevisiae glycolysis.* Eur J Biochem, 2002. **269**(16): p. 3894-904.
87. Edwards, J.S. and B.O. Palsson, *Robustness analysis of the Escherichia coli metabolic network.* Biotechnol Prog, 2000. **16**(6): p. 927-39.
88. Herrgard, M.J., et al., *Integrated analysis of regulatory and metabolic networks reveals novel regulatory mechanisms in Saccharomyces cerevisiae.* Genome Res, 2006. **16**(5): p. 627-35.
89. Schuster, R. and H.G. Holzhutter, *Use of mathematical models for predicting the metabolic effect of large-scale enzyme activity alterations. Application to enzyme deficiencies of red blood cells.* Eur J Biochem, 1995. **229**(2): p. 403-18.
90. Andrews, N.C., *Disorders of iron metabolism.* N Engl J Med, 1999. **341**(26): p. 1986-95.
91. Mendes, P. and D. Kell, *Non-linear optimization of biochemical pathways: applications to metabolic engineering and parameter estimation.* Bioinformatics, 1998. **14**(10): p. 869-83.
92. Andrews, N.C. and P.J. Schmidt, *Iron homeostasis.* Annu Rev Physiol, 2007. **69**: p. 69-85.
93. Bahram, S., et al., *Experimental hemochromatosis due to MHC class I HFE deficiency: immune status and iron metabolism.* Proc Natl Acad Sci U S A, 1999. **96**(23): p. 13312-7.
94. Cavill, I., *The preparation of 59 Fe-labelled transferrin for ferrokinetic studies.* J Clin Pathol, 1971. **24**(5): p. 472-4.

95. Vácha J., H.J., Dungel J., Znojil V., *The distribution of erythropoiesis over the various anatomical regions of the erythropoietic system in some inbred strains of mice.* Experimental Hematology, 1982. **10**: p. 6.
96. Klipp, E., *Timing matters.* FEBS Lett, 2009. **583**(24): p. 4013-8.
97. Donovan, A., et al., *Positional cloning of zebrafish ferroportin1 identifies a conserved vertebrate iron exporter.* Nature, 2000. **403**(6771): p. 776-81.
98. Glass, R.D. and D. Doyle, *On the measurement of protein turnover in animal cells.* J Biol Chem, 1972. **247**(16): p. 5234-42.
99. Haskins, D., et al., *Iron metabolism; iron stores in man as measured by phlebotomy.* J Clin Invest, 1952. **31**(6): p. 543-7.
100. Cook, J.D., C. Hershko, and C.A. Finch, *Storage iron kinetics. IV. Cellular distribution of ferritin iron stores in rat liver.* Proc Soc Exp Biol Med, 1974. **145**(4): p. 1378-81.
101. Hershko, C., J.D. Cook, and C.A. Finch, *Storage iron kinetics. VI. The effect of inflammation on iron exchange in the rat.* Br J Haematol, 1974. **28**(1): p. 67-75.
102. Van Wyk, C.P., M. Linder-Horowitz, and H.N. Munro, *Effect of iron loading on non-heme iron compounds in different liver cell populations.* J Biol Chem, 1971. **246**(4): p. 1025-31.
103. P. F. Hahn, W.F.B., R. A. Hettig, M. D. Kamen, and G. H. Whipple, *Radioactive iron and its excretion in the urine, bile and feces.* Journal of Experimental Medicine, 1939. **70**(5): p. 8.
104. Muckenthaler, M., et al., *Regulatory defects in liver and intestine implicate abnormal hepcidin and Cybrd1 expression in mouse hemochromatosis.* Nat Genet, 2003. **34**(1): p. 102-7.
105. Vujic Spasic, M., et al., *Physiologic systemic iron metabolism in mice deficient for duodenal Hfe.* Blood, 2007. **109**(10): p. 4511-7.
106. Hower, V., et al., *A general map of iron metabolism and tissue-specific subnetworks.* Mol Biosyst, 2009. **5**(5): p. 422-43.

Acknowledgements

Many people should be acknowledged for the direct and indirect support during the development of this work.
Providing me orientation, support and giving me an excellent example of how to be an advisor is Prof. Jens G. Reich. Thank you for your patience, clarifications and very dedicated work during the whole process.
From Heidelberg and Munich, Prof. Martina Muckenthaler, who was my first contact to Germany and iron metabolism, Prof. Matthias Hentze who kindly received me in his laboratory and Prof. Klaus Schümann, for providing us support with his extensive knowledge of the physiology of iron.
From our side in Berlin, I need to mention our very effective and kind secretary Edelgard Wolf. Tatjana Luganska, Dr. Klaus Rohde, Sven and Anja also should be mentioned for being very nice work colleagues and receiving me very well in Berlin.
In addition, the whole group of Dr. Miguel Andrade should be acknowledged for their friendship and kindness. Matt, Enrique, Adriano, Martin, Jean-Fred, David, Nancy and Marie.
I'm also grateful to the good friends that I made during my short stay in MDC: Maliha, Andrey Goncalves and many many others who were every Friday in the event organized by Matt and me.
And finally, my girlfriend, Katharina Rost.

Thank you all.